

**EFFECTS OF TEMPERATURE AND STRAIN RATE OF
DIFFICULT-TO-CUT PLATE ON ITS DEFORMATION BEHAVIOR
UNDER CUTTING BY WEDGE AND SQUARE PUNCH.**

(くさびと矩形パンチによる切断を受ける切断困難板材の温度とひずみ速度が変形挙動に及ぼす影響)

by

NGUYEN CONG HANH

グエン コン ハン

A Dissertation Submitted to the Graduate School of Engineering in Partial
Fulfillment of the Requirements for the Degree of

Doctoral Engineering

in

Information Science and Control Engineering

at the



Nagaoka University of Technology

December 2020

TITLE:

EFFECTS OF TEMPERATURE AND STRAIN RATE OF DIFFICULT-TO-CUT PLATE ON ITS DEFORMATION BEHAVIOR UNDER CUTTING BY WEDGE AND SQUARE PUNCH.

(くさびと矩形パンチによる切断を受ける切断困難板材の温度とひずみ速度が変形挙動に及ぼす影響)

AUTHOR: NGUYEN CONG HANH

DATE OF ISSUE: DECEMBER 2020

DEDICATION

I would like to dedicate this thesis

To my parents
NGUYEN C. THAM & BUI T. PHU

To my brothers and sisters
Nguyen C. Hiep, Nguyen T. Hoa, Nguyen C. Hung,
Nguyen T.H. Hue, Nguyen C. Hoan

This page has been intentionally left blank

ACKNOWLEDGMENT

I would like to express my honest gratitude to my academic advisor, Prof. Nagasawa Shigeru, a professor of Department of Mechanical Engineering, Nagaoka University of Technology, for his invaluable guidance, support, and deep encouragement throughout my research work. Moreover, the achievement of my study in the doctoral program could not be possible without his precious comments.

The thesis would not have come to successful completion, without the guidance that I received from all examining committees. Therefore, I would like to thank Prof. Ikuo Tanabe, Prof. Hiromi Isobe, Associate prof. Takahiko Kurahashi from Department of Mechanical Engineering, Nagaoka University of Technology, and Prof. Hideo Koguchi from Niigata Institute of Technology.

I am very much indebted to all laboratory members for their collaboration and support. Special thanks and appreciation are paid to my tutor Mr. Takahashi Tomohisa for his kindness support. I also would like to thank to Dr. Kensei Kaneko from National Institute of Technology, Nagaoka College for his support in ceramics specimen preparation.

I am grateful for the cooperation support of Mr. Daishiro Yamaguchi and Mr. Akira Hine from Katayama Steel Rule Die Inc. for supporting a research project of cutting tool development. I would like also to thank for supporting a collaboration fund and advising a role and requirement on ceramics dies as a deep drawing tool from Shimizu Industrial Co. Ltd.

My sincere thankfulness is extended to all of Division of International Affairs staffs and Machine Center technicians, Nagaoka University of Technology for their kindness support. I also wish to acknowledge the funding support from the Japanese government (Monbukagakusho scholarship), providing financial support during my studies in Japan.

Finally, I am especially indebted to my parents, sisters, and brothers, for their support and encouragement throughout my study.

NGUYEN CONG HANH

Nagaoka University of Technology

December 2020

This page has been intentionally left blank

ABSTRACT

In this research, the author investigated and revealed the effects of cutting parameters on the cutting characteristics of laminated sheet materials subjected to a wedge indentation process. Apart from this laminated sheet, the cutting characteristics of a fragile acrylic resin sheet were studied. A thermal cutting method was proposed to overcome the unstable separation and quality of the sheared profile of the worksheet. The main objectives of the research work were as follows:

First, concerning the wedge cutting of the nylon- polyethylene film (PA6/PE), the fundamental cutting characteristics of wedge indentation was reviewed. A general cutting mechanism of PA6/PE film and the factors affecting the cutting performance of wedged cutting process were presented. From the experiments, it was found that underlay stiffness and blade tip thickness were important factors that affected to the bent-up angle and cutting load response of the nylon film.

Second, to overcome the unstable cutting with a crushed blade tip, a thermal cutting technique was proposed. It was found that the appropriate range of the temperature of a blade body, a case of $T = 318\text{K}$ against a room temperature 296K is suitable for cutting the 0.16mm PA6/PE film off during a wedge indentation. An FEM model was conducted to reveal the effect of temperature on the deformation of the PA6/PE film.

Third, to reveal deformation behavior and cracking patterns of an acrylic worksheet subjected to a punch shearing or a wedge indentation was investigated under varying the mechanical conditions such as the cutting velocity, and the temperature of blade. As the results, a suitable cutting tool conditions for making a smart sheared wedging of the worksheet was proposed.

Furthermore, a developed simulation model using VCCT method was developed to predict the crack propagation in fragile materials (acrylic, ceramics) subjected to a shearing tool indentation.

This page has been intentionally left blank

NONMENCLATURE

L	Length of specimen, [mm]
B	Width of specimen, [mm]
t	Thickness of the specimen, [mm]
E	Young's modulus, [MPa]
ν	Poisson ratio
σ_Y	Yield stress, [MPa]
σ_B	Tensile strength, [MPa]
ε_B	Breaking strain
α	Blade tip angle, [degree]
w	Blade tip thickness, [mm]
t_b	Thickness of the blade, [mm]
w_b	Width of the blade, [mm]
V	Cutting velocity, mm/min
T	Temperature, [K]
f	Cutting line force, [N]
d/t	Normalized indentation depth
θ	Bent-up angle, [degree]
θ_{max}	Maximum value of bent-up angle, [degree]
f_C	Peak of cutting line force, [N]
J_T	Cutting energy, [N.mm ⁻¹]
T_r	Room/ambient temperature, [K]
T_m	Melting temperature of material
$\dot{\varepsilon}_r$	Reference strain rate
ρ	Density, [kg/mm ³]
K_I	Stress intensive facture, [MPa.m ^{1/2}]
G_C	Critical energy release rate, [N/m]
τ_{max}	Shear strength, [MPa]

This page has been intentionally left blank

TABLE OF CONTENT

Chapter 1 : INTRODUCTION	1
1.1 Motivation.....	2
1.2 Problem statement.....	4
1.3 Objectives of research work.....	7
1.4 Scope of research work.....	8
1.5 Organization of treatise.....	8
Chapter 2 : CUTTING MECHANISM OF NYLON POLYETHYLENE LAMINATED FILM SUBJECTED TO WEDGE INDENTATION	13
2.1 Introduction	14
2.2 Effect of cutting direction	16
2.2.1 Experiment method.....	16
2.2.1.1 <i>Material and specimens</i>	16
2.2.1.2 <i>Experiment condition</i>	16
2.2.1.2 <i>Experiment results</i>	18
2.2.2 Finite element analysis.....	21
2.2.2.1 <i>Simulation condition</i>	21
2.2.2.2 <i>Simulation results</i>	23
2.3 Effect of tip thickness on cutting resistance	24
2.3.1 Measurement of bent-up angle.....	25
2.3.2 Cutting load resistance and side-view deformation of worksheet	27
2.4 Conclusions.....	30
Chapter 3 : THERMAL DEPENDENCY IN CUTTING CHARACTERISTICS OF NYLON- POLYETHYLENE LAMINATED FILM	33
3.1 Introduction	34
3.2 Experiment method.....	34

3.2.1 Condition of thermal cutting system and specimens	34
3.2.2. Experiment results and discussions	38
3.2.2.1 <i>Cutting load resistance and deformation profile of worksheet</i>	38
3.2.2.2 <i>Relationship between cutting energy and cutting profile</i>	41
3.3 Simulation method	42
3.3.1 Procedure to determine Johnson – Cook material parameters.....	42
3.3.2 Friction coefficient test	49
3.3.3 Finite element analysis.....	51
3.3.3.1 <i>FEM condition</i>	51
3.3.3.2 <i>Simulation results and discussions</i>	53
3.4 Summary	59
Chapter 4 : THERMAL CUTTING AND EQUIVALENCY OF VELOCITY IN CUTTING CHARACTERISTICS OF ACRYLIC WORKSHEET	61
4.1 Introduction	62
4.2 Experiment method.....	63
4.2.1 Experiment conditions and specimens.....	63
4.2.2 Experiment results	66
4.2.2.1 <i>Cutting load resistance</i>	66
4.2.2.2 <i>Deformation profile of worksheet</i>	70
4.4 Summary	71
Chapter 5 : PREDICTION OF CRACKING BEHAVIOR OF FRAGILE SHEET USING IOSIPESCU TYPE SPECIMEN SUBJECTED TO A SHEARING- TOOL INDENTATION	73
5.1 Introduction	74
5.2 Strength estimation of silicon nitride ceramics using a round-notched specimen	75
5.2.1 Materials and experiments	75

5.2.1.1 <i>Materials</i>	75
5.2.1.2 <i>Experiment procedure of shearing</i>	77
5.2.1.3 <i>Experimental results and discussions</i>	79
5.2.2 Simulation of cracked behavior	83
5.2.2.1 <i>Principle of vcct cracking model</i>	83
5.2.2.2 <i>Preliminary simulation for determining the initiation of crack</i>	86
5.2.2.3 <i>Results of simulation and discussions</i>	89
5.3 Apply vcct model in acrylic shearing	93
5.3.1 Experiment and simulation method	93
5.3.2 Experiment and simulation results.....	93
5.4 Conclusion	95
Chapter 6 : CONCLUSIONS AND PROSPECTS	99
6.1 Conclusions.....	99
6.2 Prospects	100

LIST OF FIGURES

Figure 1-1. Some examples of die-cutting products. (a). Food packaging (b) Pen/Pencil container.....	2
Figure 1-2. Die-cutting processes for packaging and protective sheet industries.....	3
Figure 1-3. Types of die-cutting processes	3
Figure 1-4. Burrs occurred nearby the tip blade in term of $w/t=0.23$ [1.10].....	4
Figure 1-5. Cutting defects of plastics film.....	5
Figure 1-6. Generation of cracks in the worksheet	6
Figure 2-1. Typical problems in wedge indentation cutting [2.9]	14
Figure 2-2. Cutting defects of PA6/PE film. (a) General view of cutting failure (b) Sectional view of uncut part (SEM).....	15
Figure 2-3. Experiment apparatus and PA6/PE film structure.....	17
Figure 2-4. Cutting direction: (a) Normal direction. (b). Inverse direction	18
Figure 2-5. CCD side views of sheared worksheet (a) PA6-PE and (b) PE-PA6 when choosing the feed velocity $V = 5 \text{ mm.min}^{-1}$	19
Figure 2-6. Bent-up angle θ and the normalized indentation depth d/t for 2 cases of cutting direction PA6-PE and PE-PA6.	20
Figure 2-7. Cutting line force f and the normalized indentation depth d/t for different cutting directions PA6-PE and PE-PA6 when choosing the feed velocity $V = 5 \text{ mm.min}^{-1}$	20
Figure 2-8. SEM micrographs of wedged profile of laminated nylon film by varying the cutting direction (a) PA6-PE and (b) PE-PA6	21
Figure 2-9. A half symmetric cutting simulation model with respect to the effect of cutting direction (a) PA6-PE and (b) PE-PA6.	21
Figure 2-10. Representative initial meshes in the FEM model.....	22
Figure 2-11. Deformation profile of nylon film with respect to the cutting direction	23
Figure 2-12. Cutting blade tip (a) fined tip and (b) crushed tip.....	25
Figure 2-13. Maximum value of bent-up angle θ_{max} of wedged sheet at various tip thickness.....	26
Figure 2-14. Cutting line force f and the normalized indentation depth d/t at various tip thickness.	27

Figure 2-15. Relation between the cutting line force f and the normalized indentation depth d/t	28
Figure 2-16. SEM micrographs of wedged profile of laminated PA6/PE film by varying the tip thickness w/t	29
Figure 3-1. Schematic of PA6/PE specimen.....	35
Figure 3-2. Schematic diagram for thermal cutting system.....	36
Figure 3-3. Thermographic image of thermal cutting system.....	38
Figure 3-4. Relation between the cutting line force f and the normalized indentation depth d/t when choosing the temperature of blade as $T = 296, 318$ and 333K	39
Figure 3-5. CCD side views of sheared PA6/PE film by varying the temperature of blade.....	40
Figure 3-6. Photograph of wetted blade after cutting PA6/PE film at a temperature of blade $T=333\text{K}$	42
Figure 3-7. True strain-true stress data by varying strain rate at reference temperature $T_r = 239\text{K}$ (a). PA6 (b). PE	43
Figure 3-8. True strain-true stress data by varying the temperature at the reference strain rate $\epsilon_r = 0.0083/\text{s}$ (a). PA6 (b). PE	44
Figure 3-9. Yield stress as a function of strain rate (a). PA6 (b). PE.....	45
Figure 3-10. Yield stress as a function of temperature (a). PA6 (b). PE	46
Figure 3-11. The plots used to determine value B and n	47
Figure 3-12. The plots used to determine value C	48
Figure 3-13. The plots used to determine value m	48
Figure 3-14. Friction coefficient testing system at various temperature.....	50
Figure 3-15. A half symmetric cutting simulation model.....	52
Figure 3-16. Comparison temperature at point Q of the worksheet between experiment and simulation.....	54
Figure 3-17. Contour plot of the temperature at $d/t = 0.3$ when the blade is applied $T = 333\text{K}$	55
Figure 3-18. Deformation profile of the worksheet on the FEM simulation at $d/t = 0.45$ with respect to various temperature of the blade (a) $T = 296\text{K}$, (b) $T = 318\text{K}$, (c) $T = 333\text{K}$	56

Figure 3-19. Deformation profile of the worksheet when the 1st peak of cutting load (f_{CI}) with respect to various temperature of the blade (a) $T = 296K$, (b) $T = 318K$, (c) $T = 333K$	57
Figure 3-20. Cutting load response with respect to cutting temperature	58
Figure 4-1. Generation of cracks in the worksheet	62
Figure 4-2. True stress- true strain relationship of AC sheet at various temperature with constant strain rate = $0.002 s^{-1}$	64
Figure 4-3. Schematic of experiment apparatus.....	65
Figure 4-4. Thermal system setting: (a) Thermocouple in the cutting blade and (b) Thermocouple in the worksheet.....	66
Figure 4-5. Measured temperature in the blade and worksheet when (a) $d/t = -1$ (b) $d/t = 0.5$	67
Figure 4-6. Cutting line force at constant temperature $T= 296K$ with various cutting velocity.....	68
Figure 4-7. Cutting line force at constant high-velocity $V = 25 mm.min^{-1}$ with various cutting temperature	69
Figure 4-8. CCD side views of sheared AC sheet by varying the velocity.....	70
Figure 4-9. CCD side views of sheared AC sheet by varying the temperature	71
Figure 5-1. Ultrasonic testing system.	76
Figure 5-2. Size of specimen. (a). General view of workpiece, (b). Zoomed up view of profile of the notch.....	77
Figure 5-3. Notch surface was observed in lazer-mocroscope	78
Figure 5-4. Schematic of shearing experiment	79
Figure 5-5. Here, the thickness of plate was $t_s= 1 mm$, the feed velocity of punch was $V= 5mm.min^{-1}$	80
Figure 5-6. Load – displacement response. Here, the thickness was $t_s=1 mm$, the feed velocity was $V = 5mm.min^{-1}$	81
Figure 5-7. Scanning electron microscopy image two type of Si_3N_4 (a). SNP02 and (b). SNP03.....	82
Figure 5-8. Meshed node patterns for explaining the VCCT model.....	84
Figure 5-9. A simulation model and notched profile.....	85
Figure 5-10. Flow schemes of numerical procedure.....	86

Figure 5-11. Stress distribution on the notch surface.....	88
Figure 5-12. Detection of stress severe position and setting of a small crack on a groove surface. (a) Contour band of stress σ_{p1} at $d/t_s = 0.021$ (b) Introduction of a small crack for VCCT.....	88
Figure 5-13. Crack propagation in shearing simulation for SNP02.....	90
Figure 5-14. Comparing cracking profile between (a). experiment and (b). simulation for SNP02.....	91
Figure 5-15. Comparing load-displacement response between experiment and simulation.....	92
Figure 5-16. Comparing cracking profile between simulated crack propagation and experiment results	94
Figure 5-17. Simulated and experimental cutting line force.....	95

This page has been intentionally left blank

LIST OF TABLES

Table 2-1. Mechanical properties of polycarbonate underlay and nylon film.	16
Table 2-2. FEM conditions.....	23
Table 3-1. Mechanical properties of PA6/PE film, PA6 film, PE sheet and PC sheet (* A referenced data of single substance)	35
Table 3-2. Specification of Thermal system.	37
Table 3-3. Average cutting energy of PE layer from P^1_T to P^2_T with respect to the temperature of blade at a feed velocity of 5 mm.min-1 (maximum-minimum measured).....	41
Table 3-4. List of Johnson-Cook parameters.	49
Table 3-5. Testing conditions.....	50
Table 3-6. Effects of temperature on the friction coefficient of polymers (Average, max-min of 5 times).....	51
Table 3-7. Mechanical properties of polycarbonate underlay and nylon film.	53
Table 3-8. FEM conditions.....	53
Table 4-1. In-plane mechanical properties of acrylic at reference temperature $T=$ 296K, strain rate = 0.002 s^{-1}	63
Table 4-2. AC Johnson-Cook parameters.	64
Table 5-1. Mechanical properties of Si3N4 workpiece.....	76
Table 5-2. Shear strength of Si3N4 workpieces (Average, max-min of 3 samples)...	82

This page has been intentionally left blank

Chapter 1

INTRODUCTION

The purpose of this chapter is to introduce the background and to present the fundamental of plastic plate application and its cutting process. Research objectives and scope of the study are identified.

1.1 Motivation

Recently, plastics sheet is widely using in the packaging industry, the precision electronic components, such as the product of laminated LCD cover film, lenses and touch-screens in electronic devices and luxury products. Plastics have many unique properties such as a wide range of working temperatures, light-resistant and high strength. Due to the low cost and their advanced application, the annual global demand for plastic reached 245 million tonnes [1.1]. Although there are hundreds of plastic materials, only some of them are widely used in terms of their high volume and relatively low price for example low-density polyethylene (LDPE), high-density PE (HDPE), polypropylene (PP), PS and polyethylene terephthalate (PET) [1.2].

In plastics processing, a based plastics plate is converted to finished plastic parts and objects basing on die-cutting method [1.3-1.4]. For most industrial applications the quality of the products is related to the shape of the cutting profile. Some examples of sophisticated die-cutting products are presented in **Figure 1-1**.



Figure 1-1. Some examples of die-cutting products. (a). Food packaging (b) Pen/Pencil container

In general, there are two types of die-cutting systems: wedged indentation and punch/die shearing as shown in **Figure 1-2**. For the wedge indentation, it is often chosen

when cutting square shape, while the punch/die shearing is suitable for circular shape cutting. In the real industry, the wedge indentation and punch/die shearing is applied in both systems of rotary and flatbed cutting, as shown in **Figure 1-3**.

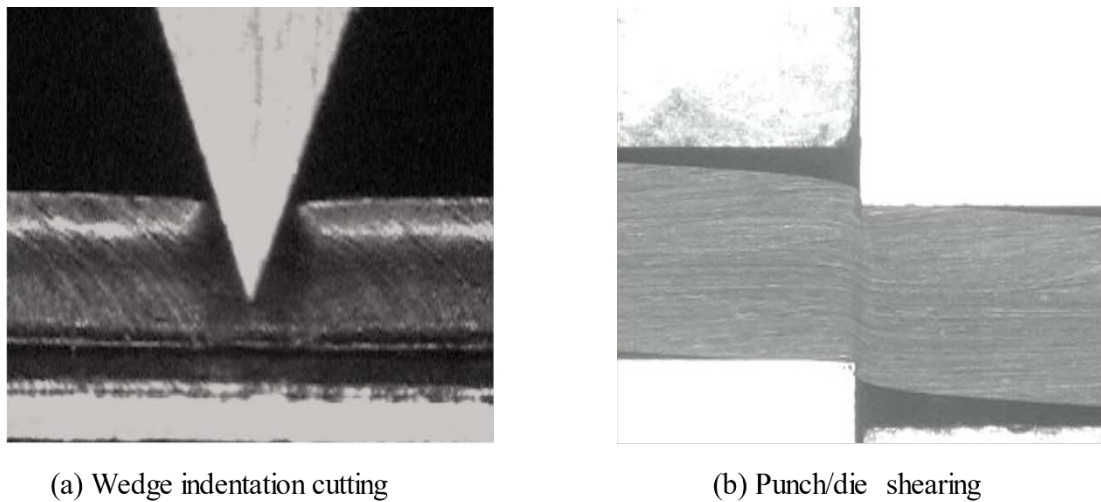


Figure 1-2. Die-cutting processes for packaging and protective sheet industries

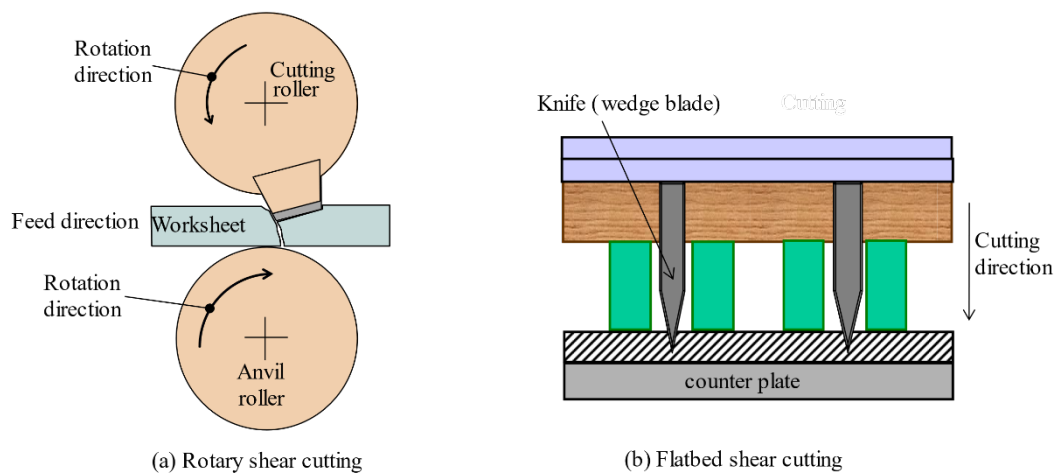


Figure 1-3. Types of die-cutting processes

Analysis of die-cutting is mainly based on phenomenological knowledge. Since, also in die-cutting processes, requirements concerning product quality, accuracy in dimension shapes, the separation performance of cutting blade, and also maintain a service life of the cutting tool are becoming more severe. The quality of the die-cutting product is affected not only by the material mechanical properties, but also other

problems caused by crushing of the blade tip. A crushed wedge is difficult to cut off in some laminated structures in comparison to a single layer. Namely, the cutting direction is affected to the cutting characteristics of the laminated worksheet sensitively. One obvious way to tackle this problem is to apply the appropriate cutting temperature and velocity that can improve the cutting processability and protect the cutting tip life.

1.2 Problem statement

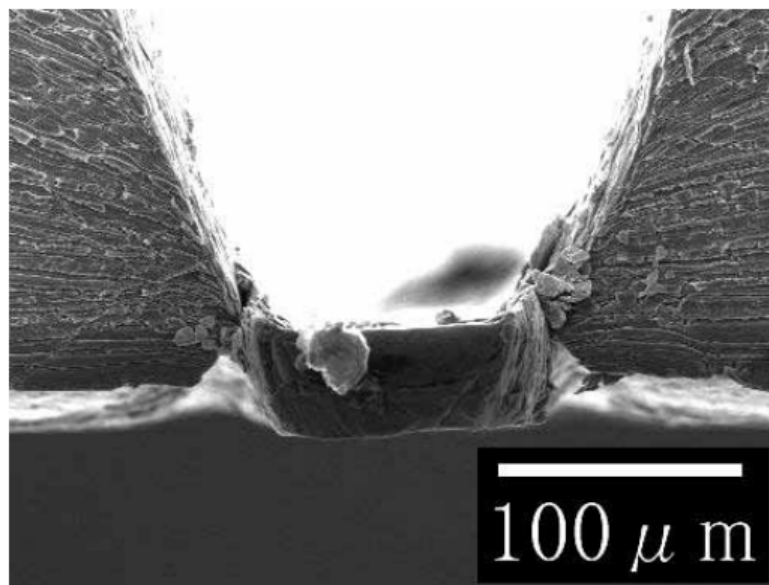


Figure 1-4. Burrs occurred nearby the tip blade in term of $w/t=0.23$ [1.10]

It is necessary to improve product quality and also maintain a service life of cutting blade on a cutting process. However, many problems affect the product quality of the wedged sheet. Previous researchers have studied how a tip blade was crushed during the processing and its effect on the occurrence string like dust in white-coated paperboard [1.5-1.7]. Murayama et al. [1.8-1.9] and Seksan et al. [1.10] also have investigated the effect of tip profile on the load response and final separation of the aluminium workpiece. In their researches, they found that if the ratio between the tip thickness of the blade and thickness of the specimen was $w/t = 0.23$, the burrs occurred at the beneath of the blade tip as shown in **Figure 1-4**. Moreover, the effect of hardness

of the blade, friction, underlay rigidity on cutting processability of the blade also have been reported by many researchers [1.11-1.18]. From these researches, many critical conditions for wedge indentation process were studied sufficiently. Nevertheless, these studies have not expanded to laminated plastics sheets, for example, PET, nylon-polyethylene film (PA6/PE) and so on. Due to their complicated structures, laminated material properties are quite different from the original sheet. **Figure 1-5** shows an example of cutting defects in a laminated nylon film which was become unstable in cutting process. Namely, the cutting failure appears in some commercial product manufacturing as shown in **Figure 1-5 (a)**. The section view of these uncut part is shown in **Figure 1-5 (b)**. This unsuccessful cutting phenomenal seems to be related to the difference in material properties between the substrate film and released film of laminated film. Another factor that affects the possibility of the cutting blade to the laminated film is the tip thickness. Namely, during the cutting, when the blade tip collides with the hard counter plate, it is normally deformed and becomes a crushed tip. Therefore, the analysis of the crushed tip blade indentation to the worksheet would be investigated experimentally and numerically.

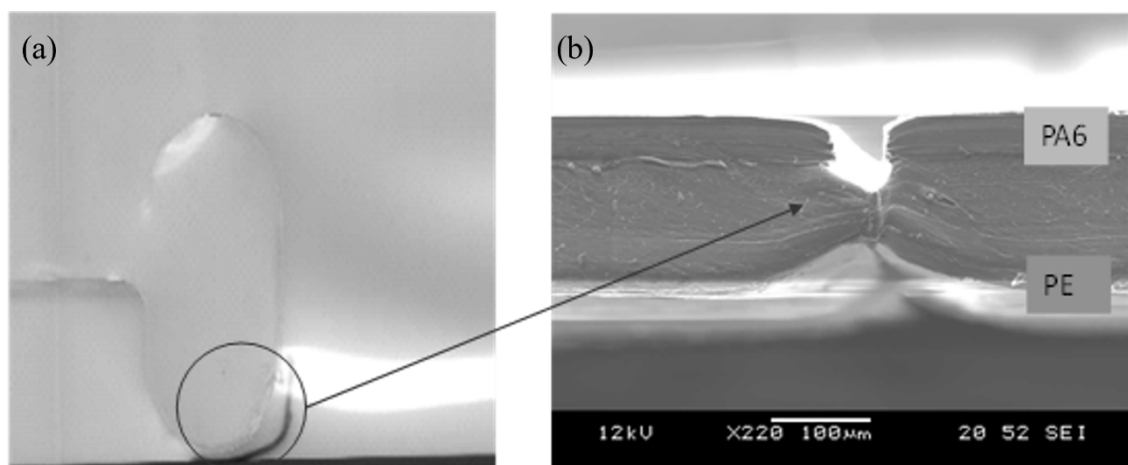


Figure 1-5. Cutting defects of plastics film.

(a) General view of cutting failure (b) Sectional view of uncut part (SEM) [1.19]

From the aspect of difficult-to-cut plate, other problems that occurred in die-cutting are the crack generation in some fragile material such as acrylic at high velocity as shown in **Figure 1-6**. The unexpected cracking seems to be caused by a fragile

property of the AC worksheet. Therefore, to find suitable cutting conditions, thermal cutting, and equivalency of the velocity effect should be clarified. These reasons indicated that the study of effect of the temperature and velocity for a cutting method would be of interest and investigated in Chapter 3 and Chapter 4.

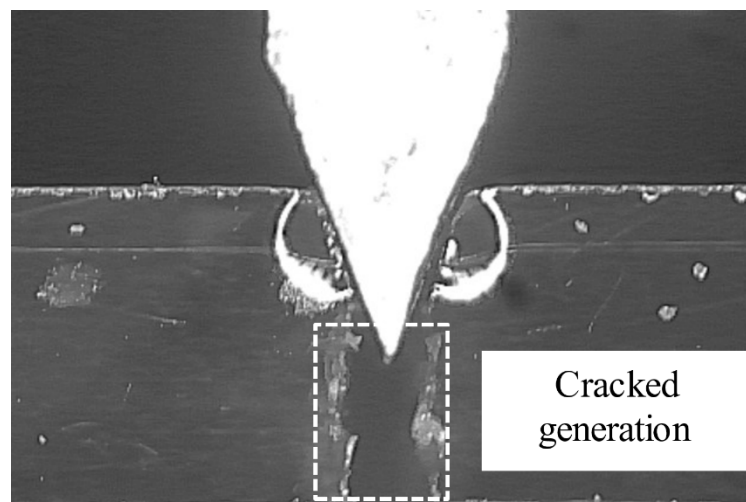


Figure 1-6. Generation of cracks in the worksheet

Moreover, the cracking behavior of plastics in wedge cutting is observed in many studies. From the literature survey, some researchers have demonstrated through the experiments and simulations for modeling of crack propagation of ductile sheet materials, and its breaking behavior [1.19-1.24]. However, the breaking behavior of ductile workpiece seems to be different from that of brittle workpieces. Crack initiation and propagation appeared to be broken randomly due to the fragile property of the brittle materials [1.25]. There are many fine cracks that seem to occur on the deformed surface pressed by a tool [1.26]. Therefore, it is limited to predict its deformation and cracking behavior due to the randomly broken of a fragile material. Previous researchers have just only investigated the deformation and stress distribution of the deformable body. There are almost not any research works that clarified the cracking behavior of a fragile workpiece. In order to promote suitable technology for cutting the fragile materials and to briefly estimate the breaking strength of that materials, the cracking behavior of

sintered Si₃N₄ workpiece and acrylic must be understood. Therefore, from the aspects of easy measuring of the strength of brittle ceramics, a notched specimen seems to be convenient for making a stable breakage, and a shearing test using Iosipescu specimen [1.27-1.28] is easy to make a shearing state at the notched zone without any gripping failure. Therefore, a study in developing a FEM cracking model to predict the crack behavior in fragile plates would be interested and discussed in Chapter 5. Consequently, this method will be applied to various resin fragile plates in wedged indentation and punch/die shearing process.

1.3 Objectives of research work

The research to be presented in this thesis aims to develop the die-cutting methods for cutting thin sheet applications such as precision electronics part, thin plastic film, and so on. The main objective of this research is designed to optimize the cutting conditions which able to cut off a thin worksheet. This study then aims to propose the essential combination methods of applying an optimal temperature and velocity to enhance the quality of the cutting profile of the thin plates. The major objectives of this study are as follow:

- To reveal the effect of underlay and crushed blade on cutting deformation of a nylon- polyethylene.
- To reveal the effect of temperature on cutting characteristics with a crushed blade tip.
- To find a suitable cutting tool conditions (cutting temperature, cutting velocity) for making a smart sheared edge of the worksheet, avoid the crack generation.
- To develop a FEM model to predict the cracking behavior of fragile worksheet in material processing.

1.4 Scope of research work

The attention in this research is focused on both the experimental and the numerical analysis. The work materials of wedged indentation processes are based on the plate material which is nylon- polyethylene film (PA6/PE) of 0.16mm thickness and an acrylic sheet of 0.5mm thickness. Meanwhile, 1mm thickness of acrylic and two types of sintered silicon nitride (Si₃N₄) plates are used for the shearing process.

Furthermore, the cracking problems of fragile materials (ceramics and acrylic) were numerically studied by a Finite Element code MSC. Marc. In this model, a virtual crack close technique (VCCT) was developed. The adaptive auto-remeshing technique has also been conducted. The adopted constitutive models are the isotropic Von Mises model incorporated in MARC and the work material is considered to be an isotropic deformation.

1.5 Organization of treatise

This treatise has been organized into six chapters. Each chapter provides the information as follows:

Chapter 1: *Introduction*. Some important problems related to thin plastic plate application and its processing were elaborated. Research objectives and scope of the study were identified.

Chapter 2: *Cutting mechanism of nylon polyethylene laminated film subjected to wedge indentation*. The fundamental cutting characteristics of wedge indentation was reviewed. In this chapter, a general cutting mechanism of PA6/PE film and the factors affecting the cutting performance of wedged cutting process were presented. It was found that underlay stiffness and blade tip thickness were important factors that affected to the bent-up angle and cutting load response of the laminated nylon film.

Chapter 3: *Thermal dependency on cutting characteristics of nylon-polyethylene laminated film.* The characteristics of nylon worksheet subjected to wedged indentation were investigated experimentally and numerically in the previous chapter. It was found that the bad cutting profile occurrence in case of using a trapezoidal cutting blade. To overcome the unstable cutting with a crushed blade tip, a thermal cutting technique was proposed.

Chapter 4: *Thermal cutting and equivalency of velocity in cutting characteristics of acrylic worksheet.* Deformation behavior and cracking patterns of an acrylic worksheet during the wedge indentation process were investigated under varying the mechanical conditions such as the punch/die cutting velocity, cutting temperature. As a result, a suitable cutting tool conditions for making a smart sheared edge of the worksheet was proposed.

Chapter 5: *Predict cracking behavior of fragile sheet using Iosipescu type specimen subjected to a shearing-tool indentation.* In this chapter, a VCCT model was applied to simulate a shearing process for investigating breaking behavior of ceramics and AC workpiece subjected to a shearing-tool indentation. This proposed model can be developed and apply to simulate the AC cutting in wedge indentation process.

Chapter 6: *Conclusions and prospects.* This chapter summarized the major contributions of this research. It then provides recommendations for further studies.

REFERENCES

- [1.1] PlasticsEurope (2008). The compelling facts about plastics, analysis of plastics production, demand and recovery for 2006 in Europe, January 2008. Belgium: PlasticsEurope
- [1.2] Andrady, A. L., & Neal, M. A. (2009). Applications and societal benefits of plastics. *Philosophical Transactions of the Royal Society B: Biological Sciences*, 364(1526), 1977–1984.

- [1.3] Inaba, Y., "Flatbed Diecutting and Maintenance of Diecutter (DSJ 囊・8 Seminar text)". CARTON BOX, 1998. Vol.17(200): pp. 17-20.
- [1.4] Mizuguchi, S.e., "Advanced Technology on Industrial Packaging and
- [1.5] Nagasawa, S., H. Sato, D. Yamaguchi, Y. Fukuzawa, I. Katayama, and A.Yoshizawa, "Effects of Tip Clearance and Blade Hardness on Cutting Resistance and Tip Shape in Paperboard Die Cutting". Journal of Japan Society for Technology of Plasticity, 2001. Vol.42(480): pp. 38-42.
- [1.6] Nagasawa, S., I. Sekikawa, M. Murayama, Y. Fukuzawa, and I. Katayama, "Effect of initial tip profile on crushing of center bevelled cutter-numerical anakysis of crushing of cutter tip indented on paperboard". Journal of Japan Society for Technology of Plasticity, 2004. Vol.45(524): pp. 747-751.
- [1.7] Nagasawa, S., Y. Fukuzawa, T. Yamaguchi, M. Murayama, Y. Daishiro, and I. Katayama, "Effect of tip shape on thread dross occurrence in paperboard die cutting". Journal of Japan Society for Technology of Plasticity, 2002. Vol.43(498): pp. 50-54.
- [1.8] Murayama, M., N. Shigeru, F. Yasushi, and K. Isamu, "Effect of sheet thickness and friction on load characteristic of crushed center bevel cutter indented to aluminum sheet". Computational Methods in Contact Mechanics VI, WIT Press, 2003. Vol.38: pp. 115-124.
- [1.9] Murayama, M., S. Nagasawa, Y. Fukuzawa, and I. Katayama, "Cutting Mechanism and Load Characteristic of Trapezoidal Center Bevel Cutter Indented on Aluminum Sheet". JSME International Journal Series C Mechanical Systems, Machine Elements and Manufacturing, 2004. Vol.47(1): pp. 21-28.
- [1.10] Seksan Chaijit, Shigeru Nagasawa, Yasushi Fukuzawa, Mitsuhiro MUrayment, Isamu Katayama, "Effect of Tip Profile on Cutting Processability of Trapezoidal Cutting Blade Indented to Aluminum Sheet", Journal of Mechanics of Materials and Structures. Vol.1, No.8, (2006), pp.1301-1322.
- [1.11] Seksan Chaijit, Shigeru Nagasawa, Yasushi Fukuzawa, Mitsuhiro Murayama and Isamu Katayama: "Effect of Hardness Combination on Contact Deformation of Center Bevel Blade with Counter Plate Subjected to a

- Pushing Load”, JSME Journal of Solid Mechanics and Materials Engineering, Vol.1 No.7, (2007), pp907-918.
- [1.12] Shigeru Nagasawa, Satoshi. Nagae, Yasushi Fukuzawa, Seksan Chaijit, Ken Yamashita, Mitsuhiro Murayama and Isamu Katayama, “Effect of surface hardness of counter plate on crushing of blade tip during pushing shear of paperboard”, Journal of Materials Processing Technology,192-193(2007),pp265-275.
- [1.13] Seksan Chaijit, Yoshikazu Yajima, Kazuya Kikuchi, Shigeru Nagasawa, Yasushi Fukuzawa, and Akira Hine, “Deformation Characteristics on Surface Layer of White-Coated Paperboard by Center Bevel Blade Subjected to Pushing Load”, Journal of Materials Science Forum, 2008
- [1.14] Seksan Chaijit, Shigeru Nagasawa, Yasushi Fukuzawa, Mitsuhiro Murayama and Akira. Hine: Effect of Underlay Rigidity on Cutting Characteristic of Aluminum Foil during Wedge Shearing Process, JSME Journal of Advanced Mechanical Design, Systems, and Manufacturing (submitted, 3rd April 2008).
- [1.15] Hesse F, Tenzer H J. Grundlaren der Papierverarbeitung. VeB Verlag fur Buch und Bibliothekswesen. 1963; 58-60.
- [1.16] Grebe W, Hofer H. Praktische hinweise zur schonung der messer in bandstahl werkzeugen. Papier-varbeitung und druck. 1973; 9: 292-300.
- [1.17] Grebe W, Hofer H. Untersuchungen an bandstahlwerkzeugen. Verpackungs-rundschau . 1972; 3: 17-24.
- [1.18] Sugihara T, Udupa A, Viswanathan K. A Plastic Boundary Layer in Wedge Indentation of Aluminum. Materials Transactions, The Japan Institute of Metals and Materials. 2006; 1-6.
- [1.19] Hanh C. Nguyen, S. Nagasawa, Cutting characteristics of nylon-polyethylene laminated film subjected to wedge indentation and its thermal dependency, Advances in Materials and Processing Technologies, (2020) 1-12
- [1.20] Brokken D, Brekelmans WAM, Baaijens FPT (2000) Predicting the shape of blanked products: a finite element approach. J Mater Process Technol 103: 51–56.

- [1.21] Goijaerts AM, Govaert LE, Baaijens FPT (2001) Evaluation of ductile fracture models for different metals in blanking. *J Mater Process Technol* 110: 312–323.
- [1.22] Goijaerts AM, Govaert LE, Baaijens FPT (2002) Experimental and Numerical Investigation on the Influence of Process Speed on the Blanking Process. *J Manuf Sci Eng* 124: 416-419.
- [1.23] Zhou Y, Yang W, Hu M, et al. (2016) The typical manners of dynamic crack propagation along the metal/ceramics interfaces: A molecular dynamics study. *Comput. Mater. Sci* 112: 27–33.
- [1.24] Zhou Y, Yang Z, Lu Z (2014) Dynamic crack propagation in copper bicrystals grain boundary by atomistic simulation. *Mater. Sci. Eng. A* 599: 116–124.
- [1.25] Yang Z, Zhou Y, Wang T, et al. (2014) Crack propagation behaviors at Cu/SiC interface by molecular dynamics simulation. *Comput. Mater. Sci* 82: 17–25.
- [1.26] Pusit M, Nagasawa S (2013) Cutting Behavior of Acrylic Thick Sheet Subjected to Squared Punch Shearing. *J Chem Chem Eng.* 7: 653-665.
- [1.27] Kojima M, Mitsomwang P, Nagasawa S. (2016) Effect of cutter tip angle on cutting characteristics of acrylic worksheet subjected to punch/die shearing. *AIMS Mater Sci* 3: 1728-1747.
- [1.28] Barnes JA, Kumosa M, Hull D (1987) Theoretical and experimental evaluation of the Iosipescu shear test. *Compos Sci Technol* 28: 251–268

Chapter 2 :

**CUTTING MECHANISM OF NYLON POLYETHYLENE
LAMINATED FILM SUBJECTED TO WEDGE INDENTATION**

In the previous studies, the fundamental cutting characteristics of wedge indentation were reviewed. In this chapter, a general cutting mechanism of PA6/PE film and the factors affecting the cutting performance of wedge cutting process are presented. It is found that underlay stiffness and blade tip thickness were an important factor affected by the bent-up angle and cutting load response of the nylon film.

2.1 Introduction

A cutting method with a 42 degrees center bevel blade into a sheet material is widely used in many packaging industries for converting metal films, laminated resin sheets, and other similar materials [2.1-2.2]. Recently, laminated structure material is increasingly used in packaging applications due to two desirable features: the first one is their high stiffness and high strength and the second is their properties that can be tailored to various components with strength far that of the original materials [2.3]. However, there are many problems that affect the product quality of the wedged sheet are caused by many mechanical conditions for making the cutting process such as the tip thickness, hardness, mechanical properties of underlay [2.4-2.6]. Experimentally and numerically studies the effect of crushed tip to the cutting characteristic of white-coated paperboard has been reported recently [2.7-2.8]. The effect of blade tip profile, apex angle, friction on cutting processability on an aluminum sheet was also reported by Seksan [2.9] and Sugihara [2.10]. **Figure 2-1** shows an example of burrs that were generated when a blade has become a crushed in wedge indentation cutting.

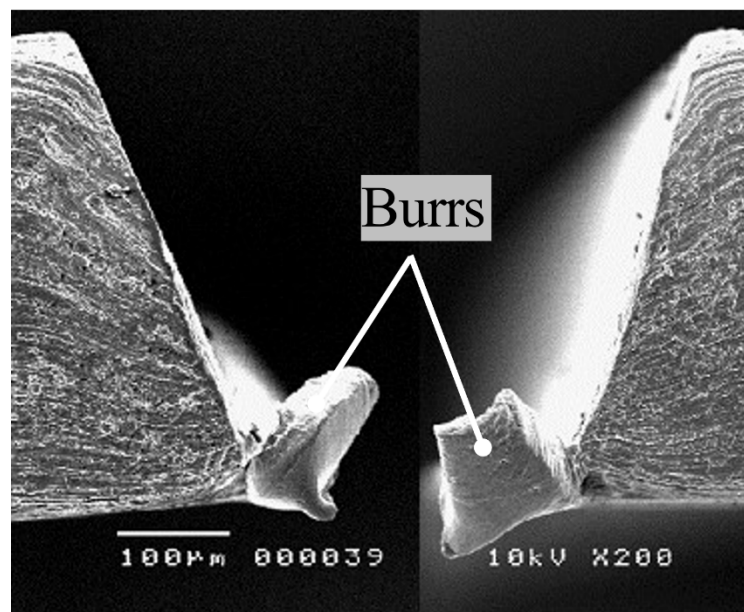


Figure 2-1. Typical problems in wedge indentation cutting [2.9]

Nevertheless, these investigations were not expanded to other laminated structures. Recently, although a nylon film is widely used in a field of food packaging due to its unique properties such as low cost, high stiffness, high transparency, thermoformability, there are not any academic reports of cutting deformation of this kind of hard material. One of common nylon film is PE-PA6 laminated film, which consists of a high tear and puncture resistance PA6 “structural” layers and a water vapour permeability PE “barrier” layers [2.11]. In laminated structure processing, crushed wedge is difficult to cut off in some laminated worksheet in comparison to a single layer. **Figure 2-2** shows an example of commercial based PA6/PE films which had cutting defects. **Figure 2-2(a)** shows a general view of stacked films after a cutting process. **Figure 2-2(b)** shows a sectional view of uncut part by zooming up a cutting line. Therefore, the same PA6/PE film was used for the cutting test in this work by changing/crushing the tip thickness of blade to reveal the effect of tip thickness to the possibility of cutting blade to the laminated worksheet. Moreover, due to the difference in material properties between the substrate film and release film, the cutting direction is sensitively affected to the cutting characteristics of the laminated worksheet. Accordingly, in the first study of difficult-to-cut plate, the cutting direction of nylon polyethylene (PA6/PE) laminated film subjected to wedge indentation was investigated.

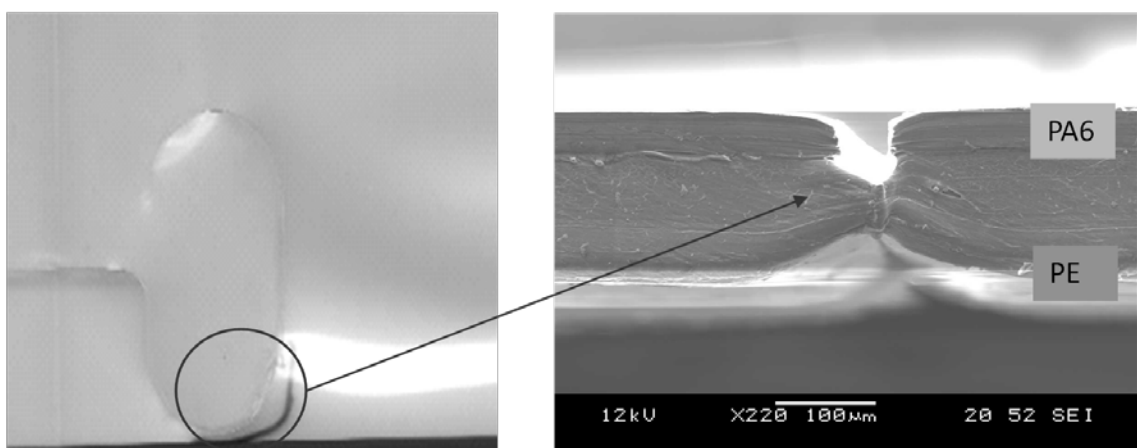


Figure 2-2. Cutting defects of PA6/PE film. (a) General view of cutting failure (b) Sectional view of uncut part (SEM)

2.2 Effect of cutting direction

2.2.1 Experiment method

2.2.1.1 Material and specimens

The material is used in the experiment is a commercial nylon polyethylene film. This laminated film is composed of 0.03 mm polyamide 6 (PA6) and 0.13 mm Polyethylene (PE). These layers are bonded perfectly by a very thin adhesive layer. The mechanical properties of the nylon polyethylene film and PC counter plate are shown in **Table 2-1**.

Table 2-1. Mechanical properties of polycarbonate underlay and nylon film.

Material	Thickness t/mm	Young modulus E/MPa	Yield stress σ_Y/MPa	Tensile strength σ_B/MPa	Breaking strain ε_B
PC	1	2650	55	153.7	0.57
PA6	0.03	2000	33	128	1.35
PE	0.13	175	10	12.7	6

2.2.1.2 Experiment condition

Figure 2-3 shows a schematic view of the experiment and specimen configuration. In this experiment, the fine cutting blades had an average tip thickness of $w = 5\mu\text{m}$ and the thickness of $t_b = 0.9\text{ mm}$ and width of $w_b = 30\text{mm}$. Experiments were carried out 5 times for each condition. On the experiment apparatus, the upper crosshead had the cutting blade mounted on the load cell with a maximum of load 20kN. The upper crosshead comoved downward with a constant speed $V = 5\text{mm}\cdot\text{min}^{-1}$ and indented to the nylon film specimens, which were placed onto polycarbonate (PC) underlay fixed on the lower crosshead until the nylon film was cut off totally. The indentation depth d

of the blade into the laminated sheet was calculated by the displacement meter of the upper crosshead. The cutting load response F was recorded by the load cell. Then, the cutting line force was calculated as $f = F/B$, $\text{N}\cdot\text{mm}^{-1}$.

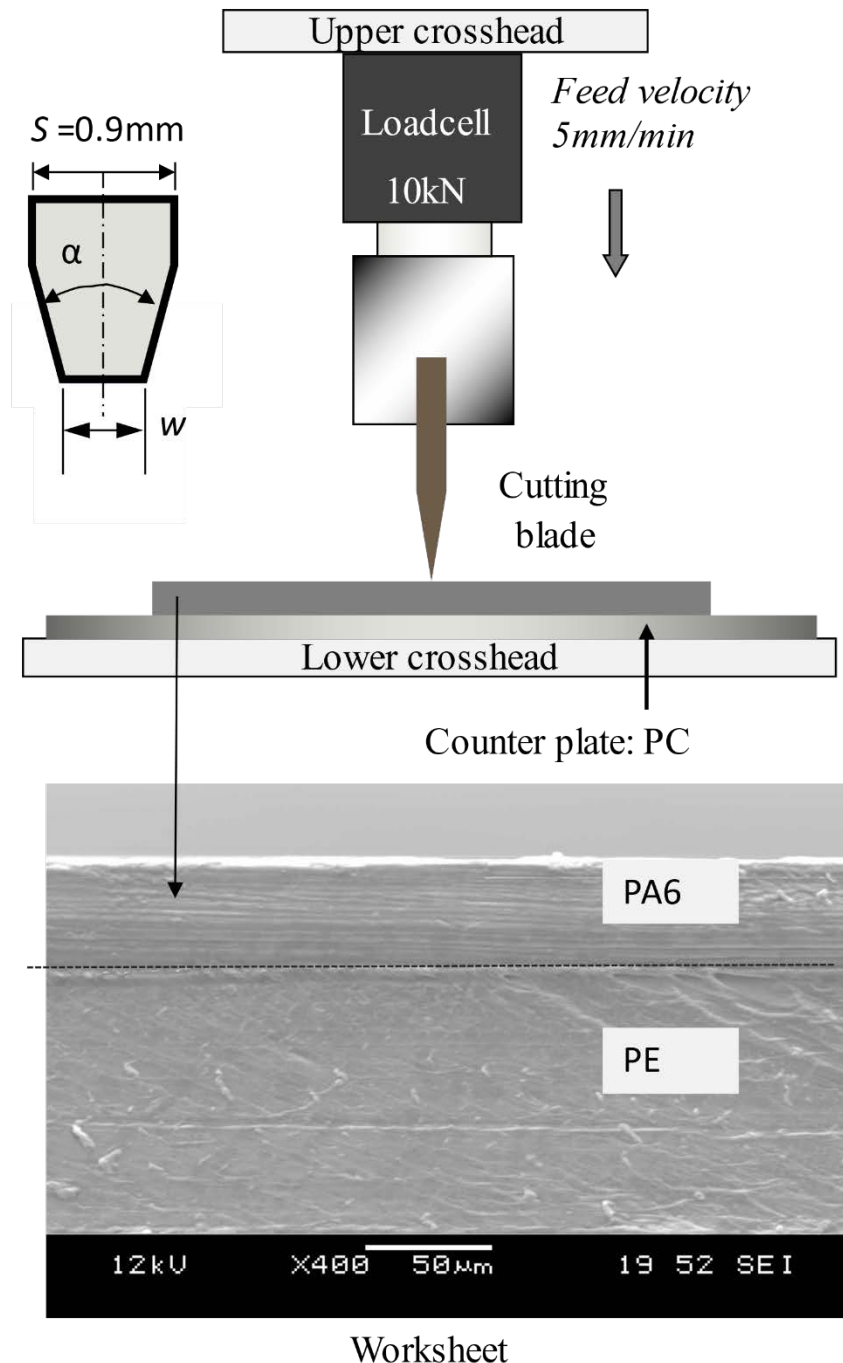


Figure 2-3. Experiment apparatus and PA6/PE film structure.

In this experiment, the effect of laminated structure was clarified by varying the cutting direction of the laminated worksheet. The normal cutting direction is specified when PA6 layer is in the upper and PE layer is in the lower. On the other hand, inverse direction is defined when PE layer is in the upper and PA6 is in the lower. The difference in the material properties of these layers seems to be affected to the cutting characteristics of the laminated worksheet.

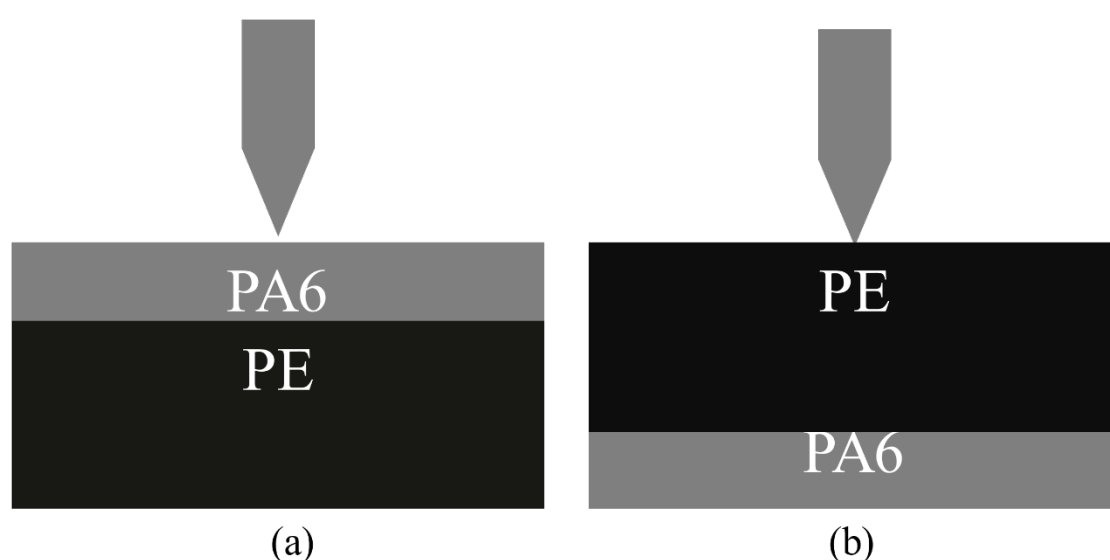


Figure 2-4. Cutting direction: (a) Normal direction. (b). Inverse direction

2.2.1.2 Experiment results

Figure 2-5(a), (b) shows the deformation profile of the laminated wedged worksheet with the tip thickness $w/t = 0.03$ at the normalized indentation depth of $d/t = 0.71$ of PA6-PE and PE-PA6, respectively. For PA6-PE, the PE lower layer is remarkably deformed, and the worksheet was in a large bending. In contrast, the laminated worksheet is almost cut off at the normalized indentation depth of $d/t = 1$ with a small bending phenomenon in the case of PE-PA6.

Figure 2-6 shows the bent-up angle θ of the laminated worksheet and the normalized indentation depth d/t for 2 cases of cutting direction PA6-PE and PE-PA6. Here, the bent-up angle θ is defined as the angle between the lower surface of the worksheet against the horizontal axis as shown in **Figure 2-5(a)**. In the case of normal

cutting direction with PA6-PE, for $0 < d/t < 0.13$, there was a slight bent-up of the laminated worksheet due to a small contact of the cutter tip and the worksheet. In the next stage, the bent-up angle was linear increase for $0.14 < d/t < 0.6$ and reached a pick at $d/t = 0.6$ mm. Seeing **Figure 2-6** and **Figure 2-7**, it was observed that the peak of maximum cutting line for f_{CI} and peak of maximum bent-up angle occurred at the same normalized indentation depth $d/t = 0.6$. After reaching a peak at 35° , the bent-up angle declined significantly and stayed at the same level from $d/t = 0.91$. In contrast, there is not any bending phenomenon in the case of PE-PA6 for $0 < d/t < 0.8$. This tendency was almost similar to cut off a soft worksheet to a hard underlay [2.12].

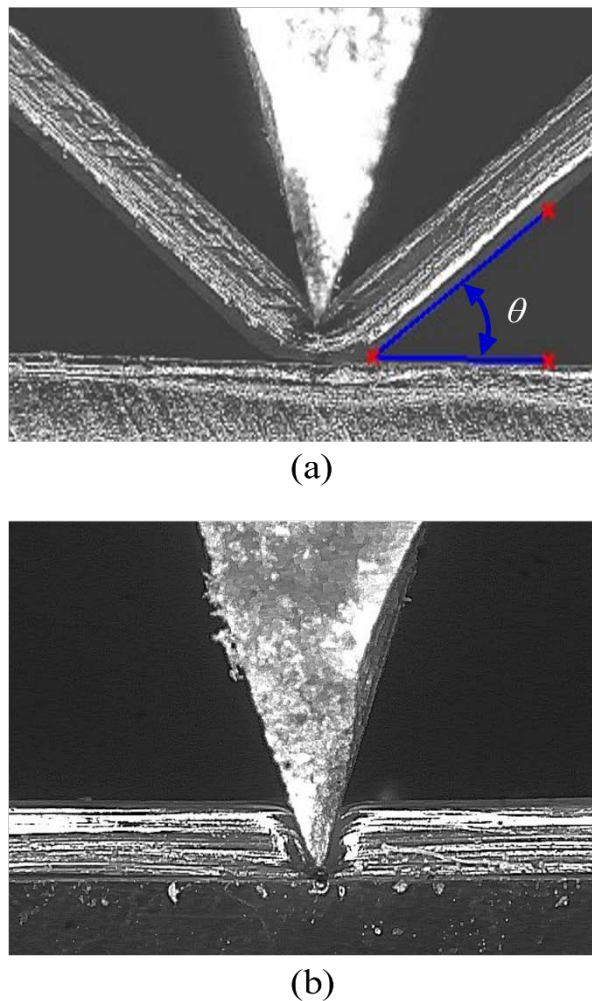


Figure 2-5. CCD side views of sheared worksheet (a) PA6-PE and (b) PE-PA6 when choosing the feed velocity $V = 5 \text{ mm} \cdot \text{min}^{-1}$.

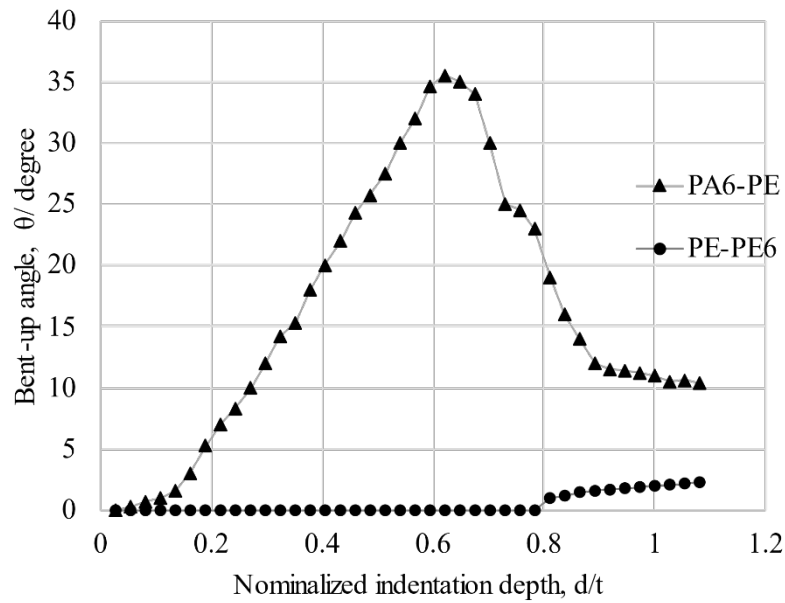


Figure 2-6. Bent-up angle θ and the normalized indentation depth d/t for 2 cases of cutting direction PA6-PE and PE-PA6.

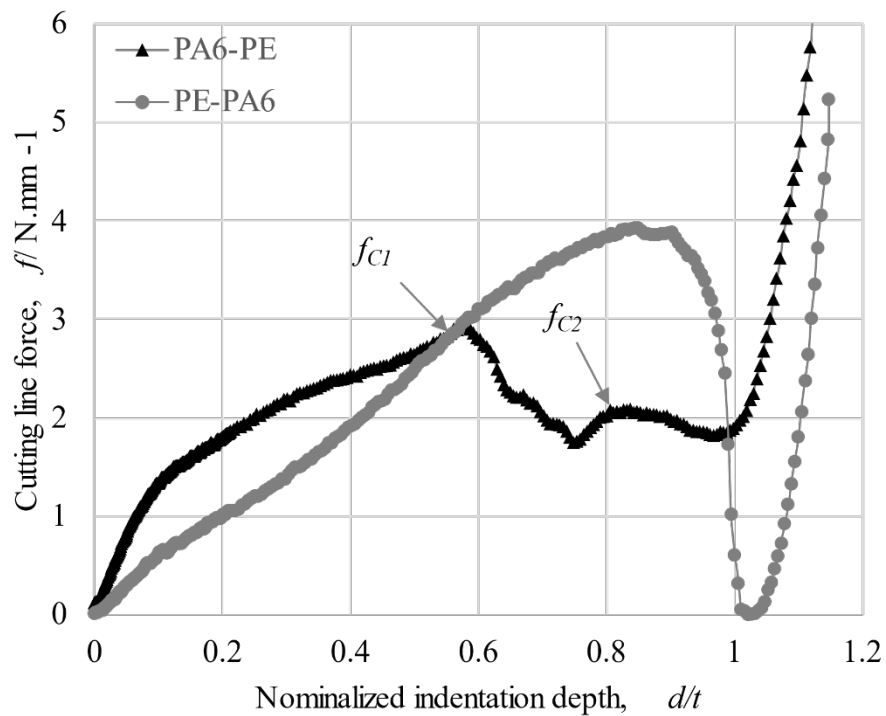


Figure 2-7. Cutting line force f and the normalized indentation depth d/t for different cutting directions PA6-PE and PE-PA6 when choosing the feed velocity $V = 5 \text{ mm} \cdot \text{min}^{-1}$.

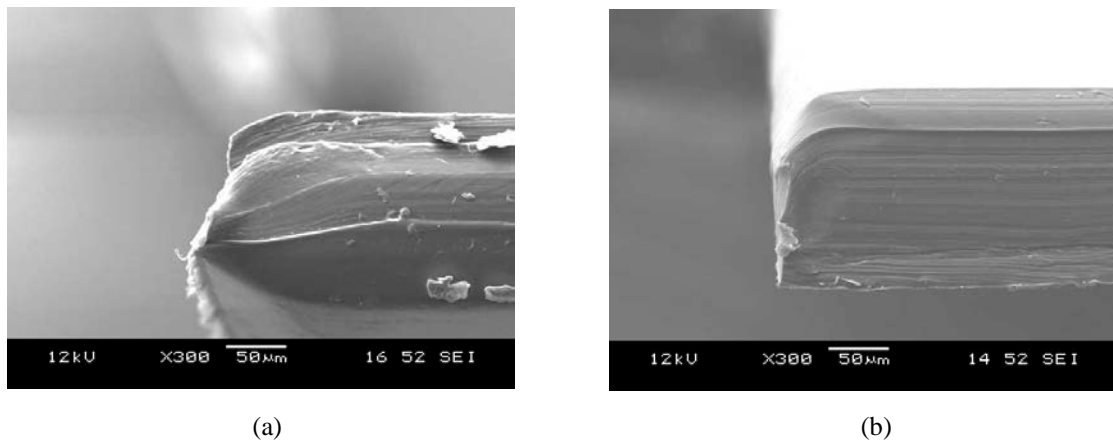


Figure 2-8. SEM micrographs of wedged profile of laminated nylon film by varying the cutting direction (a) PA6-PE and (b) PE-PA6

2.2.2 Finite element analysis

2.2.2.1 Simulation condition

In order to simulate the cutting deformation of the nylon laminated structure, a FEM code, MSC MARC 2015.0.0, was used. **Figure 2-9** shows a half symmetric cutting simulation model that had the same dimension as the experimental system with respect to the effect of cutting direction (a) PA6-PE and (b) PE-PA6.

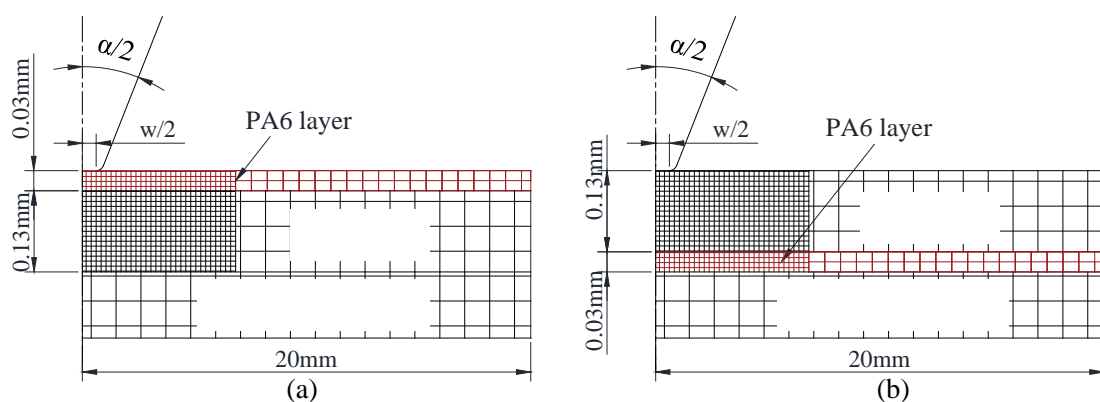


Figure 2-9. A half symmetric cutting simulation model with respect to the effect of cutting direction (a) PA6-PE and (b) PE-PA6.

In the finite element model, a plane strain model with 4280 elements was used for defining the initial mesh of the laminated workpiece. Here, the fine meshes are created for the contacting areas between the worksheet and cutting blade as shown in **Figure 2-10**. The blade was assumed to be a rigid body while the nylon film and underlayer were assumed to be isotropic elastoplastic deformation bodies. Glue contact function was used to define the contact between PA6 layer and PE layer.

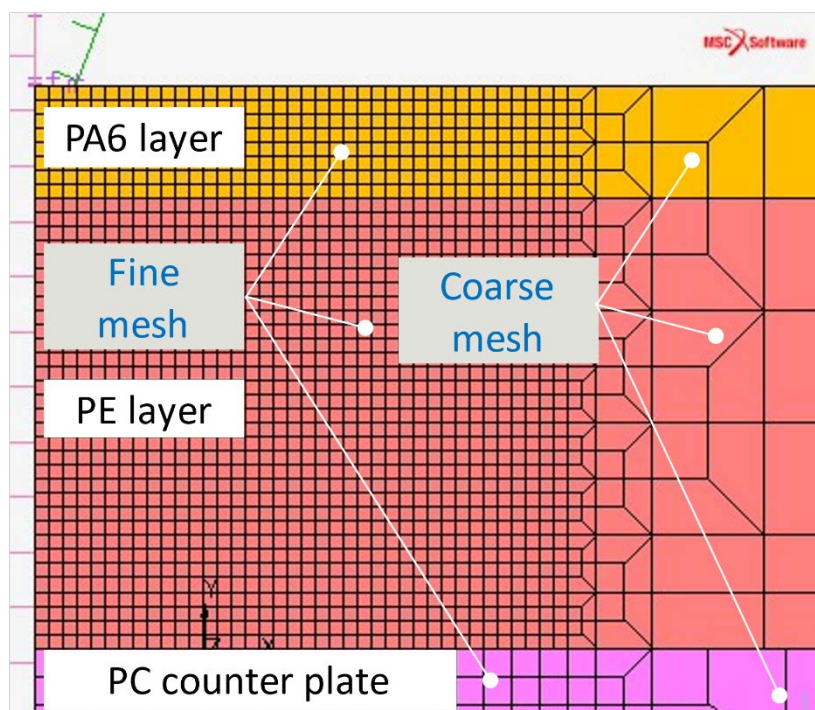


Figure 2-10. Representative initial meshes in the FEM model.

To discuss the effect of cutting direction on the nylon film subjected to wedge indentation process, simulation conditions were defined as shown in **Table 2-2**. During the downward process of the cutting blade, there was a largely deformed near the blade tip; the simulation calculation could not continuous due to crushing of the element. To overcome the poor mesh, an automatic remeshing function (2D solid: Advancing Front Quad) was used in the FEM simulation. There is not any damage model was considered in this study.

Table 2-2. FEM conditions.

Sheet symbol	Nylon film		Counter plate PC
	PA6	PE	
Young modulus, E/MPa	2000	175	2650
Yield stress, σ_Y/MPa	33	10	55
Friction coefficient	Blade and nylon film $\mu_b = 0.23$ Nylon film and counter plate $\mu_c = 0.4$		
Blade tip angle/ degree	$\alpha = 42$		
Blade tip thickness/ μm	$w = 5$		
Cutting velocity/ $\text{mm}\cdot\text{min}^{-1}$	$V = 5$		

2.2.2.2 Simulation results

Comparing the deformation profile of wedged worksheet with respect to the cutting direction PA6-PE and PE-PA6 as shown in **Figure 2-8**, it found that, for the inverse cutting direction PE-PA6, a good cutting profile was obtained. While a large bending leads to a bad cutting profile in case of normal cutting direction PA6-PE.

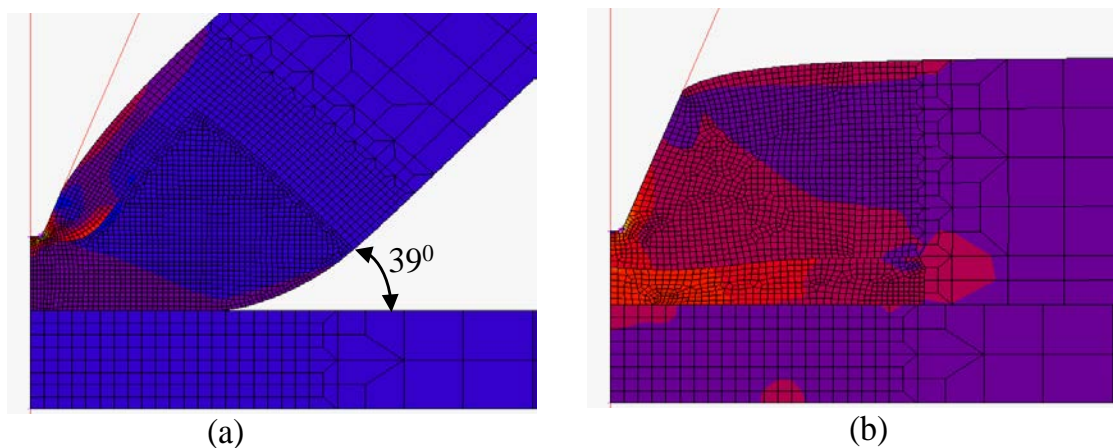


Figure 2-11. Deformation profile of nylon film with respect to the cutting direction

As we mentioned in section 2.2.1, the laminated nylon film was composed of a PA upper layer and PE lower layer. From the tensile test of PA6 and PE as shown in **Table 2-1**, Young's modulus of PA6 was estimated to be approximately 2000 MPa, and its value was significantly large in comparison to 175 MPa of PE. These have led to a significant difference in the bending phenomenon in two cases of cutting. **Figure 2-11** shows the deformation profile of the laminated nylon film with respect to the cutting direction PA6-PE and PE-PA6 in the FEM simulation. Comparing **Figure 2-11** with **Figure 2-8**, the simulated profile of the nylon film shows good agreement with experimental results. For the normal direction cutting with PA6-PE, the PE lower layer was in a large deform, and the blade could not sufficiently be indented to the worksheet. Hence, the cutting line force increased and reached the first peak f_{C1} at the indentation depth $d_{C1} = 0.6$. Here, the PA6 layer was successfully separated, and the blade continuously indented to the PE lower layer until the second peak $d_{C1} = 0.82$. For the inverse side cutting with PE-PA6, the cutting line force generally linear increased concerning the indentation depth. From this numerical and experimental investigation, we found that the cutting load response and the deformation profile of the nylon film mainly depend on Young's modulus of upper layer and lower layer of laminated worksheet.

2.3 Effect of tip thickness on cutting resistance

In order to discuss the effect of tip thickness on cutting characteristics of laminated PA6/PE film, the blade tip was varied. The blade was indented to the top surface of PA6/PE film which was placed on a PC underlay. In this experiment, the non-filled blades had a thickness of $t_c = 0.9$ mm width of $w_c = 30$ mm and average tip thickness of $w = 5\mu\text{m}$ as shown in **Figure 2-12** (a). The tips of trapezoidal bevel blades were filed using sandpapers to various tip thicknesses $w = 11, 21, 32, 42$ and $60\mu\text{m}$. These blade tips had the bevel apex angle of 42° and a hardness of 600HV (JIS Z 2244). **Figure 2-12** (b) shows an example of crushed tip of cutting blade with tip thickness $t = 32\mu\text{m}$. The experimental measurements were carried out 5 times for each case of tip thickness.

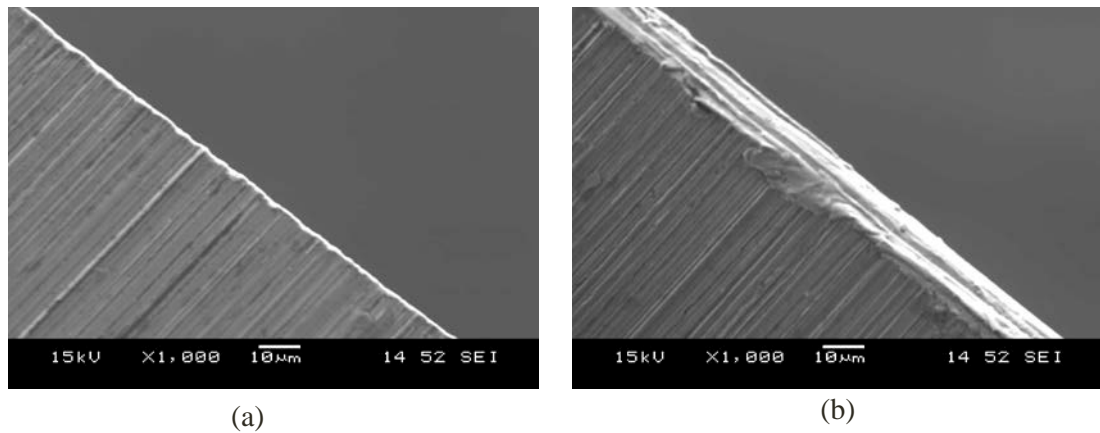
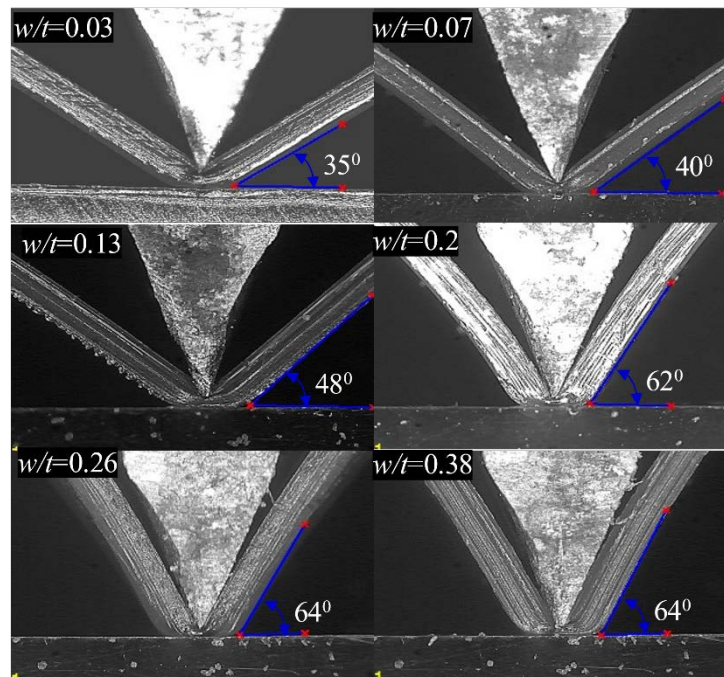


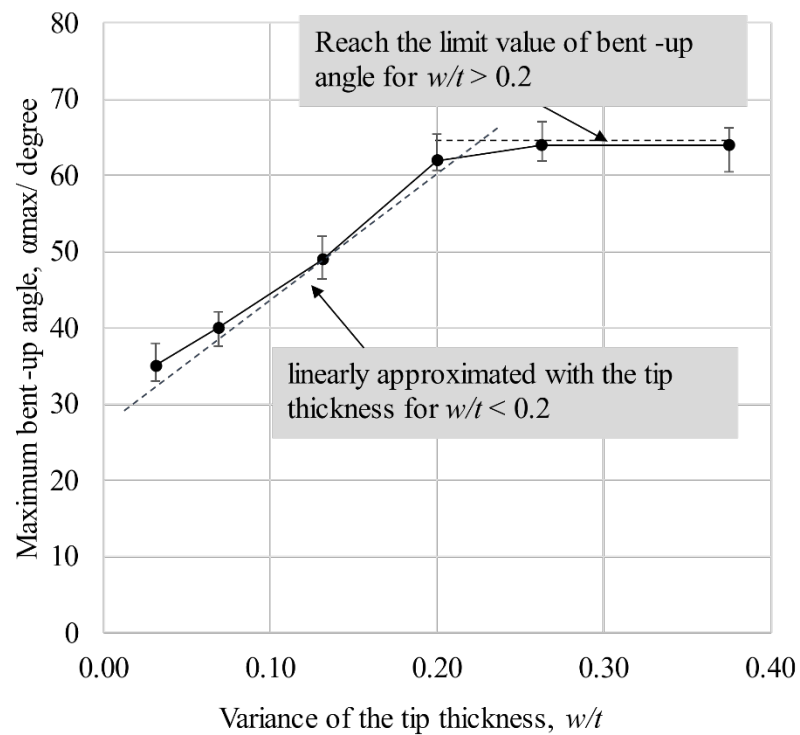
Figure 2-12. Cutting blade tip (a) fined tip and (b) crushed tip

2.3.1 Measurement of bent-up angle

Figure 2-13 shows the maximum value of bent-up angle θ_{max} of the laminated worksheet with respect to thickness w/t . Here, the bent-up angle θ is defined as the angle between the lower surface of the worksheet against the horizontal axis as shown in **Figure 2-13(a)**. It is recognized that the maximum value of bent-up angle θ_{max} was linearly approximated with the tip thickness for $w/t < 0.2$ and reached a saturated state of $\theta_{ms}=64^\circ$ at $w/t = 0.26$ when the worksheet was touched to the side of cutting blade. Here, θ_{ms} was 93% of $69^\circ (=90^\circ - \alpha/2)$ due to the contact limitation of wedge blade. The residual difference of $69 - \theta_{ms} = 5^\circ$ appeared to be an elastic detaching deformation. From this experiment, it was found that the cutting load response and the deformation profile of PA6/PE film remarkably depended on the tip blade thickness.



(a)



(b)

Figure 2-13. Maximum value of bent-up angle θ_{max} of wedged sheet at various tip thickness.

The occurrence of a large bent-up angle of PA6/PE film seemed to be caused by the dissimilar mechanical properties of PA6 and PE layers. Namely, since a PA6 layer had 3 times large yield stress and 10 times large tensile strength from **Table 2-2**, compared to that of a PE layer, the PE layer seemed to be easily elongated in the in-plane direction before cutting the PA6 layer off during the cutting process.

2.3.2 Cutting load resistance and side-view deformation of worksheet

Figure 2-14 shows the experimental of the relationship between the cutting line force f and the normalized indentation depth d/t with respect to the w/t for cutting direction PA6/PE. The maximum load points are indicated (f_{C1} , d_{C1}/t) and (f_{C2} , d_{C2}/t), where f_{C1} , f_{C2} is the line force; d_{C1} , d_{C2} is the corresponding indentation depths of the blade at two peaks of load. The cutting line force was reached the first peak f_{C1} when the PA6 layer was separated. The blade continuously indented to the PE layer until the second peak f_{C2} when the PE layer was cut off.

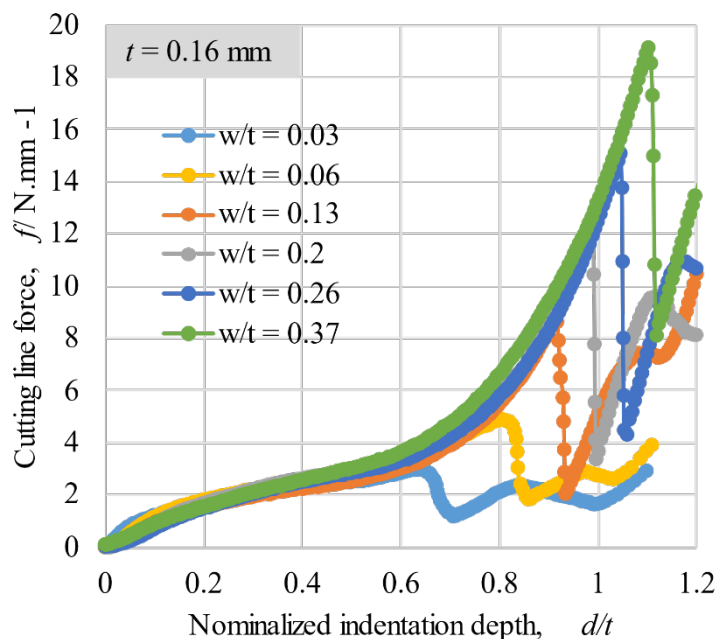


Figure 2-14. Cutting line force f and the normalized indentation depth d/t at various tip thickness.

The linear approximations of f_{C1} , f_{C2} by the least-squares method were derived as Eq. (1), (2), (3), (4) as shown in **Figure 2-15**. There were slightly changes at $w/t = 0.13$ with f_{C1} and at $w/t = 0.06$ with f_{C2} .

$$f_{C1} = 33.06(w/t) + 2.65 \text{ N.mm}^{-1} \quad (w/t < 0.13) \quad (2-1)$$

$$f_{C1} = 49.61(w/t) - 0.92 \text{ N.mm}^{-1} \quad (w/t > 0.13) \quad (2-2)$$

$$f_{C2} = 32(w/t) + 1 \text{ N.mm}^{-1} \quad (w/t < 0.06) \quad (2-3)$$

$$f_{C2} = 28.76(w/t) - 2.03 \text{ N.mm}^{-1} \quad (w/t > 0.06) \quad (2-4)$$

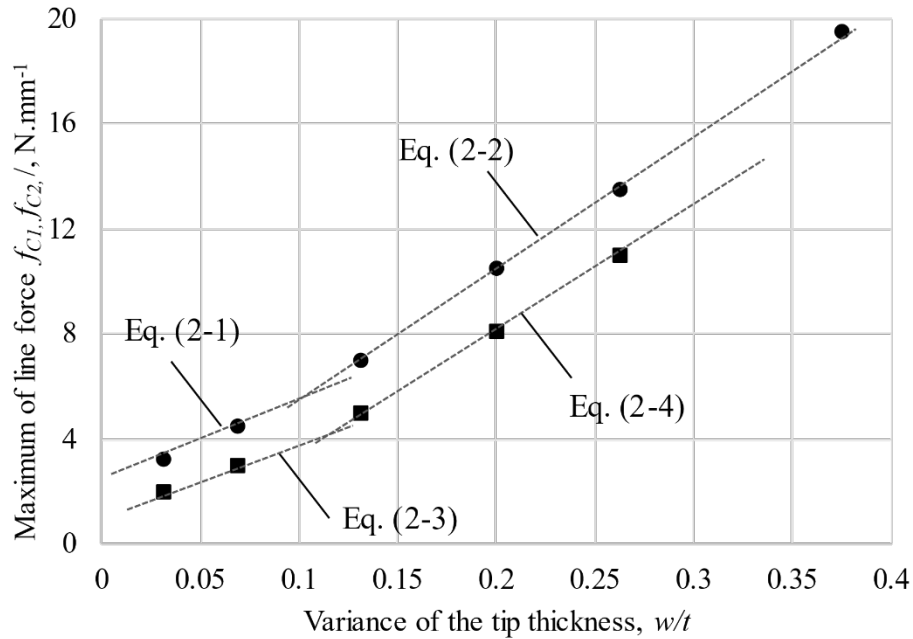
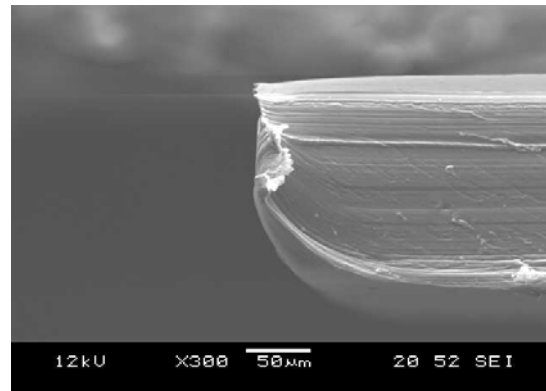


Figure 2-15. Relation between the cutting line force f and the normalized indentation depth d/t .

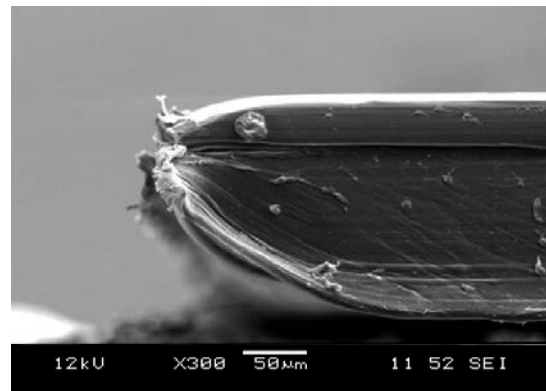
Figure 2-16 shows the SEM micrographs of wedged profile of laminated PA6/PE film by varying the tip thickness w/t . When w/t was varied from 0.03 to 0.37, there were 3 kinds of load response with respect to the indentation depth d/t : (a) $0.03 < w/t < 0.07$. The blade was smoothly indented to the PA6/PE film and successfully cut off the film at $d/t \approx 1$. (b) When choosing $0.07 < w/t < 0.26$, a large force dropped occurred without any residual resistance at the breaking stage of PA6 layer and many

string-like dusts occurred. (c) For $w/t > 0.26$, the blade tip generally pushed the PA6/PE film without any separation in the final stage. Namely, the PC underlay was deformed with a high pressure from a sort of built-up edge which consisted of blade tip and adhered PA6 layer.

(a) $w/t < 0.13$



(b) $0.13 < w/t < 0.26$



(c) $w/t > 0.26$

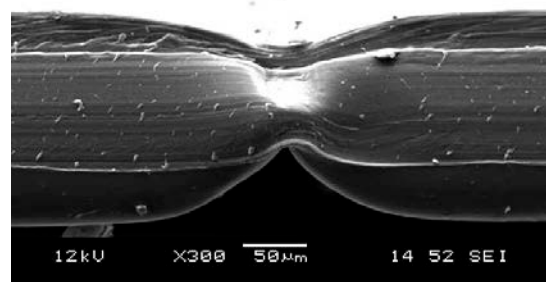


Figure 2-16. SEM micrographs of wedged profile of laminated PA6/PE film by varying the tip thickness w/t .

2.4 Conclusions

In this work, a cutting test of a 0.16mm PA6/PA laminated film subjected to a 42 degrees wedge indentation was carried out experimentally under the cutting velocity $V= 5 \text{ mm.min}^{-1}$. By varying the cutting direction and crushed tip thickness w , the following results were obtained.

- i. By varying the cutting direction PA6-PE and PE-PA6, the bent-up angle θ of the laminated worksheet and cutting load response were remarkably affected by the laminated structure.
- ii. A bad cutting profile occurred in this case of normal cutting direction PA6-PE. While a good cutting profile was observed for reversed cutting direction PE-PA6. From this result, a good cutting condition can be chosen for a similarity laminated worksheet cutting in the mass industrial.
- iii. The simulated profile of the nylon film shows good agreement with experimental result. The bent-up angle and the deformation profile of the nylon film mainly depend on Young's modulus of the upper layer and lower layer of the laminated worksheet.
- iv. The bent-up angle and the deformation profile of worksheet remarkably depended on the normalized tip thickness of the cutting blade w/t . When choosing $w/t < 0.13$, the bent-up angle was less than 50degrees (72% of saturated maximum angle) and the cutting peak maximum was less than 7 N/mm at normal temperature. This seemed to be a preferable mechanical condition for smoothly cutting a PA6-PA film off.

References

- [2.1] Inaba Y, Flatbed die-cutting and maintenance of diecutter (DSJ '98 seminar text), carton and box, 1998;17(200): 17-20.
- [2.2] Mizuguchi S, eds, Advanced Technology on Industrial Packaging and Transportation, Fuji Techno System, Tokyo.2002; 58-59 (in Japanese).
- [2.3] Masud A, Tham C, Computational Mechanics in Structural Engineering, Recent Developments; 1999. p. 295-307.
- [2.4] Hesse F, Tenzer H J. Grundlagen der Papierverarbeitung. VeB Verlag fur Buch und Bibliothekswesen. 1963; 58-60.
- [2.5] Grebe W, Hofer H. Praktische hinweise zur schonung der messer in bandstahl werkzeugen. Papier-verarbeitung und druck. 1973; 9: 292-300.
- [2.6] Grebe W, Hofer H. Untersuchungen an bandstahlwerkzeugen. Verpackungs-rundschau . 1972; 3: 17-24.
- [2.7] Nagasawa S, Sato H, Yamaguchi D, Fukuzawa Y, Katayama I, and Yoshizawa A. Effect of tip clearance and blade hardness on cutting resistance and tip shape in paper board die cutting. J Japan Society Technol Plastic. 2006;42(480): 38-42.
- [2.8] Nagasawa S, Sekikawa H, Murayama D, Fukuzawa Y, Katayama I. Effect of initial tip profile on crushing of center bevelled cutter-numerical analysis of crushing tip indented on paperboard. J Japan Society Technol Plastic, 2004; 45(524): 747-751.
- [2.9] Chaijit S, Nagasawa S, Fukuzawa Y, Murayama D, Katayama I. Effect of tip profile on cutting processability of a trapezoidal cutting blade indented to an aluminum sheet, J Mechanics of Materials and Structures, 2006;1(8): 1301-1321.
- [2.10] Sugihara T, Udupa A, Viswanathan K. A Plastic Boundary Layer in Wedge Indentation of Aluminum. Materials Transactions, The Japan Institute of Metals and Materials. 2006; 1-6.
- [2.11] Information on <https://www.gruber-folien.de/?q=en/products/pape-film>, accessed 20th March 2020.

- [2.12] S. Chaijit, S. Nagasawa, Y. Fukuzawa, D. Murayama, A. Hine, Effect of underlay rigidity on cutting characteristic of aluminum foil during wedge shearing process, *J. Adv. Mech. Des. Syst. Manuf.* 2(2008), 800-811.

Chapter 3 :

**THERMAL DEPENDENCY IN CUTTING CHARACTERISTICS OF
NYLON- POLYETHYLENE LAMINATED FILM**

The characteristics of nylon worksheet subjected to wedged indentation were investigated experimentally and numerically in the previous chapter. It is found that the bad cutting profile occurrence in case of using a trapezoidal cutting blade. To overcome the unstable cutting with a crushed blade tip, a thermal cutting technique was proposed. It was found that the appropriate range of the temperature of a blade body, which is suitable for cutting the 0.16mm PA6/PE film off during wedge indentation.

3.1 Introduction

In the wedged indentation process, many problems that affected on the quality of the products. One of them is caused by plastic crushing or abrasion of the blade tip. Nagasawa et al [3.1-3.3] and Nagae [3.4-3.5] have investigated how the tip profile was crushed and its effect to the cutting characteristic of white-coated paperboard. In their study, it was found that the fine cutting tip became a crushed form when the cutting tip contacted to the hard-counter plate after multiple cutting processes. In the previous chapter, it was also shown that the bad cutting profile occurrence in case of using a trapezoidal cutting blade with $w/t > 0.07$. In this study, a thermal system was used to overcome the unstable cutting with a crushed blade tip. To develop new countermeasures, temperature elevation effect is considered. Namely, changing the temperature of the work body is seems to be effective to change the material properties and improve the edge profile. Therefore, in this chapter, in order to reveal the effect of cutting parameters on the cutting features, a 42 degrees wedge indentation test of 0.16 mm thickness PA6/PE film was conducted. The cutting line force was gotten using a recording unit; the cutting profile of the PA6/PE film was observed using a CCD camera. In this study, in order to reveal the effect of elevated temperature of blade on the cutting resistance and deformation state of the film, a rubber heater was mounted on the blade and the cutting test was investigated. Moreover, the FEM simulation was applied the Johnson-Cook model to simulate the effect of temperature on the cutting characteristic of PA6/PE film. The transition heat conduction and load response in the experiment have been discussed with the FEM simulation results.

3.2 Experiment method

3.2.1 Condition of thermal cutting system and specimens

In the wedge indentation experiment, the specimens of the laminated nylon film were prepared which has a thickness of 0.16mm (composed of 0.03mm polyamide 6 (PA6) and 0.13mm Polyethylene (PE)). The mechanical properties of the PA6/PE film

were determined by uniaxial tensile test by using JIS K 7161 standard. The specimen of nylon film was a rectangle sheet that has an average total thickness of $t = 0.16\text{mm}$ (0.157-0.165), $L= 50\text{mm}$ length and a 20mm width. The cutting position was across the crossing direction (CD) as shown in **Figure 3-1**. The mechanical properties of the PA6/PE film and PC underlay were shown in **Table 3-1**.

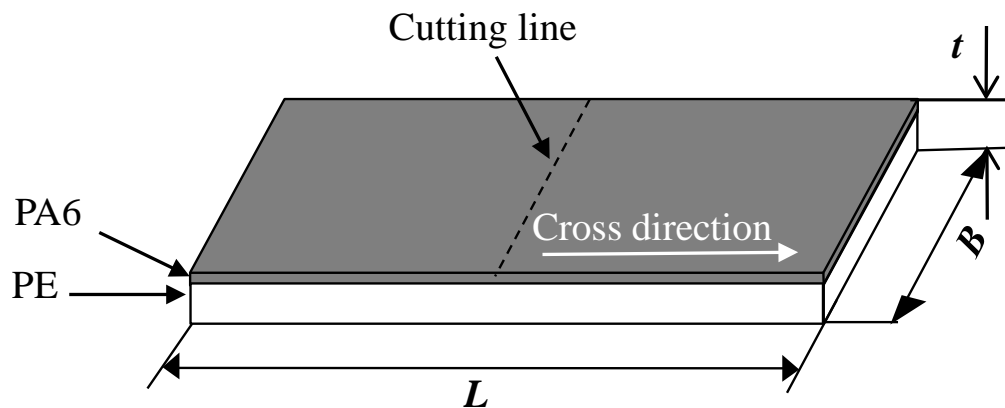


Figure 3-1. Schematic of PA6/PE specimen.

Table 3-1. Mechanical properties of PA6/PE film, PA6 film, PE sheet and PC sheet (* A referenced data of single substance)

Sheet symbol	Thickness t/mm	Young modulus E/MPa	Yield stress σ_Y/MPa	Tensile strength σ_B/MPa
PA6/PE (CD)	0.16	495	15	55
PA6*	0.17	2000	33	128
PE*	0.25	175	10	12.7
PC	1	2650	55	153.7

Figure 3-2 shows a schematic diagram of the thermal cutting system experiment. A specimen of the PA6/PE film was placed onto a polycarbonate (PC) underlay fixed on the lower crosshead. The upper crosshead moved downward with a constant velocity

$V = 5 \text{ mm.min}^{-1}$. The cutter was indented to the laminated PA6/PE film until the lower layer was cut off. The blade edge was indented to the upper surface of PA6 layer and the PA6 layer was equivalently stacked on the PE layer without detaching. The normalized indentation depth of the cutting blade into the laminated sheet was estimated by the displacement of the upper crosshead. The load response F was measured by the load cell with a maximum load of 20kN and the cutting line force $f = F/B$, N.mm^{-1} was calculated. All the experiment was carried out at a temperature 296K and relative humidity of 50% in a controlled room.

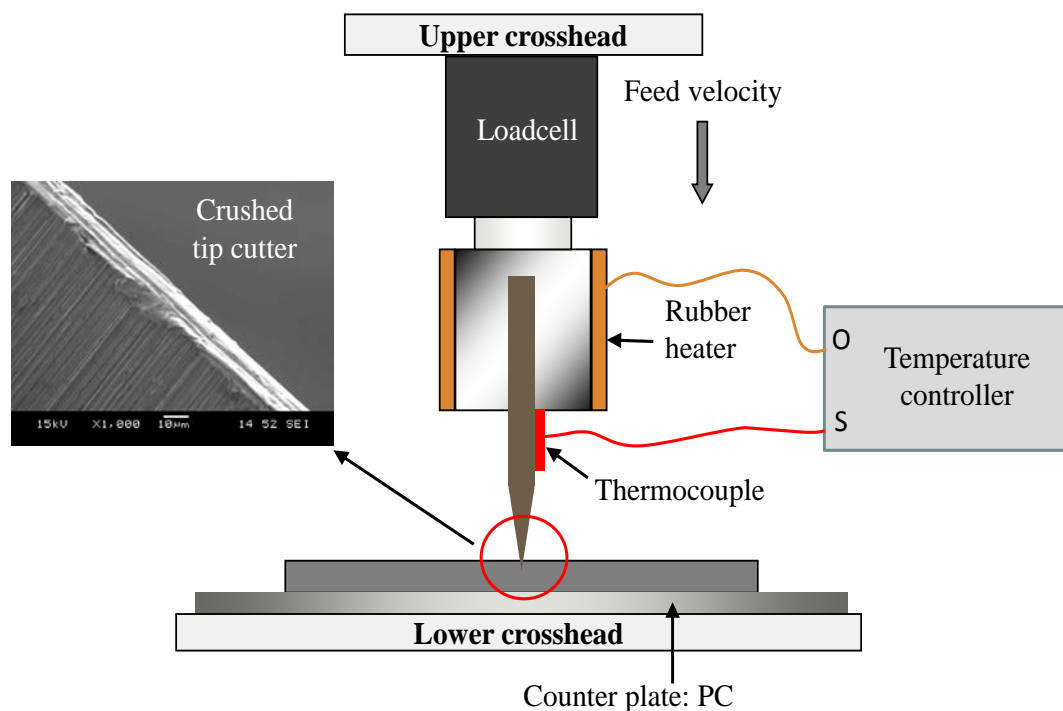


Figure 3-2. Schematic diagram for thermal cutting system.

In this system, heat was generated from the rubber heater and transferred to the tip blade. A thermocouple was mounted to the blade to measure the real temperature in the tip blade. A temperature controller was used to compare the temperature signal to the setpoint (desired temperature) and actuated the rubber heater. Another thermocouple was placed at a 2mm off-set from the cutting line to measure the heat transfer from the blade to the worksheet. A thermal imaging camera was used to capture the temperature in the cutting system area as shown in **Figure 3-3**. Thermal system components and

their specifications are explained in **Table 3-2**. In this experiment, a crushed blade tip with the tip thickness $w/t = 0.13$ ($w=21\mu\text{m}$) was used to investigate the effect of cutting temperature to the cutting profile and cutting load response. Other experiment conditions, for example, feed velocity, worksheet and counter plate were kept as the same with the previous investigation, which was explained in Chapter 2, section 2.3 effect of tip thickness on cutting resistance. The cutting temperature of blade was varied at room temperature (296K), 318K, 333K.

Table 3-2. Specification of Thermal system.

Component	Model, specification
Thermal controller	E5CC-RX3ASM-000
Thermocouple	Type K; 273K – 453K
Silicone rubber heater	Maximum operating temperature: 473K Heat generation density: 0.8 W/cm ² Voltage: 100 V, Power: 10 W
Thermal imaging camera	Flir C3 Thermal sensitive < 0.1 °C Temperature range -263K~ +423K



Figure 3-3. Thermographic image of thermal cutting system.

3.2.2. Experiment results and discussions

3.2.2.1 Cutting load resistance and deformation profile of worksheet

Figure 3-4 shows the relationship between the cutting line force f and the indentation displacement d/t with varying temperatures. The peak of cutting line force was indicated (f_{c1} , $dc1/t$) and (f_{c2} , $dc2/t$), where f_{c1} , f_{c2} was the line force; $dc1$, $dc2$ was the corresponding indentation depths of the blade at two peaks of load. It was found that the cutting line force remarkably decreased when increasing the temperature of blade. At room temperature ($T = 296K$), a large force dropped without any residual resistance at the breaking stage of the PA6 upper layer when using the crushed tip blade. Namely, the blade was indented to the worksheet with high pressure. As a result, a bad profile was observed in **Figure 3-5 (a)**. On the contrary, in cases of $T = 318K$, the cutting line force tended to be same as the first cutting mode with a fine tip blade which was explained in chapter 2, section 2.3.2. In this case, after passing the first peak of load, the cutting line force residually decreased when the PA6 layer was separated. Therefore, it seemed that the cutting line force decreased due to the effect of temperature on the

yield stress of PA6/PE film. In addition, the cutting profile was improved with a good profile as shown in **Figure 3-5 (b)**. When we applied a high temperature larger than 333K, the second peak of load has not appeared in the red curve in **Figure 3-4**. The plastic flow phenomenon was observed with an unsuccessful cutting mode as shown in **Figure 3-5 (c)**. This seemed to be caused by reaching the heat deflection temperature of PE layer (333K-363K) [3.6]. From these results, it was found that the cutting temperature significantly affected the load response and cutting profile of the PA6/PE film.

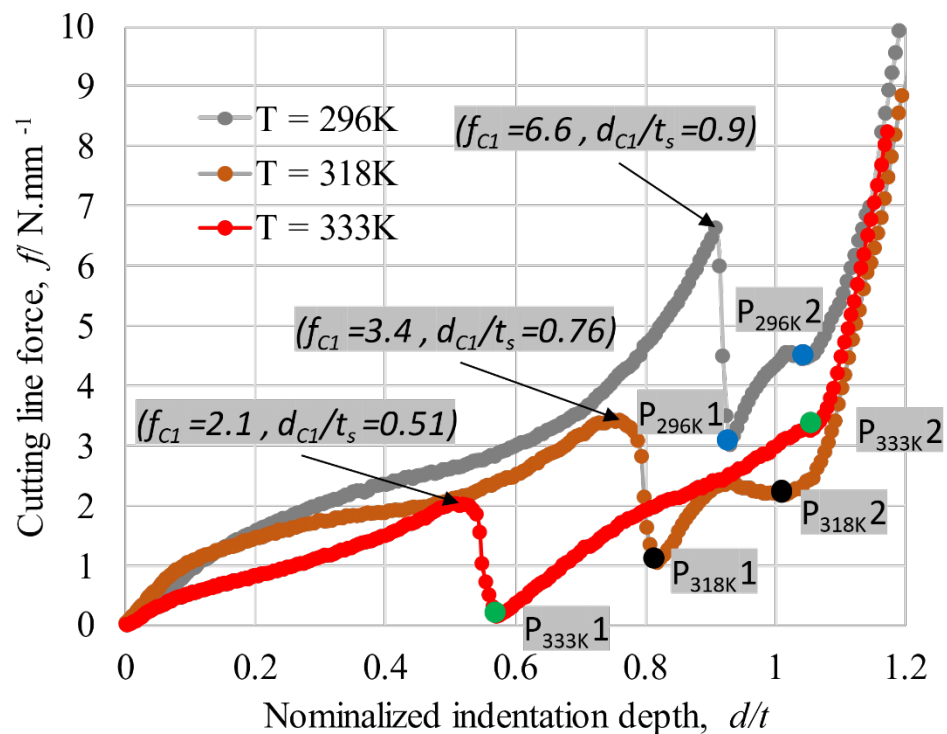
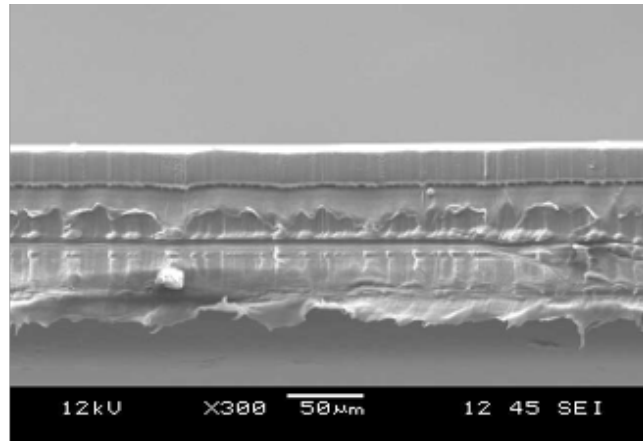
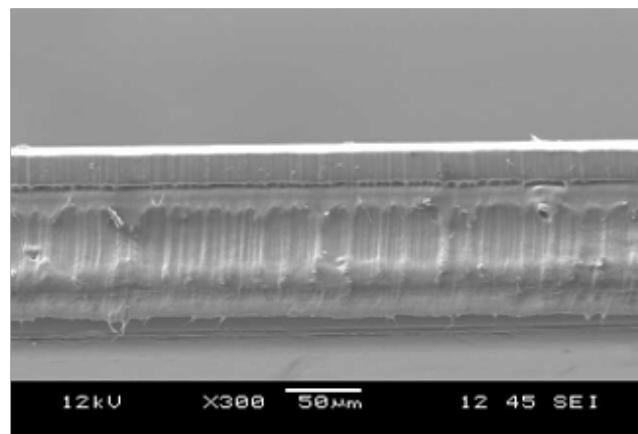


Figure 3-4. Relation between the cutting line force f and the normalized indentation depth d/t when choosing the temperature of blade as $T = 296, 318$ and $333K$.

a) $T = 296\text{K}$



(b) $T = 318\text{K}$



(c) $T = 333\text{K}$

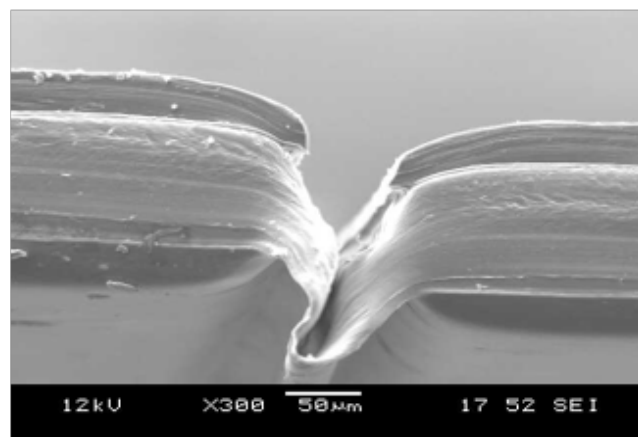


Figure 3-5. CCD side views of sheared PA6/PE film by varying the temperature of blade.

3.2.2.2 Relationship between cutting energy and cutting profile

The cutting energy J_T from a point P_t^1 to point P_t^2 was expressed as follows:

$$J_T = \int_{P_t^1}^{P_t^2} f d(d/t) \quad (3-2)$$

In the equation, f was the cutting line force, d/t was the nominalized indentation depth, the P_T^1 and P_T^2 were positions of blade indentation when PA6 and PE layers were cut off respectively at the specified temperature T in **Figure 3-4**. Here, the trapezoidal rule was used to approximate the definite integral using the increment pitch of indentation depth of 0.005. Finally, the results of average cutting energy at various temperatures were shown in **Table 3-3**.

Table 3-3. Average cutting energy of PE layer from P_T^1 to P_T^2 with respect to the temperature of blade at a feed velocity of 5 mm.min⁻¹ (maximum-minimum measured).

Temperature of blade T, K	Cutting energy $J_T, N.mm^{-1}$	Maximum-minimum of J_T measured
296	3.97	(3.85-4.15)
318	2.42	(2.37-2.61)
333	4.23	(4.13-4.42)

From **Table 3-3**, it was found that the cutting energy was large in the case of room temperature and $T = 333K$, while this value was small at $T = 318K$. It was possible to decrease the cutting energy when choosing the appropriate temperature of blade. However, the cutting energy was large in case of $T=333K$ (at a higher temperature) due to the half melting state of PE layer and the wetting of blade surface as shown in **Figure 3-6**. It appeared that the larger cutting energy the cutting process had, the worse profile the sheared edge of PA6/PE film had. From these results, it was found that appropriate temperature of blade was an effective method to cut off smoothly the PA6/PE film during a cutting process.

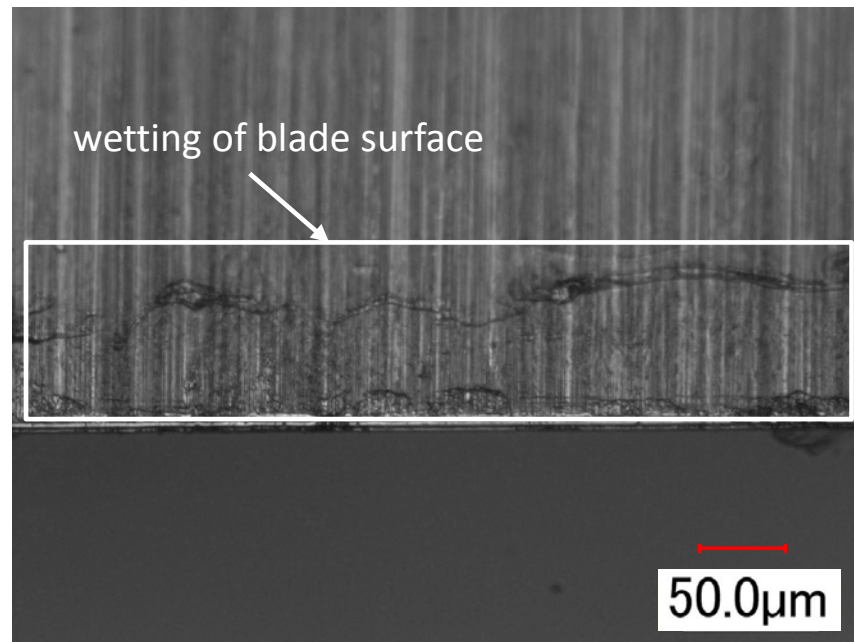


Figure 3-6. Photograph of wetted blade after cutting PA6/PE film at a temperature of blade $T=333\text{K}$.

3.3 Simulation method

3.3.1 Procedure to determine Johnson – Cook material parameters

The temperature effect was numerically investigated based on the Johnson-Cook model. This model is used for explaining the flow stress of materials when strain rate hardening and elevated-temperature softening are considered as Equation 3.3.

$$\sigma = [A + B\varepsilon^n] \left[1 + C \ln \frac{\dot{\varepsilon}}{\dot{\varepsilon}_r} \right] [1 - \hat{T}^m] \quad (3-3)$$

Where, parameters A, B, C, m, and n are material constants. $\dot{\varepsilon}$ is a strain rate and $\dot{\varepsilon}_0$ is a reference strain rate. \hat{T} is homologous temperature. It can be calculated by the Equation 3-3.

$$\hat{T} = \frac{T - T_r}{T_m - T_r} \quad (3-$$

4) Where:

- T is the material temperature
- T_r is the room/ambient temperature
- T_m is the melting temperature of material

In Johnson-Cook (JC) model (Equation 3-3), the three groups of terms in the blanket express elastoplastic deformation, viscous-plastic deformation and thermal softening, respectively [3.7-3.8]. To determine JC constant parameters, a series of compressive tests of PA6 and PE material was conducted. **Figure 3-7** and **Figure 3-8** show the representative true stress and true strain by varying strain rate at reference temperature $T_r = 239\text{K}$ and varying the temperature at the reference strain rate $\dot{\epsilon}_r = 0.0083/\text{s}$, respectively. From these figures, it can be found that PE is more sensitive to the velocity and temperature changes than PA6. PE has reached the heat deflection temperature at $T = 333\text{K}$ as shown in **Figure 3-8 (b)**.

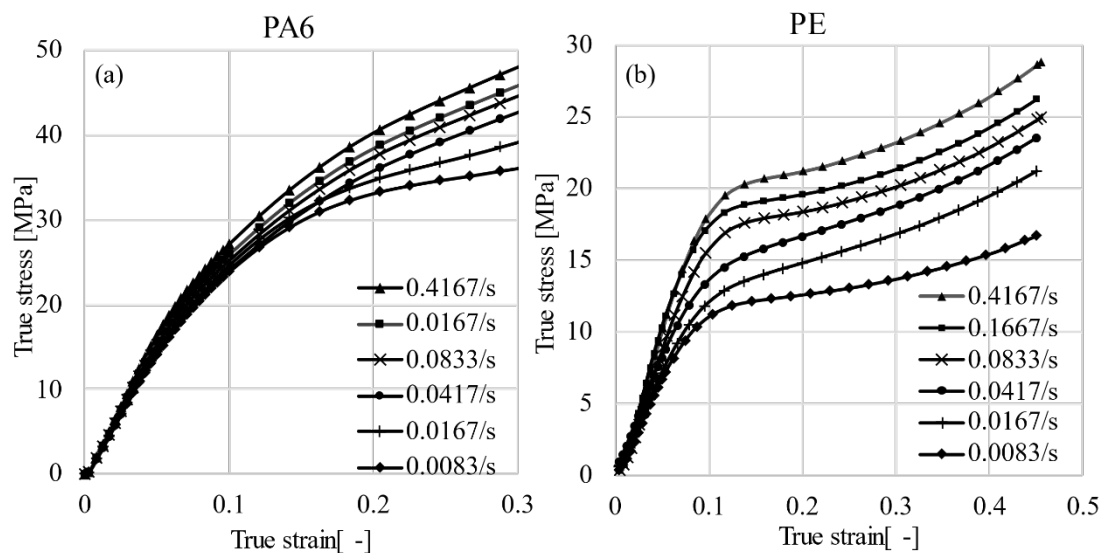


Figure 3-7. True strain-true stress data by varying strain rate at reference temperature $T_r = 239\text{K}$ (a). PA6 (b). PE

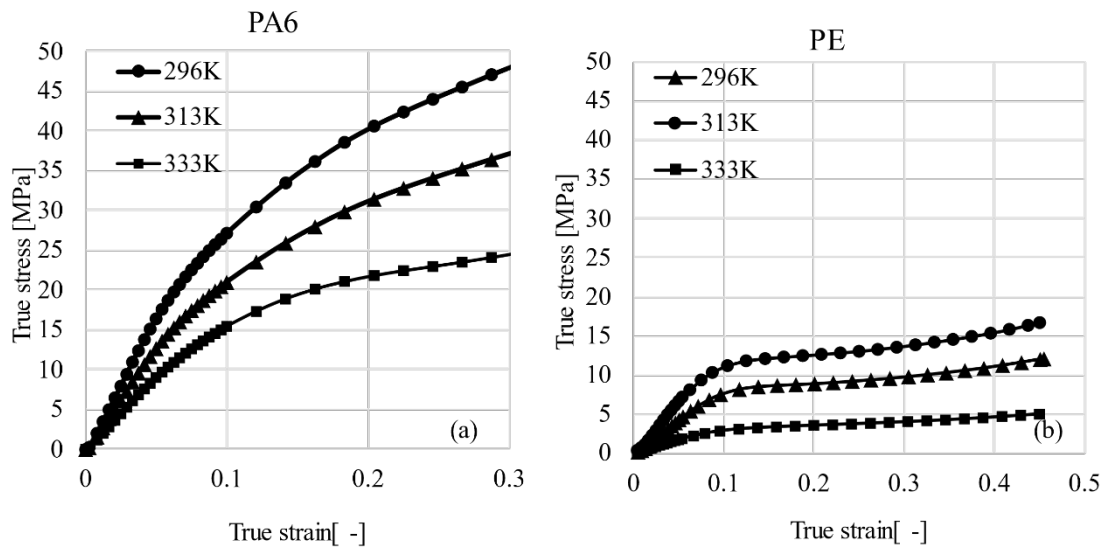


Figure 3-8. True strain-true stress data by varying the temperature at the reference strain rate $\dot{\epsilon}_r = 0.0083/s$ (a). PA6 (b). PE

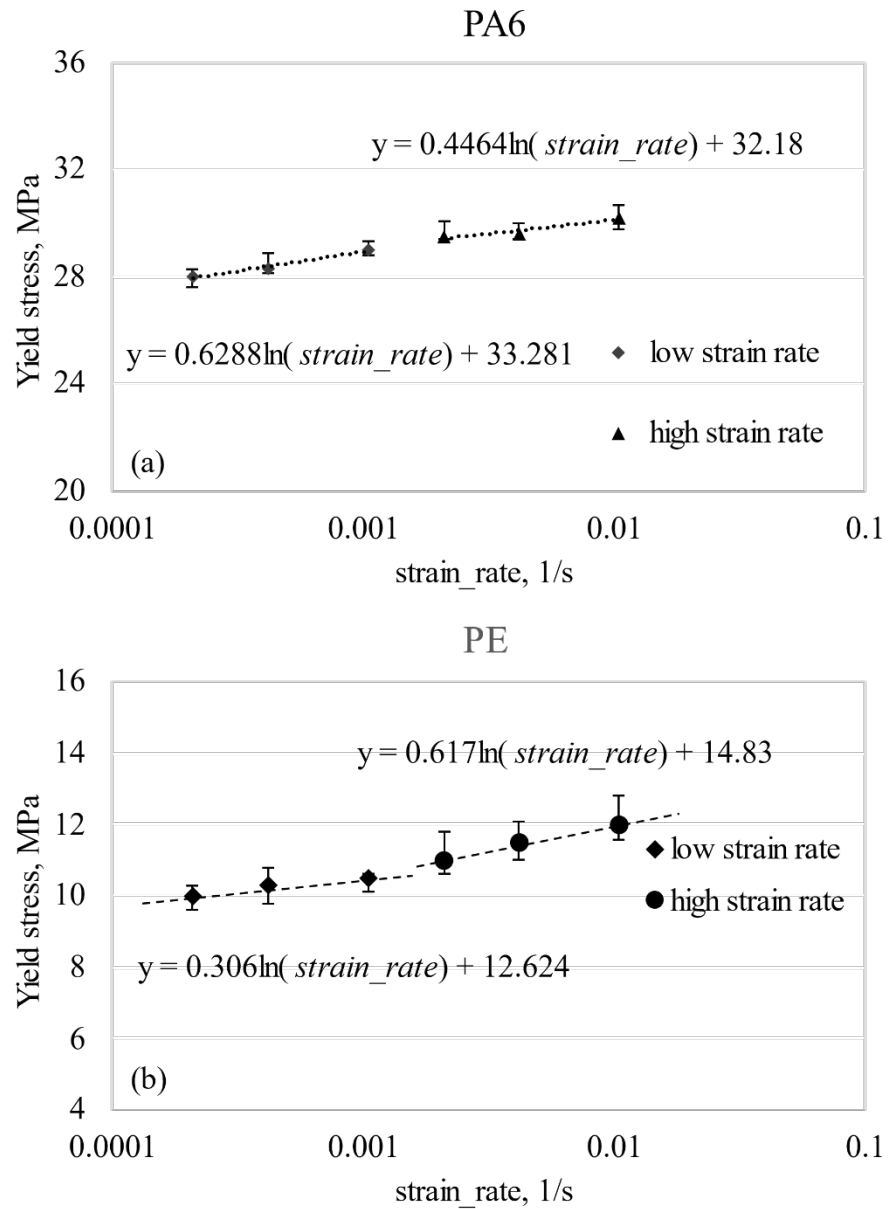


Figure 3-9. Yield stress as a function of strain rate (a). PA6 (b). PE

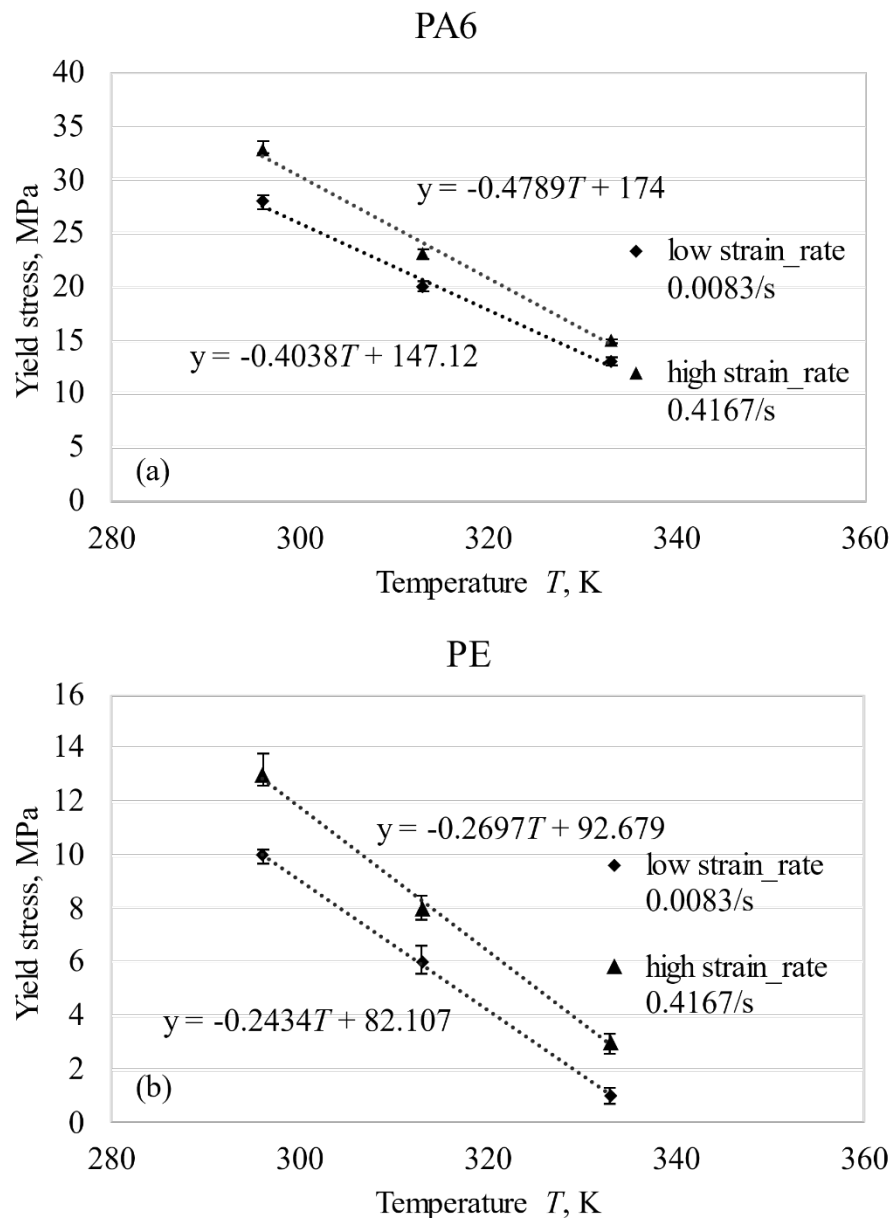


Figure 3-10. Yield stress as a function of temperature (a). PA6 (b). PE

In this study, the lowest temperature $T_r = 296\text{K}$ and strain rate $\dot{\epsilon}_r = 0.0083/\text{s}$ was assigned as the reference values. Therefore, value A can be obtained from **Figure 3-9**.

At the reference temperature and strain rate, Eq. (3-3) simplifies as:

$$\sigma = (A + B\varepsilon^n) \text{ or } \sigma - A = B\varepsilon^n \quad (3-5)$$

Taking natural logarithm from each sides of the latter equation gives:

$$\ln(\sigma - A) = \ln B + n \ln \varepsilon \quad (3-6)$$

Therefore, value B and n can be determined from **Figure 3-11**.

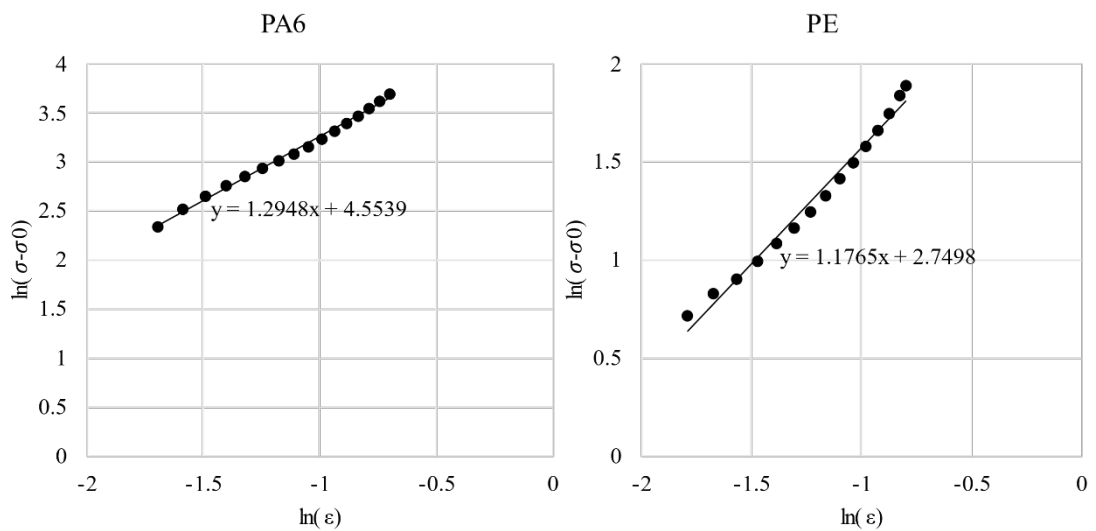


Figure 3-11. The plots used to determine value B and n

At the reference temperature, Eq. (3-3) can also be simplified as:

$$\sigma = (A + B\varepsilon^n) (1 + C \ln(\dot{\varepsilon}/\dot{\varepsilon}_r))$$

$$\rightarrow \sigma / (A + B\varepsilon^n) = 1 + C \ln(\dot{\varepsilon}/\dot{\varepsilon}_r)$$

Therefore, the slope of the plot of $\sigma / (\sigma_0 + B\varepsilon^n)$ and $\ln \dot{\varepsilon}/\dot{\varepsilon}_r$ at constant strain 0.1-0.3 at various strain rates gives the value of C as shown in **Figure 3-12**.

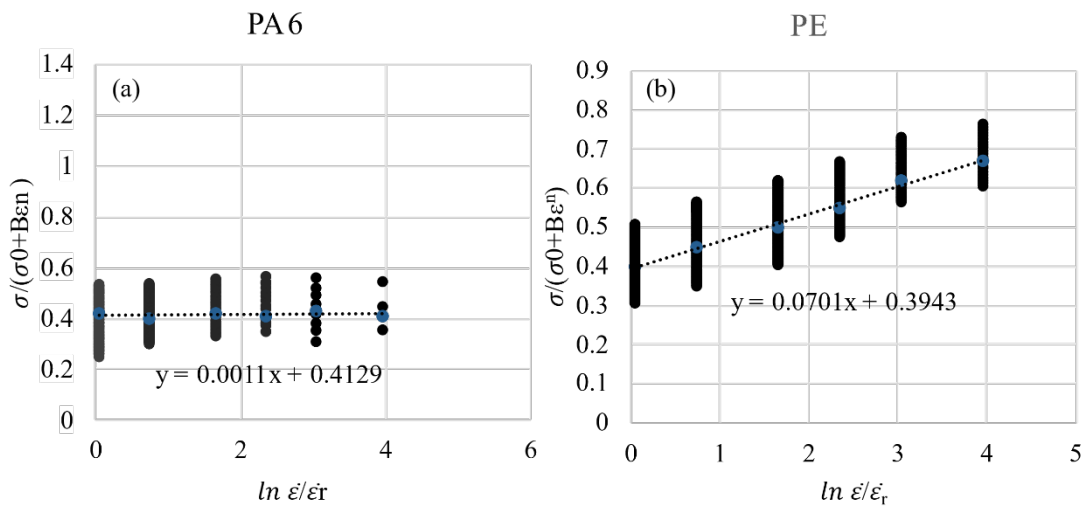


Figure 3-12. The plots used to determine value C

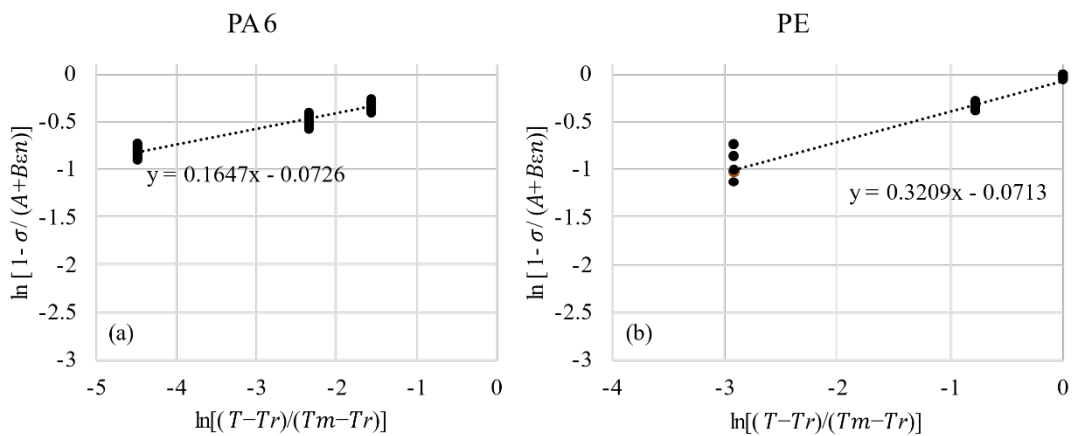


Figure 3-13. The plots used to determine value m

At the reference strain rate, Eq. (3-3) can also be simplified as:

$$\sigma = (A + B\varepsilon^n) \left(1 - \frac{T - T_r}{T_m - T_r}^m\right)$$

$$\rightarrow \frac{T - T_r}{T_m - T_r}^m = 1 - \sigma / (A + B\varepsilon^n)$$

Taking natural logarithm from both sides of this equation gives:

$$\ln [1- \sigma/ (A + B\varepsilon^n)]=m\ln\left[\frac{T-T_r}{T_m-T_r}\right]$$

Therefore, the slope of the plot of $\ln [1- \sigma/ (A + B\varepsilon^n)]$ and $\left[\frac{T-T_r}{T_m-T_r}\right]$ in **Figure 3-13** at constant strain 0.1-0.3 and various temperatures give the value of m .

As a result, a list of Johnson-Cook parameters of PA6 and PE was determined as shown in **Table 3-4**.

Table 3-4. List of Johnson-Cook parameters.

Parameter	PA6	PE	PC
$A, [Mpa]$	28.2	10.1	80
$B, [Mpa]$	94.6	15.6	75
$C, [-]$	0.001	0.07	0.052
$m, [-]$	0.16	0.32	0.548
$n, [-]$	1.29	1.18	0.9
$T_m, [K]$	473	333	562
$\rho, [kg/mm^3]$	1.73e-6	0.95e-6	1.2e-6

3.3.2 Friction coefficient test

From a literature review of the previous study [3.9-3.10], it is found that, in plastic processing, the rise of temperature obviously influences the coefficient of friction of the material. Namely, the friction coefficient of some polymers (Polycaprolactam, Polyethylene) increased with the rise of temperature. While this value decreased in polytetrafluoroethylene (PTFE). These previous studies also show that the friction coefficient of polymers gradually increased above the glass transition temperature point. Therefore, to obtain the effect of temperature on the friction

coefficient of the blade and nylon-polyethylene sheet, the friction test at various temperatures was investigated. **Figure 3-14** shows the schematic of the friction test system. Here, to apply the heat in the polyethylene sheet and steel plate, a rubber heater was set up and controlled by a thermal controller. A thermocouple mounted in the polyethylene surface to measure the real contacting temperature between nylon-polyethylene sheet and steel plate surface. The tests were performed with a sliding velocity of 5mm/min for 10mm sliding distance, and temperatures between 296K–333K. These tests were made in dry condition (no lubrication) at an environmental humidity of 50%. Two cases of the contact surface were investigated as indicated in **Table 3-5**.

Table 3-5. Testing conditions

Case No.	plane material	worksheet material
1	Steel	PA6
2	PC	PE

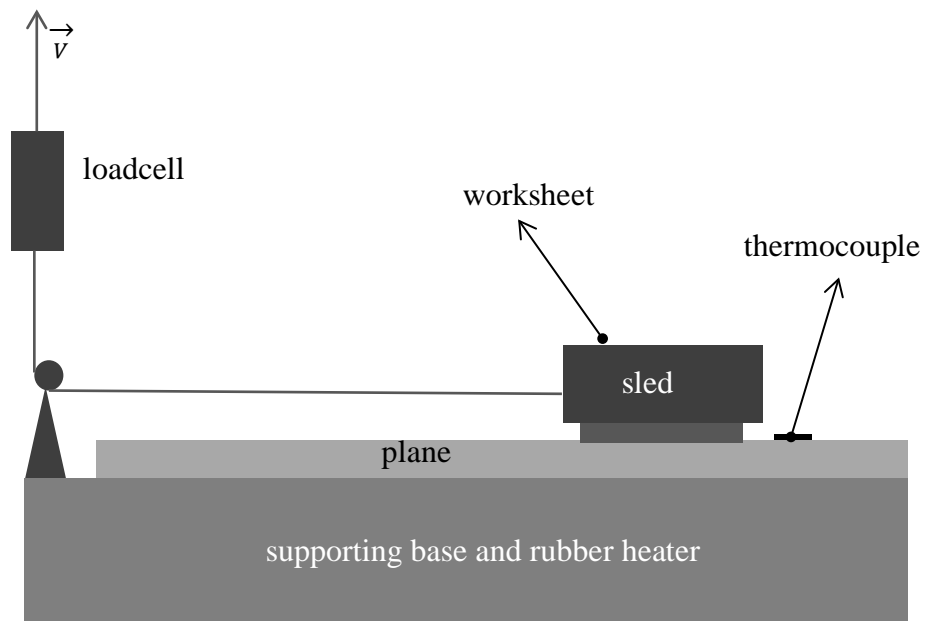


Figure 3-14. Friction coefficient testing system at various temperature

As a result, the friction coefficient of contacting surface between the cutting blade and upper PA6 surface; lower PE surface and PC counter plate were explained in Table 3-6. Here, friction coefficient of PA6 against steel has risen 9% when the contacting temperature changed from 296K to 333K. While this value is calculated at 15% for PE against PC. The obtained values of friction coefficients will be used to define in the FEM model that will be explained in section 3.3.3.

Table 3-6. Effects of temperature on the friction coefficient of polymers (Average, max-min of 5 times)

Contact type	μ ($T = 296\text{K}$)	μ ($T = 313\text{K}$)	μ ($T = 333\text{K}$)
PA6 against Steel	0.54 (0.53-0.55)	0.56 (0.54-0.57)	0.59 (0.58-0.60)
PE against PC	0.23	0.26 (0.24-0.27)	0.30 (0.29-0.31)

3.3.3 Finite element analysis

3.3.3.1 FEM condition

In order to simulate the effect of temperature on the cutting deformation of the nylon laminated structure, a FEM code, MSC MARC 2015.0.0, was used. **Figure 3-15** shows a half symmetric cutting simulation model that had the same dimension as the experimental system with respect to the effect of temperature. In the finite element model, a plane strain model with 4280 elements was used to define the initial mesh of the laminated workpiece. The blade was assumed to be a rigid body while the nylon film and underlayer were assumed to be isotropic elastoplastic deformation bodies. Glue contact function was used to define the contact between PA6 layer and PE layer. To discuss the effect of temperature on the nylon film subjected to wedge indentation process, mechanical properties of the worksheet, underlayer and simulation conditions were defined as shown in

Table 3-7 and **Table 3-8**, respectively. Moreover, the Johnson-Cook material parameters used in the simulation are presented in **Table 3-4**. List of Johnson-Cook parameters. Here, the properties of PA6 and PE were obtained from the experiment, which was explained in the previous section. Meanwhile, the Johnson-Cook parameters of PC counter plate were calculated by A. Dwivedi et al [3.9] as shown in the right column of this **Table 3-4**.

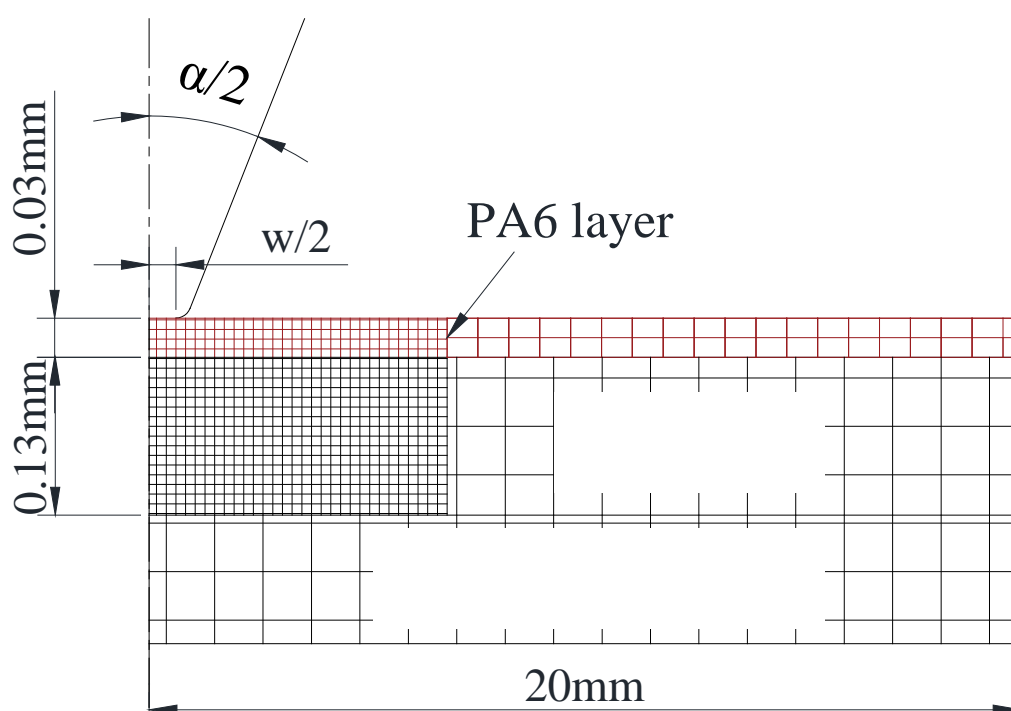


Figure 3-15. A half symmetric cutting simulation model

During the downward process of the cutting blade, there was a largely deformed near the blade tip; the simulation calculation could not continuous due to crushing of the element. To overcome the poor mesh, an automatic remeshing function (2D solid: Advancing Front Quad) was used in the FEM simulation. There is not any damage model was considered in this study.

Table 3-7. Mechanical properties of polycarbonate underlay and nylon film.

Material	Thickness t/mm	Young modulus E/MPa	Yield stress σ_Y/MPa
PC	1	2650	55
PA6	0.03	1995	28.2
PE	0.13	185	10.1

Table 3-8. FEM conditions.

Blade tip angle/ degree	$\alpha = 42^\circ$
Blade tip thickness/ μm	$w = 5 \mu\text{m}$
Cutting velocity/ $\text{mm}.\text{min}^{-1}$	$V = 5 \text{ mm/min}$

3.3.3.2 Simulation results and discussions

In order to discuss the effect of temperature on the nylon film subjected to wedge indentation process, a normal side PA6-PE cutting direction was investigated. Here, the cutting blade was applied at various temperatures $T = 296\text{K}$, 318K and 333K . Meanwhile, the nylon film was initially assumed at the room temperature ($T = 296\text{K}$). In this model, thermal contact between cutting blade and the worksheet was defined by interface heat transfer coefficient at approximately $4700 \text{ W}/(\text{m}^2.\text{K})$ [3.11]. To comparing the heat conduction from the blade to the worksheet between the experiment and simulation, temperature of point Q was measured and compared in **Figure 3-16**. Here, point Q is the position of thermocouple in the worksheet surface, which is placed at 2mm off-set from the cutting line to avoid the damage from the cutting blade. From this figure, it is found that the transferred temperature in the experiment is slightly less than in the simulation. This small mismatching seems to be caused by the heat transfer

from the worksheet surface to the air in the experimental investigation. On the other hand, in this simulation model, the heat transfer to the air has not been investigated. From this result, it can reveal the matching between the experiment and simulation in heat conduction from the cutting blade to the worksheet. Therefore, this simulation is suitable to predict the heat transition in the experiment.

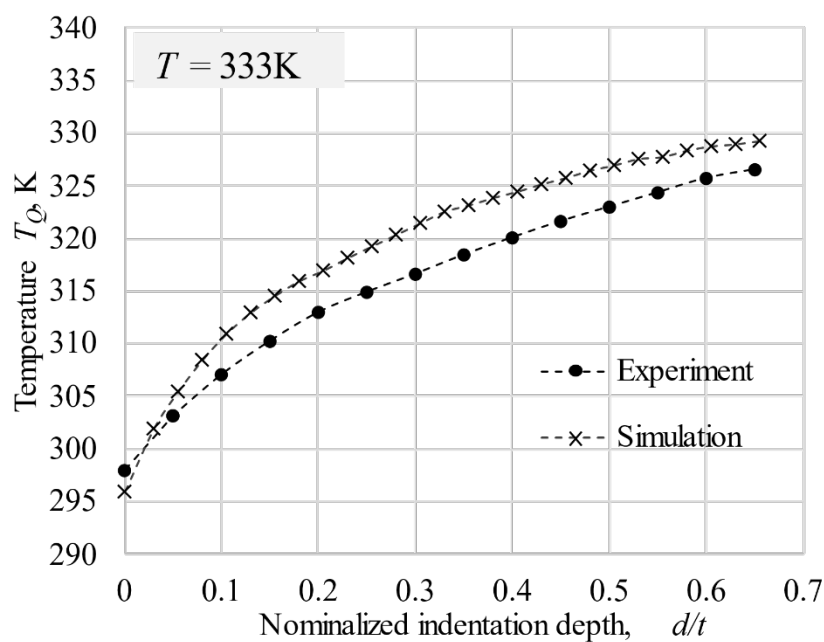


Figure 3-16. Comparison temperature at point Q of the worksheet between experiment and simulation

Seeing **Figure 3-16** and **Figure 3-16 (a)**, it is also found that the temperature at point Q was smaller than in applied temperature in the cutting blade ($T = 333\text{K}$) in both experiment and simulation. However, seeing **Figure 3-17 (b)**, the temperature of the worksheet body beneath the cutting blade was almost similar to the applied temperature in the cutting blade. Therefore, the heat transfer was sufficient to make a change in the PA6, PE material properties.

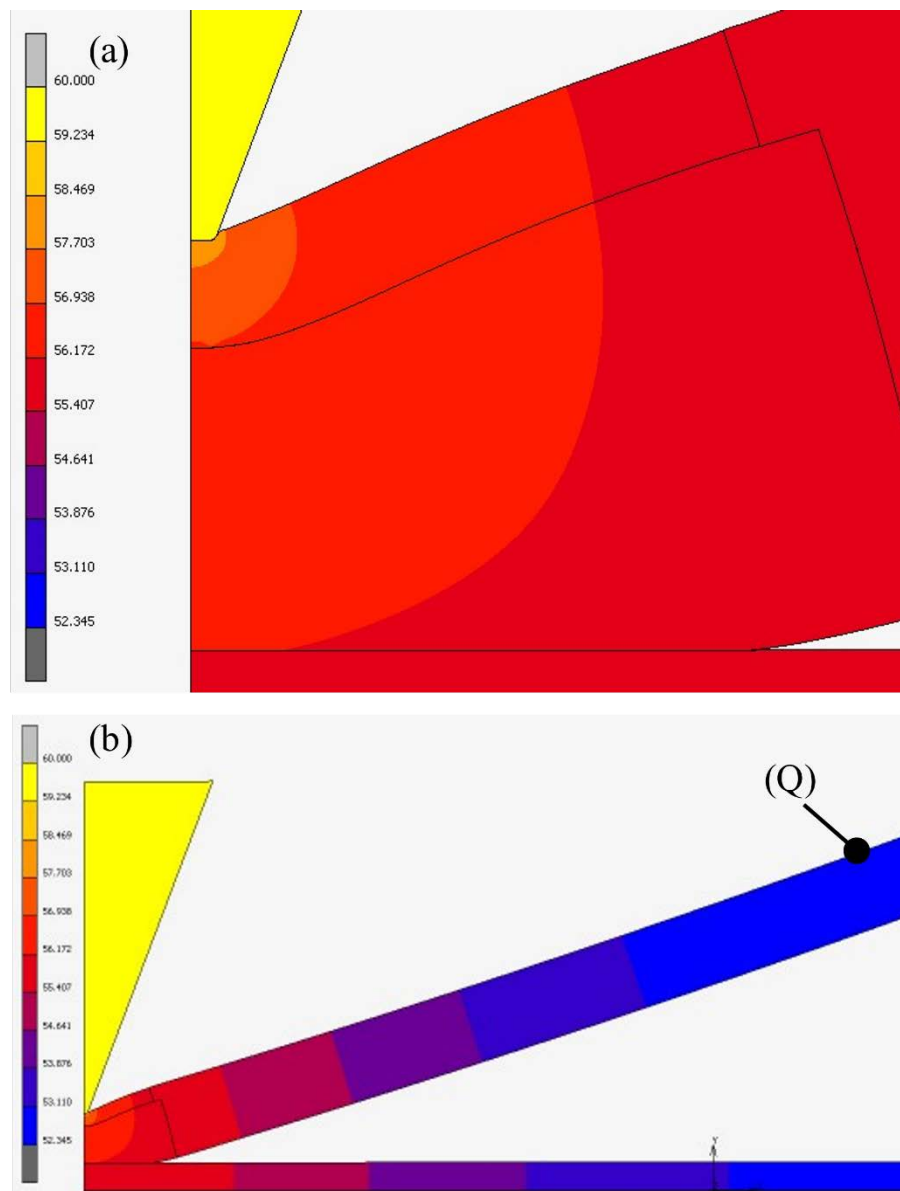


Figure 3-17. Contour plot of the temperature at $d/t = 0.3$ when the blade is applied $T = 333\text{K}$.

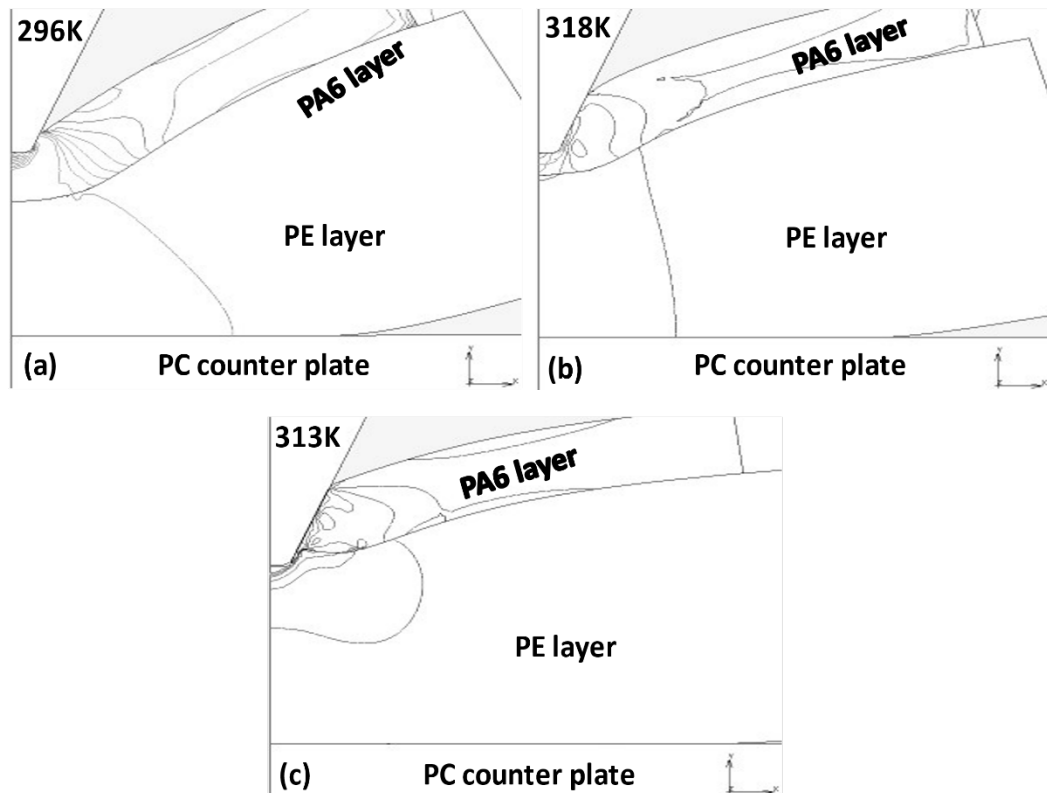


Figure 3-18. Deformation profile of the worksheet on the FEM simulation at $d/t = 0.45$ with respect to various temperature of the blade (a) $T = 296\text{K}$, (b) $T = 318\text{K}$, (c) $T = 333\text{K}$

Figure 3-18 shows the deformation profile of the laminated wedged worksheet with the tip thickness $w/t = 0.13$ at the normalized indentation depth of $d/t = 0.45$ at $T = 296\text{K}$, $T=318\text{K}$, $T=333\text{K}$ respectively. From the compressive test of PA6 and PE at room temperature as shown in

Table 3-7, Young's modulus of PA6 was estimated to be approximately 1995 MPa, and its value was significantly large in comparison to 185 MPa of PE. Due to this significant difference, the PE lower layer was remarkably deformed, and the blade was generally pushed to the worksheet. This tendency was almost similar to cut off a soft worksheet to a hard underlay [3.12]. Meanwhile, when a 318K of temperature was initially applied to blade, the PA6 and PE yield stress was significantly decreased. As a

result, the PA6 layer was in large deform as shown in **Figure 3-18 (b)** and totally separated at $d/t = 0.67$ as shown in **Figure 3-19(b)**.

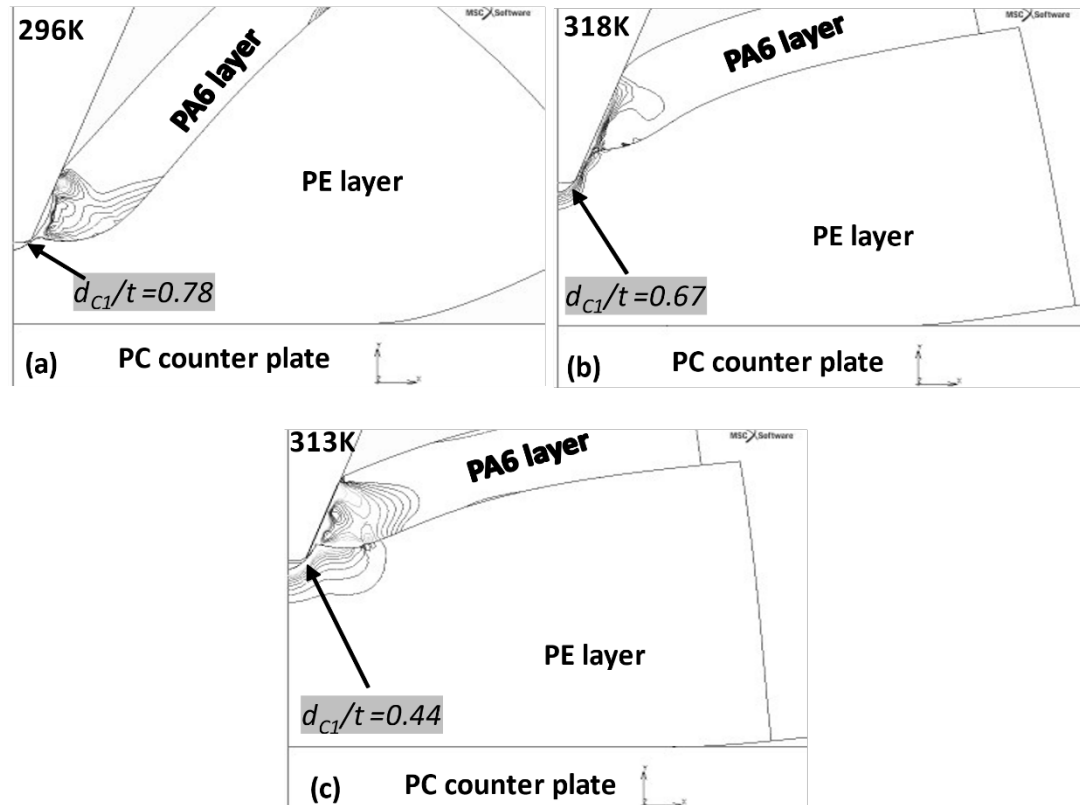


Figure 3-19. Deformation profile of the worksheet when the 1st peak of cutting load (f_{C1}) with respect to various temperature of the blade (a) $T = 296K$, (b) $T = 318K$, (c) $T = 333K$

Figure 3-20 shows the relationship between the cutting line force f and the indentation displacement d/t with varying temperatures. The peak of cutting line force was indicated (f_{C1} , d_{C1}/t), where f_{C1} was the line force; d_{C1} was the corresponding indentation depths of the blade at two peaks of load. It was found that the cutting line force remarkably decreased when increasing the temperature of the blade. At room temperature ($T = 296K$), the blade was indented to the worksheet with high pressure when using the crushed tip blade. On the contrary, in cases of $T = 318K$, the cutting line force tended to be decreased and the PA6 layer was totally separated at $d/t = 0.67$. When

the high temperature was up to 333K as shown in **Figure 3-19(b)**, f_{CI} continued to considerably decrease and the PA6 was almost cut off at the normalized indentation depth of $d/t = 0.44$. However, at $T = 333K$, the PE layer was reached the heat deflection temperature and the plastic flow phenomenon was observed with an unsuccessful cutting mode as described in the previous section.

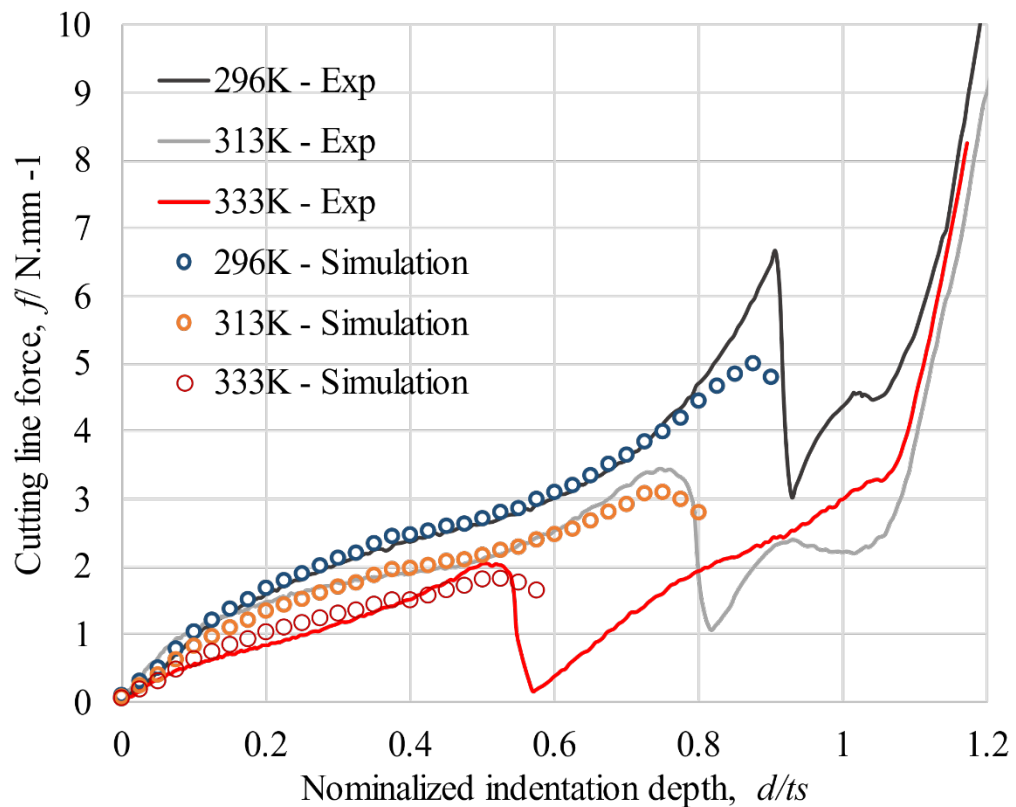


Figure 3-20. Cutting load response with respect to cutting temperature

Comparing **Figure 3-20** with **Figure 3-4**, the simulated cutting load response of the nylon film shows good agreement with experimental result. However, there was not any damage model has been investigated in this model. Therefore, this model was not successfully simulated the breaking behavior of PA6 layer and the second peak of load as the experiment results.

3.4 Summary

In this study, the cutting characteristics of 0.16mm nylon film subjected to a wedged indentation were investigated experimentally and numerically. By varying the cutting temperature of blade body T , features on the cutting resistance and profile deformation mode were revealed as follows:

- i. The cutting deformation and cutting force of the laminated PA6/PE film was remarkably changed. It was found that the temperature elevation of blade body significantly affected the temperature of PA6/PE film under the specified cutting velocity, and then the temperature elevation of PA6/PE film reduced the first load peak also changed the cutting profile of PA6/PE film. There was an appropriate range of the temperature of a blade body, a case of $T = 318\text{K}$ against a room temperature 296K was suitable for cutting the 0.16mm PA6/PE film off during wedge indentation.
- ii. An FEM model also was conducted to reveal the effect of temperature in the deformation of the PA6/PE film. The effect of temperature, velocity was defined by Johnson-Cook parameters that was obtained from series of experiment as various temperature and strain rate. From the simulation results, the simulated cutting load response of the nylon film shows good agreement with experimental result.

References

- [3.1] Nagasawa S, Sato H, Yamaguchi D, et al. Effect of tip clearance and blade hardness on cutting resistance and tip shape in paper board die cutting. J Jpn Soc Technol Plastic. 2006;42(480):38–42.
- [3.2] Nagasawa S, Sekikawa H, Murayama D, et al. Effect of initial tip profile on crushing of center bevelled cutter-numerical analysis of crushing tip indented on paperboard. J Jpn Soc Technol Plastic. 2004;45(524):747–751.

- [3.3] Chaijit S, Nagasawa S, Fukuzawa Y, et al. Effect of tip profile on cutting processability of a trapezoidal cutting blade indented to an aluminum sheet. *J Mech Mater Struct.* 2006;1 (8):1301–1321.
- [3.4] Nagae, S., Endurance characteristics of die tools on pushing shear of paperboard, in *Mechanical Engineering.* 2006, Nagaoka University of Technology.
- [3.5] Nagae, S., S. Nagasawa, Y. Fukuzawa, A. Hine, and I. Katayama, "Effects of Quenching Hardness on Cutting Resistance and Crushing of Blade Tip Indented on Paperboard". *Journal of Japan Society for Technology of Plasticity*, 2004. Vol.45(524): pp. 742-746.
- [3.6] Cornelia V, Mihaela P. *Practical guide to polyethylene.* Smithers Rapra Technology; 2005. Grzesik, W., Niesłony, P., & Laskowski, P. (2017).
- [3.7] Determination of Material Constitutive Laws for Inconel 718 Superalloy Under Different Strain Rates and Working Temperatures. *Journal of Materials Engineering and Performance*, 26(12), 5705–5714.
- [3.8] Mirzadeh, H. (2015). Constitutive modeling and prediction of hot deformation flow stress under dynamic recrystallization conditions. *Mechanics of Materials*, 85, 66–79.
- [3.9] A. Dwivedi, J. Bradley, D. Casem Mechanical response of polycarbonate with strength model fits, *Army Research Laboratory* (2012)
- [3.10] Dawson, A., Rides, M., Allen, C. R. G., & Urquhart, J. M. (2008). Polymer–mould interface heat transfer coefficient measurements for polymer processing. *Polymer Testing*, 27(5), 555–565.
- [3.11] S. Chaijit, S. Nagasawa, Y. Fukuzawa, D. Murayama, A. Hine, Effect of Underlay Rigidity on Cutting Characteristic of Aluminum Foil during Wedge Shearing Process, *Journal of Advanced Mechanical Design, Systems, and Manufacturing*, vol.2, no 4, 2008, pp.800-811

Chapter 4 :

**THERMAL CUTTING AND EQUIVALENCY OF VELOCITY IN
CUTTING CHARACTERISTICS OF ACRYLIC WORKSHEET**

In this chapter, deformation behaviour and cracking patterns of an acrylic worksheet during the wedge indentation process were investigated under varying the mechanical conditions such as the punch/die cutting velocity, cutting temperature. As a result, a suitable cutting tool conditions for making a smart sheared edge of the worksheet was proposed.

4.1 Introduction

Because of many advanced characteristics, for example, low density, visible light, high shattered resistance, good resistance, an acrylic sheet is proposed to be an ideal material for making control panels, advertising boards, dental applications, etc. [4.1-4.4]. To cut a based acrylic sheet into net shape products, a wedged indentation process is one of the attractive cutting methods. Previous researchers have paid a lot of attention to the cutting of ductile metallic sheet materials [4.5] and paper board. Experimentally and numerically studies the effect of crushed tip to the cutting characteristic of white-coated paperboard has been reported recently [4.6-4.7]. From the above literature survey, most researchers have investigated the cutting of ductile sheets due to the stable in cutting profile of its worksheet. On the other hand, acrylic is a fragile material, which has some difficulties for smooth processing. Concretely, the acrylic worksheet appears to be randomly broken by the propagation of several initiated cracks when it is subjected to a wedged indentation and shearing process [4.2, 4.5]. The unexpected cracking seems to be caused by a fragile property of the acrylic worksheet.

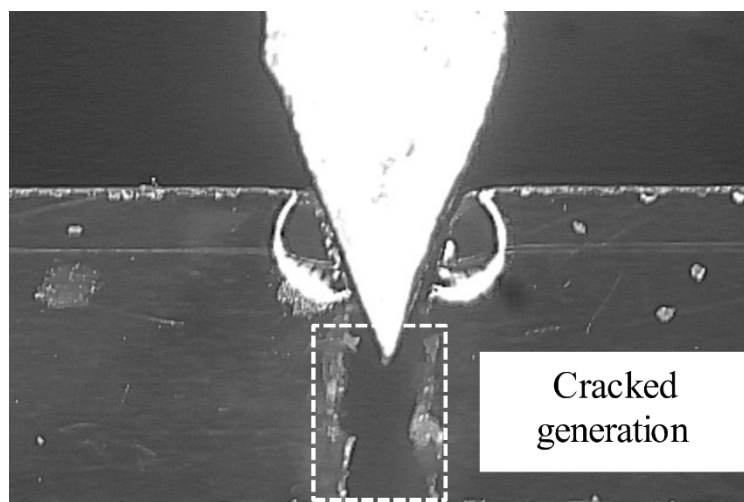


Figure 4-1. Generation of cracks in the worksheet

Figure 4-1 shows an example of cracks generation in an acrylic cutting. In order to enhance the wedge indentation technology for cutting the fragile worksheets, the

cutting characteristics of acrylic sheet must be understood furthermore. In this study, deformation behavior and cracking patterns of an acrylic worksheet during the wedge indentation process were investigated under varying the mechanical conditions such as the cutting velocity, cutting temperature. As a result, a suitable cutting tool conditions for making a smart sheared edge of the worksheet was proposed.

4.2 Experiment method

4.2.1 Experiment conditions and specimens

In order to evaluate the in-plane mechanical properties of the AC worksheet, the uniaxial tensile test (based on JIS-K7127 standard) was carried out. The stress-strain relationship of the AC worksheet at various temperatures, and reference strain rate = 0.002 s^{-1} was shown in **Figure 4-2**, and its mechanical properties were concluded into **Table 4-1**.

Table 4-1. In-plane mechanical properties of acrylic at reference temperature $T=296\text{K}$, strain rate = 0.002 s^{-1}

$t_s = 0.5 \text{ mm}$, strain rate = 0.002 s^{-1}			
Young's modulus E / MPa	Yield strength σ_Y / MPa	Breaking strength σ_B / MPa	Breaking strain ϵ_B
2200	40	47	0.015

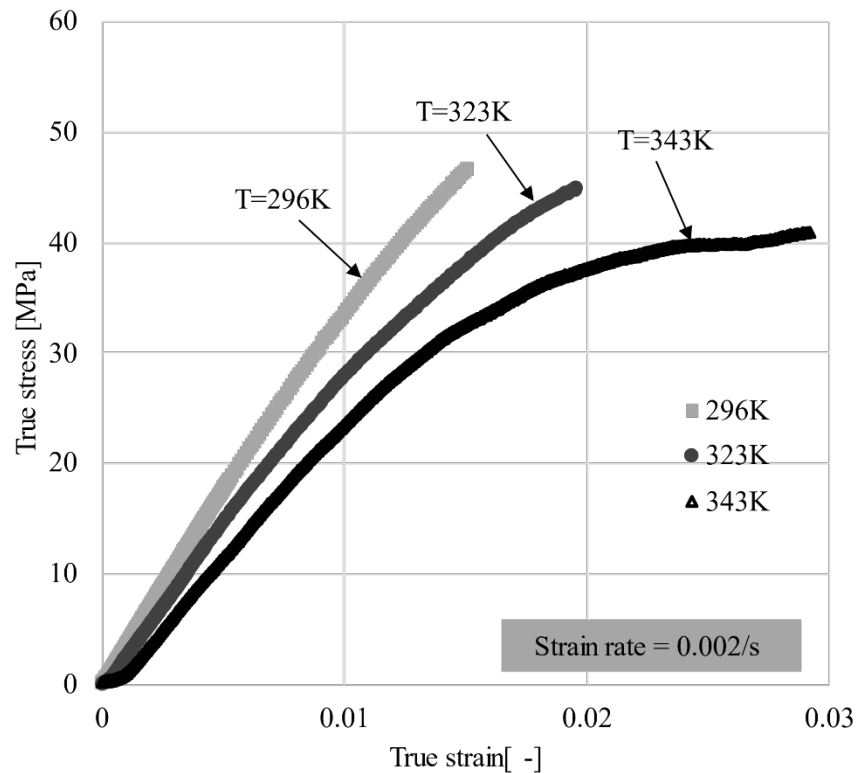


Figure 4-2. True stress- true strain relationship of AC sheet at various temperature with constant strain rate = 0.002 s^{-1}

The effect of temperature and strain rate on the deformation behaviour of AC is presented in **Table 4-2**. Here, JC parameters were calculated as the same method that was explained in the previous chapter.

Table 4-2. AC Johnson-Cook parameters.

Parameter	$A,$ [Mpa]	$B,$ [Mpa]	$C,$ [-]	$m,$ [-]	$n,$ [-]	$T_m,$ [K]	$\rho,$ [kg/mm ³]
AC	53	64	0.049	0.53	0.75	433	9.4e-7

To observe the cutting behaviour of AC sheet, the wedge indentation experiments were carried out as shown in **Figure 4-3**. During the cutting process, the blade was pushed into the AC worksheet by the moveable of the upper crosshead of the

universal testing machine. When the worksheet was completely separated, the upper crosshead was moved upward. For observing side view deformation of worksheet, a high-speed camera was installed with the cutting apparatus.

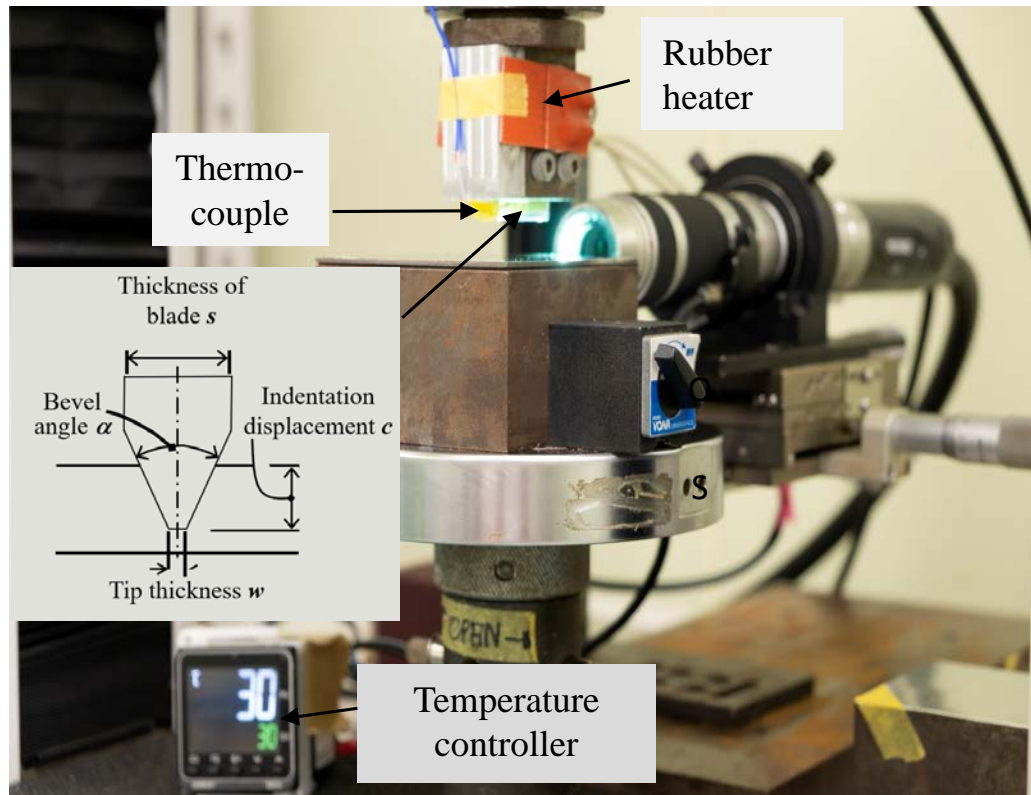


Figure 4-3. Schematic of experiment apparatus

In this thermal cutting system, the rubber heater was mounted in the blade holder to generate heat and transfer it to the worksheet when the cutting blade moved downward and indented into the worksheet. Here, the temperature in the blade was controlled by the left temperature controller in **Figure 4-5 (a)**. Two thermocouples were used. The first thermocouple was mounted in the blade to measure the real temperature at the blade tip (**Figure 4-4 (a)**). The second thermocouple was placed 2 mm off-set from the cutting line to measure the heat transfer from the blade to the worksheet as shown in **Figure 4-4 (b)**. The measured temperature in the worksheet was observed on the right display unit in **Figure 4-5 (a)**.

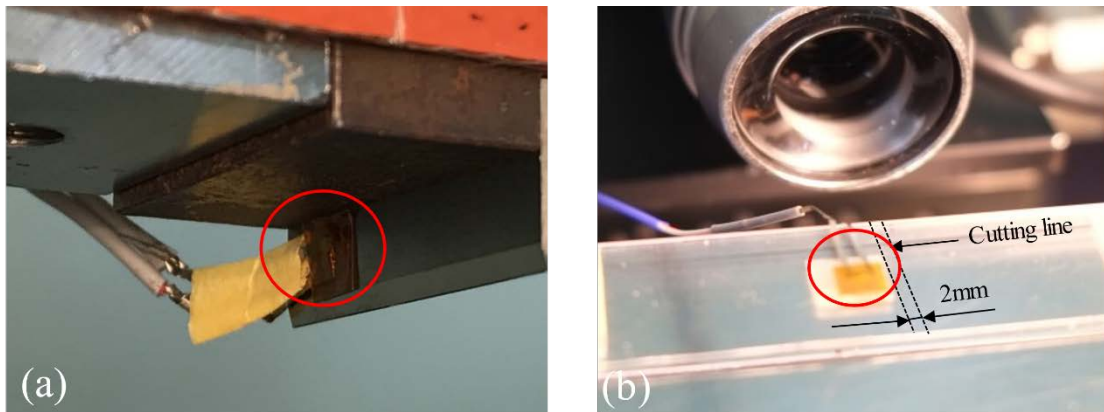


Figure 4-4. Thermal system setting: (a) Thermocouple in the cutting blade and (b) Thermocouple in the worksheet.

In this experimental investigation, an acrylic (AC) rectangle specimen of 20 x 60 mm with thickness $t=0.5$ mm was used. To propose a suitable cutting tool conditions for making a smart sheared edge of the worksheet, a series of cutting tests were conducted on AC worksheet at various temperature and velocity to characterize its mechanical response. First, the experiment was conducted at room temperature ($T=296\text{K}$) and varied the feed velocity at 1, 5 and 25 $\text{mm}\cdot\text{min}^{-1}$. Second, the cutting experiments were kept at a constant velocity $V=25$ $\text{mm}\cdot\text{min}^{-1}$ and varied the cutting temperature $T=296\text{K}$, 323K and 343K. The cutting load resistance and the side-view deformation behaviour of the worksheet were compared and discussed.

4.2.2 Experiment results

4.2.2.1 Cutting load resistance

When the cutting blade indented to the worksheet, the heat was transferred from the blade to the worksheet surface. **Figure 4-5** shows the representative measured temperature in the blade (T_b) and worksheet (T_w) during the blade indentation when a 313K of temperature was set for the cutting blade. When $d/t = -1$ (the blade is above the worksheet surface 0.5mm), T_w was calculated at 298K (25°C). This value was a bit larger than room temperature (296K) due to the heat transfer from the blade to worksheet. After that, the blade was indented to the worksheet when the upper crosshead moved downward to the worksheet. To protect the thermocouple from the cutting tip blade, the

thermocouple was setup a 2mm off-set from the cutting line force. Therefore, the measured temperature was smaller than the real temperature at the cutting line, where the blade contacted the worksheet as shown in **Figure 4-5** (b). As a result, the heat transfer was sufficient to make a change in the worksheet material properties.

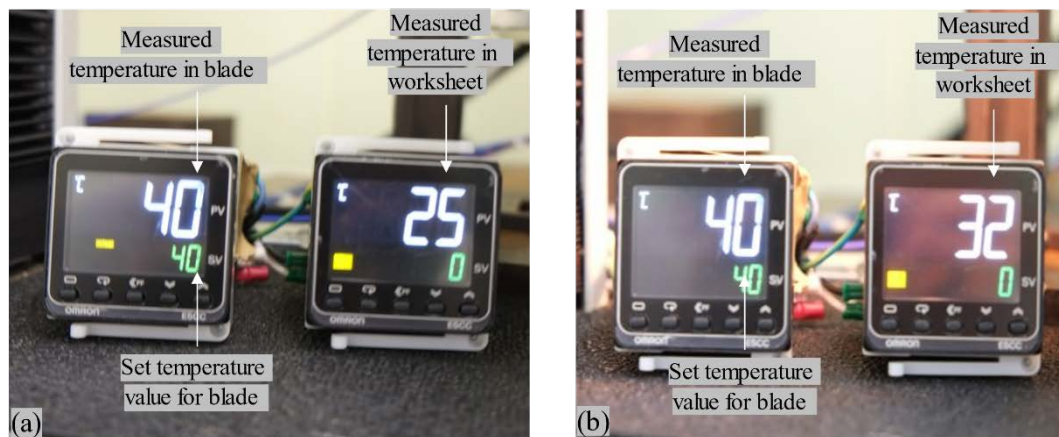


Figure 4-5. Measured temperature in the blade and worksheet when (a) $d/t = -1$ (b) $d/t = 0.5$.

Figure 4-6 and **Figure 4-7** shows the experimental results of the relationship between the line force f and the normalized indentation depth d/t for at various cutting velocity and various temperature, respectively.

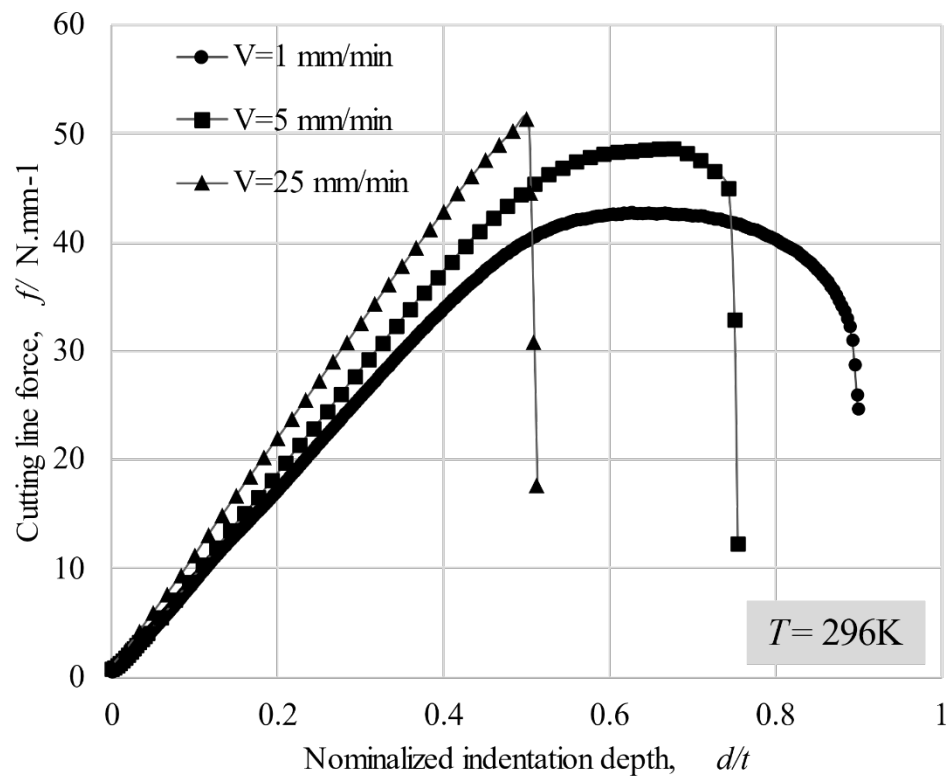


Figure 4-6. Cutting line force at constant temperature $T= 296K$ with various cutting velocity

Seeing **Figure 4-7**, the cutting line force was gradually decreased when the cutting velocity decreased. At low-velocity of $V = 1 \text{ mm}\cdot\text{min}^{-1}$ and $V = 5 \text{ mm}\cdot\text{min}^{-1}$, AC sheet had a plastic deformation before breaking off. Meanwhile, the cutting line fore was approximately linear increased and suddenly breaking off when the force reached a peak. The breaking behaviour is almost similar to the ceramics worksheet subjected to the shearing process due to the brittle behaviour [4.8]. Namely, cracks were generated, and an unstable cutting phenomenon occurred. The relation between the peak of cutting line force F_c and the cutting velocity V is linear approximate as Equation 4-1.

$$f_c = 0.48V + 43.37 \text{ [N]} \quad (4-1)$$

In the second series experiment, the cutting experiments were kept at a constant high velocity of $25 \text{ mm}\cdot\text{min}^{-1}$ and varied the cutting temperature $T= 296K, 323K$ and

343K. Seeing the **Figure 4-7**, it was found that the cutting load response was significantly decreased when we applied the cutting temperature to the cutting plate. This tendency is almost similar to the case of decreasing the cutting velocity. The relation between the peak of cutting line force F_c and the cutting temperature T is linear approximate as Equation 4-2.

$$f_c = 0.3T - 57.13 \text{ [N]} \quad (4-2)$$

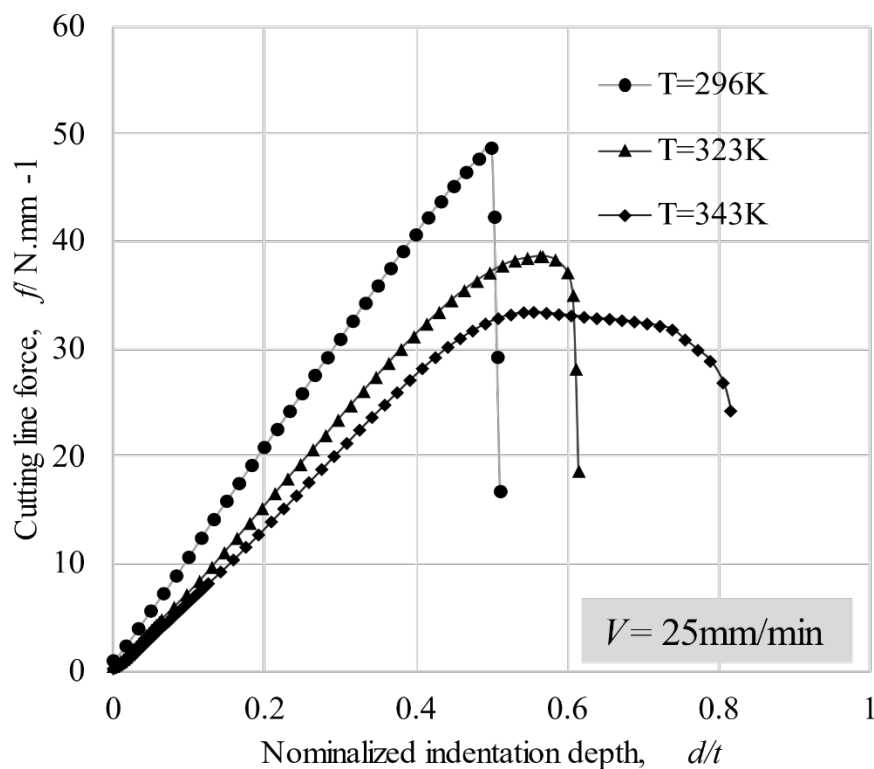


Figure 4-7. Cutting line force at constant high-velocity $V = 25 \text{ mm} \cdot \text{min}^{-1}$ with various cutting temperature

From the equation 4-1 and equation 4-2, a suitable value of T and V for making a smart sheared edge of the worksheet could be obtained.

4.2.2.2 Deformation profile of worksheet

Figure 4-8 and **Figure 4-9** show the representative sheared surfaces with respect to the effect of V and T , respectively. Here, c/t_s is the ratio of cracking length and thickness of the worksheet ($t_s = 0.5\text{mm}$). Comparing values of c/t_s in **Figure 4-8(a)** and **Figure 4-9(c)**, it was found that the crack generation in the AC cutting could be overcome when an optimum value of V and T were applied.

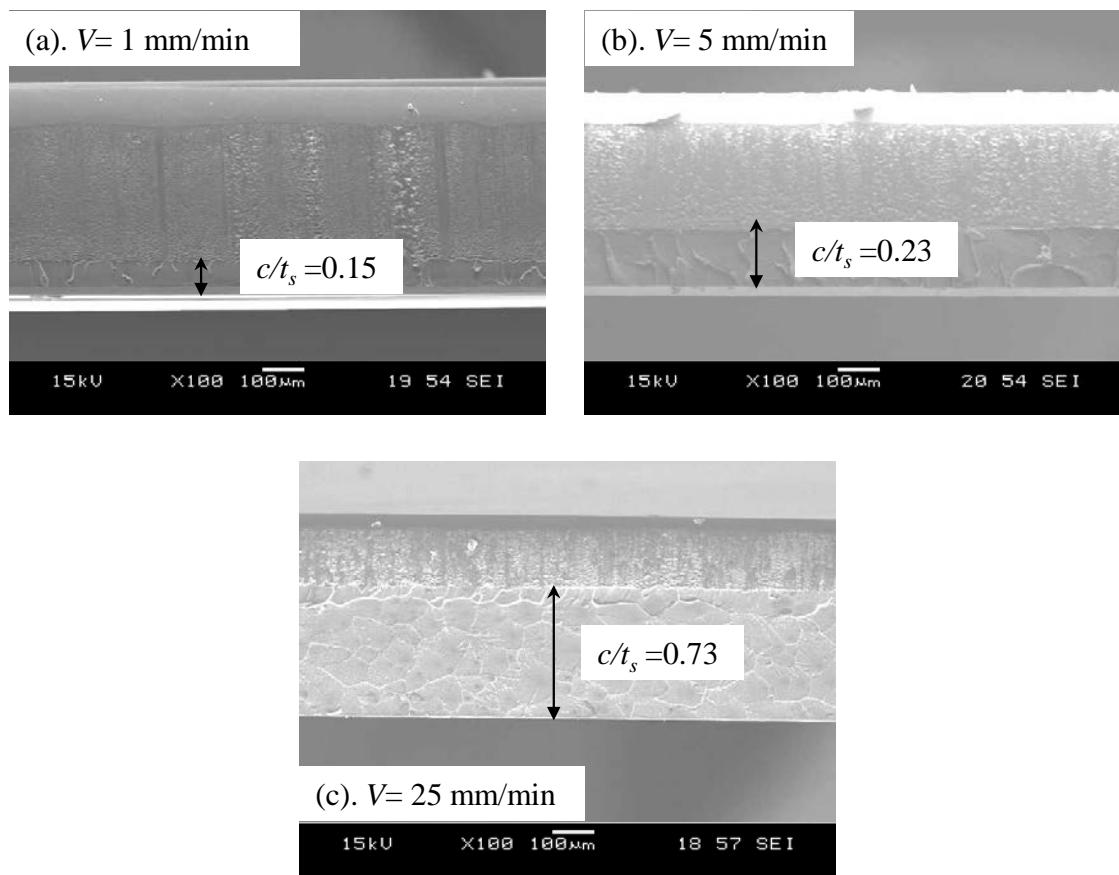


Figure 4-8. CCD side views of sheared AC sheet by varying the velocity

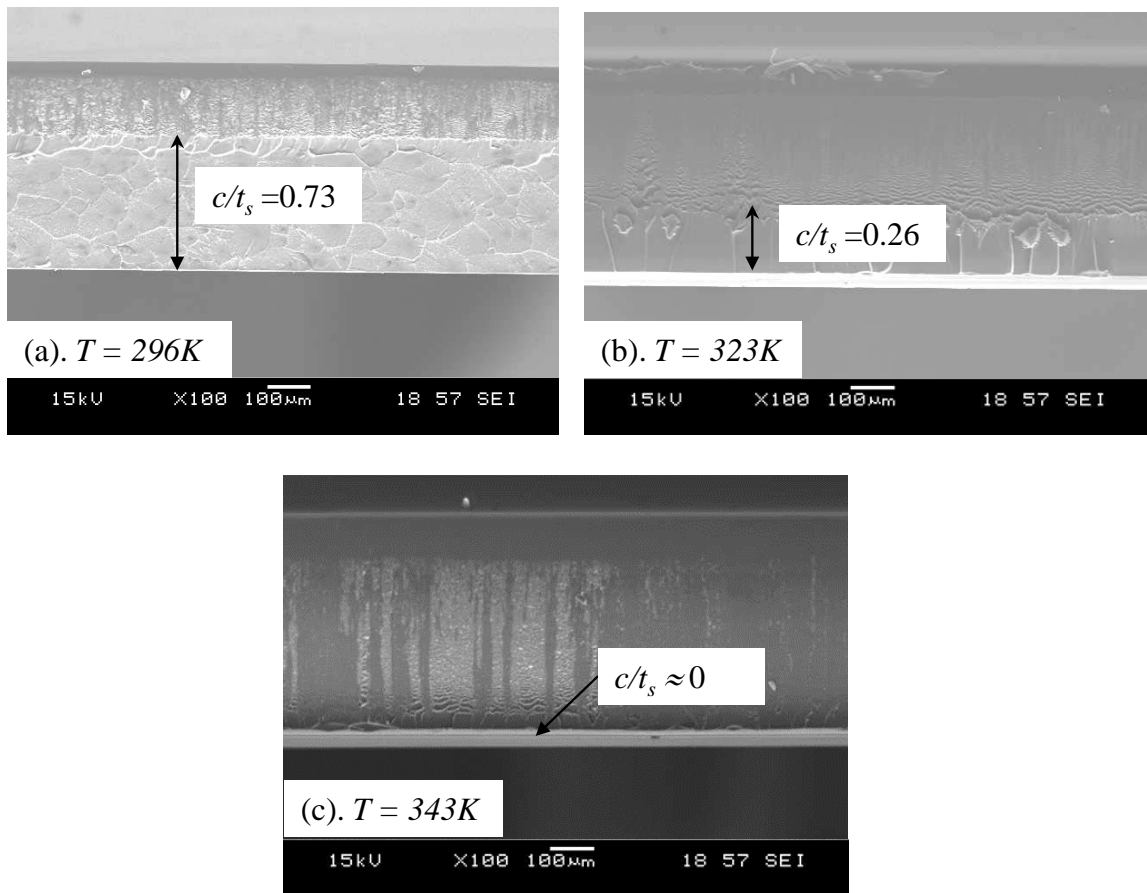


Figure 4-9. CCD side views of sheared AC sheet by varying the temperature

4.4 Summary

In this study, the cutting characteristics of 0.5mm acrylic worksheet subjected to a wedged indentation were investigated experimentally and numerically. By varying the cutting temperature of blade body T and cutting velocity v features on the cutting resistance and profile deformation mode were revealed as follows:

- i. The cutting load response and the deformation profile of the worksheet remarkably depended on the cutting velocity and applied temperature of the cutting blade.

- ii. An appropriate range of the temperature of a blade body and cutting velocity can be optimized to enhance the quality of the sheared surface of the cutting worksheet.

References

- [4.1] Crawford RJ (1999) *Plastics Engineering*, 3 Eds., Burlington: Elsevier Butterworth-Heinemann, 1–40.
- [4.2] Masami Kojima, Pusit Mitsomwang, Shigeru Nagasawa. Effect of cutter tip angle on cutting characteristics of acrylic worksheet subjected to punch/die shearing. *AIMS Materials Science*, 2016, 3(4): 1728-1747.
- [4.3] Al-Rifaiy MQ (2010) The effect of mechanical and chemical polishing techniques on the surface roughness of denture base acrylic resins. *Saudi Dent J* 22: 13–17.
- [4.4] Shimizu H, Tsue F, Chen Z, et al. (2008) Bonding of auto polymerizing acrylic resins to magnetic stainless-steel alloys using metal conditioner. *J Dent* 36: 138–142
- [4.5] Pusit Mitsomwang, et al., An Experimental Behavior of Acrylic Worksheet Subjected to Squared Punch Shearing, *Proc. of the 2012 Japanese spring conference for the technology of plasticity.*, pp.135-136
- [4.6] Nagasawa S, Sato H, Yamaguchi D, et al. Effect of tip clearance and blade hardness on cutting resistance and tip shape in paper board die-cutting. *J Jpn Soc Technol Plastic*. 2006;42(480):38–42.
- [4.7] Nagasawa S, Sekikawa H, Murayama D, et al. Effect of initial tip profile on crushing of center bevelled cutter-numerical analysis of crushing tip indented on paperboard. *J Jpn Soc Technol Plastic*. 2004;45(524):747–751.
- [4.8] Hanh C. Nguyen, Shigeru Nagasawa, Kensei Kaneko. Strength estimation of silicon nitride ceramics using a round-notched specimen subjected to shearing-tool indentation. *AIMS Materials Science*, 2020, 7(5): 518-533.

Chapter 5 :

**PREDICT CRACKING BEHAVIOR OF FRAGILE SHEET USING
IOSIPESCU TYPE SPECIMEN SUBJECTED TO A SHEARING-TOOL
INDENTATION**

The thermal cutting and equivalency of velocity effect on acrylic (AC) wedge cutting was discussed in the previous chapter. It is found that the cracking behaviour in AC cutting was significantly affected by the cutting temperature and velocity. Due to the time-delay of crack propagation from initiation, the cracking behaviour in AC worksheet is unstable in FEM simulation. Therefore, in the first stage of study, an Iosipescu specimen, which has a rounded-notch on the top, is proposed for analysing a stable cracking in fragile material. In this model, a VCCT model is applied to simulate a shearing process for investigating breaking behaviour of ceramics and AC workpiece subjected to a shearing-tool indentation. This proposed model can be developed and apply to simulate the AC cutting in wedge indentation process.

5.1 Introduction

From the literature survey, there are some researchers have demonstrated through the experiments and simulations for modelling of crack propagation of ductile sheet materials, and its breaking behaviour [5.1-5.6]. However, the breaking behaviour of ductile workpiece seems to be different from that of brittle workpieces. Crack initiation and propagation appeared to be broken randomly due to the fragile property of the brittle materials [5.7]. There are many fine cracks seem to occur on the deformed surface pressed by a tool [5.8]. Therefore, it is limited to predict its deformation and cracking behaviour due to the randomly broken of fragile material. Previous researchers have just only investigated the deformation and stress distribution of the deformable body. There are almost not any research works which clarified a cracking behaviour of a fragile workpiece. In order to promote the suitable technology for cutting the fragile materials and also to briefly estimate the breaking strength of that materials, the cracking behaviour of sintered Si₃N₄ workpiece and acrylic must be understood. Therefore, from the aspects of easy measuring of the strength of brittle ceramics, a notched specimen seems to be convenient for making a stable breakage, and a shearing test using Iosipescu specimen [5.9-5.10] is easy to make a shearing state at the notched zone without any gripping failure.

In this work, the VCCT model was applied to simulate a shearing process for investigating breaking behaviour of Si₃N₄ and AC workpiece subjected to a shearing-tool indentation. By considering the appropriate resistance of crack propagation from the pre-cracked bending test, a propagation behaviour of initial surface crack was numerically detected and compared with the shearing experiment of Si₃N₄ and AC workpieces.

In this study, so far, the shear strength of two types of sintered silicon nitride (Si₃N₄) plate [5.11] was estimated using a round-notched specimen subjected to shearing-tool indentation. Although the Iosipescu specimen, which has a symmetric pair of round-edges on the top and bottom side, is more convenient for analysing a pure

shearing state, to make a pair of round-edges at the just same position on the upper and lower part in a specimen is empirically difficult, especially for machining brittle ceramics. Therefore, a shearing test of one side-notched specimen was proposed here to estimate the shear strength. In this case, a CO₂ laser-assisted diamond cutting wheel abrasion was used for making a round-edge on the upper side of a Si₃N₄ specimen. Also, a finite element method (FEM) analysis was conducted in order to further discuss about the resistance of crack propagation in ceramics and acrylic workpiece subjected to a shearing-tool indentation.

5.2 Strength estimation of silicon nitride ceramics using a round-notched specimen

5.2.1 Materials and experiments

5.2.1.1 Materials

This study was performed by using two types of commercial silicon nitride (Si₃N₄), SNP02 and SNP03 (made by Japan Fine Ceramics Co.,Ltd.). SNP02 was a sintered reaction bonded silicon nitride (SRBSN) while SNP03 was prepared via gas-pressure sintering of silicon nitride (SSN) method. Both of SNP02 and SNP03 had the same hardness at 15 GPa which was conducted by Vickers hardness test based on JIS R 1601 standard test method.

Silicon nitride (Si₃N₄) is a brittle material at the ambient temperature since the yielding is very small [5.12-5.13]. To detect the mechanical properties of Si₃N₄ workpiece, a non-destructive test method based on ASTM E 494 – 15, was investigated. In this test method, an ultrasonic pulse generator and sensors plus an oscilloscope was used to measure the sound velocity. **Figure 5-1** indicates a schematic of the ultrasonic testing system. Young's modulus E and Poisson's ratio ν of a ceramics specimens were calculated from the longitudinal wave velocity v_l , transversal wave velocity v_s and density ρ using Eqs. (5-1, 5-2) [5.14-5.15]. and its mechanical properties were concluded into **Table.5-1**. It was found that SNP03 had slightly low stiffness compared

with that of SNP02. The Young's modulus of SNP03 was almost similar to that of Si₃N₄ which was estimated in [5.16].

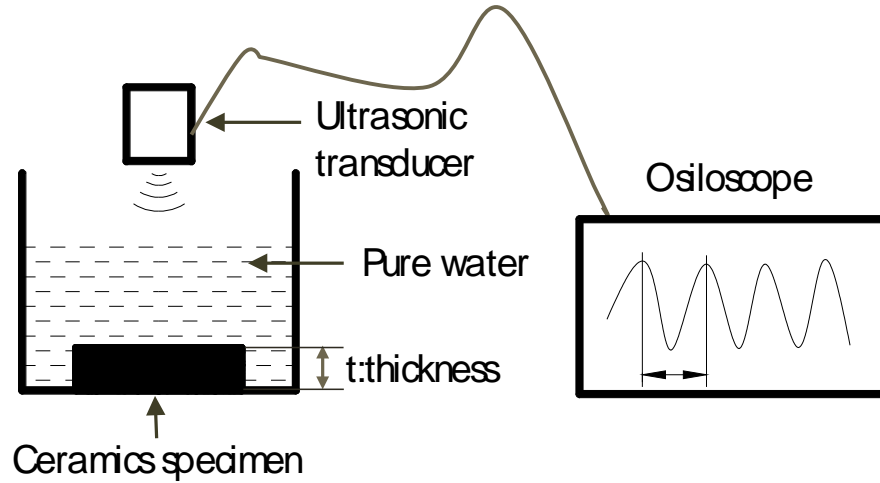


Figure 5-1. Ultrasonic testing system.

$$\nu = \left[1 - 2(v_s / v_l)^2 \right] / 2 \left[1 - (v_s / v_l)^2 \right] \quad (5-1)$$

Table 5-1. Mechanical properties of Si₃N₄ workpiece.

Physical parameters		SNP02	SNP03
Density, ρ	[kg/m ³]	3200	3200
Poisson ratio, ν	[-]	0.29	0.3
Young's modu. E	[MPa]	271	297
Vickers hardness. H_v	[VHN]	1500	1500
Str. Intensive.fac. K_I	[MPa.m ^{1/2}]	6	7
Critical enr. rel. rate G_C	[N/m]	19	21

$$E = \left[\rho v_s^2 (3v_l^2 - 4v_s^2) \right] / (v_l^2 - v_s^2) \quad (5-2)$$

There are many test methods to detect the fracture toughness of ceramics, including chevron-notched beam test, surface crack in flexure method and pre-cracked beam method. In this study, pre-cracked beam test (ASTM C 1421-10), which is easy to prepare the straight through pre-crack, was used. Crack intensive factor of two types

of silicon nitride was calculated from the fracture force, the measured pre-crack length and the specimen size. The critical value of energy release rate G_C is calculated from Young's modulus, Poison's ratio and stress intensive factor K_I shown as Eq. (5-3) [5.17]. The calculated stress intensive factor K and energy release rate G_C is shown in the last two rows of **Table 5-1**. These calculated stress intensive factors were nearly similar to that of Si_3N_4 reported in [5.16]. However, these values were quite larger than 5.3 [$\text{MPa}\cdot\text{m}^{1/2}$] of Kadin et al's estimation [5.18]. Microstructure and manufacturing conditions seem to be reasons leading the difference between these kinds of ceramics.

$$G_C = \frac{K_I^2(1-\nu^2)}{E} \quad (5-3)$$

5.2.1.2 Experiment procedure of shearing

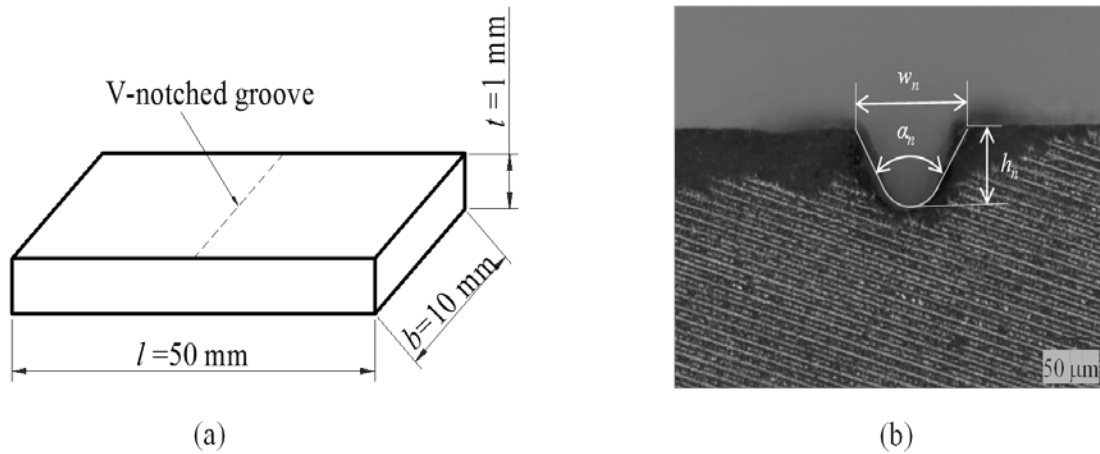


Figure 5-2. Size of specimen. (a). General view of workpiece, (b). Zoomed up view of profile of the notch.

Specimens of SNP02, SNP03 were prepared as a rectangle shape which had a thickness of $t = 1 \pm 0.01 \text{ mm}$, a length l of $50 \pm 0.05 \text{ mm}$ and a width b of $10 \pm 0.04 \text{ mm}$, using a diamond abrasive cutting wheel. A CO_2 laser machine (HAJIME CL1 PLUS) was used under a specific condition: 30W power laser was scanned 7 times with a velocity of $1 \text{ mm}\cdot\text{s}^{-1}$ to heat the surface of specimen and also the diamond abrasive machine was used for making a V-notched groove on the specimen. A single line V-

sharp was generated as the following profile parameters: $w_n = h_n = 0.15 \pm 0.01 \text{ mm}$ and $\alpha_n = 63^\circ$. Machined notch has surface roughness Ra of $0.417\text{-}0.439 \mu\text{m}$, which was observed by laser microscope (**Figure 5-3**). Various dimensions of a workpiece and round-notched groove are shown in **Figure 5-2**. All specimens were sufficiently washed with alcohol and naturally dried in a room with a temperature of $296 \text{ K} \pm 1 \text{ K}$ and a humidity of $50\% \pm 1\% \text{ RH}$ for approximately 24 hours before the shear test.

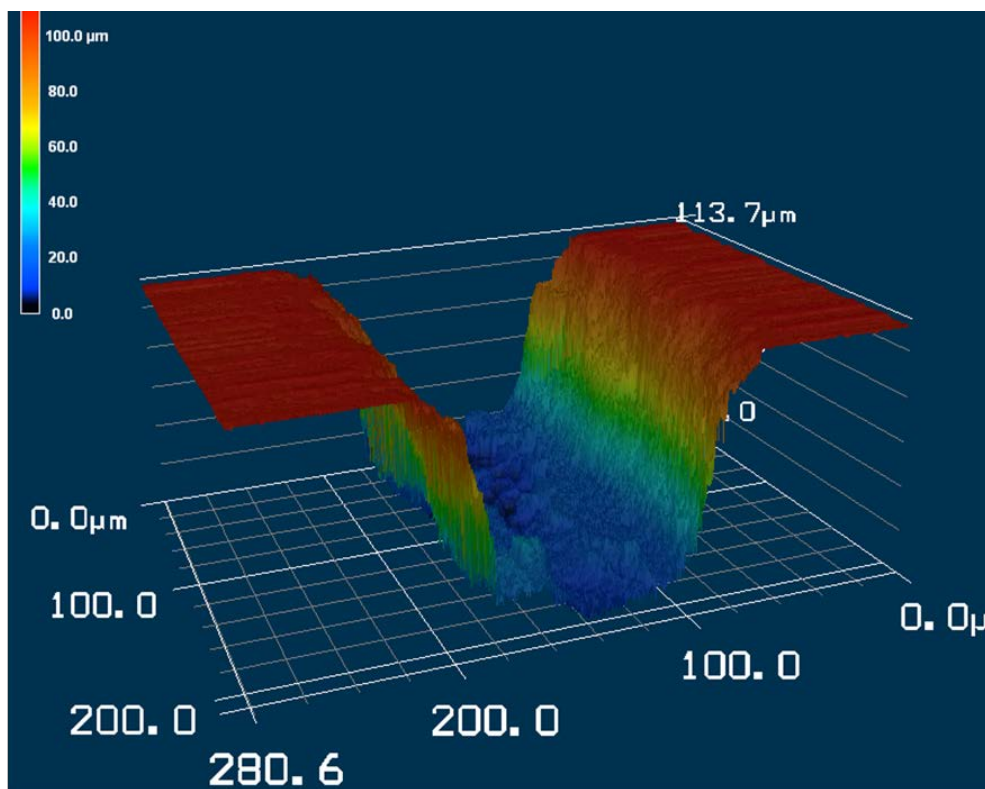


Figure 5-3. Notch surface was observed in lazer-mocroscope

Figure 5-4 indicates a schematic of the experimental-press machine apparatus in configuration with a ceramics specimen. The shearing die set contains four main components: punch, dies, blank holders and counter punch. These parts were made of SKD11 steel (cold-work steel) which had a hardness of $58 \sim 60 \text{ HRC}$. In this shearing apparatus, the right blank holder and the right die, indicated by the dashed lines in **Figure 5-4**, were not used (the specimen was not put in this area). The clearance ratio between punch and die c/t was empirically chosen as 0.15, which was equal to a ratio

of the width of the V-notch w_n by the thickness t . A force of blank holder (counter punch) and their displacement are controlled by the back-up springs with the stiffness of 5.0 and 4.5 N.mm⁻¹, respectively.

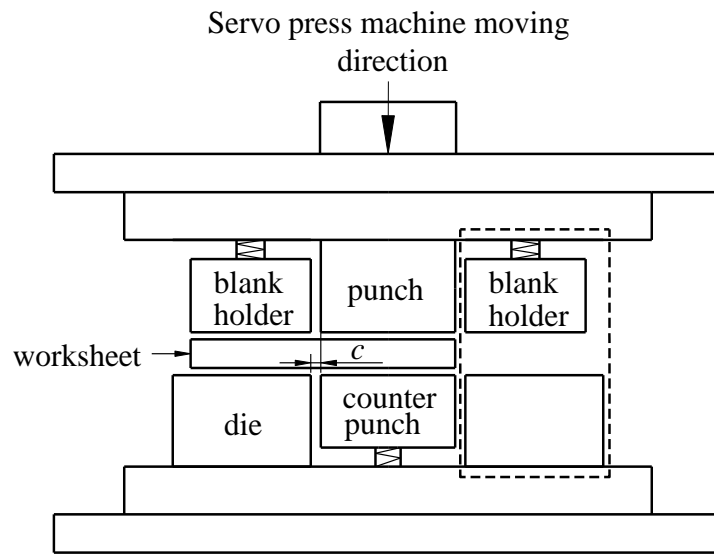


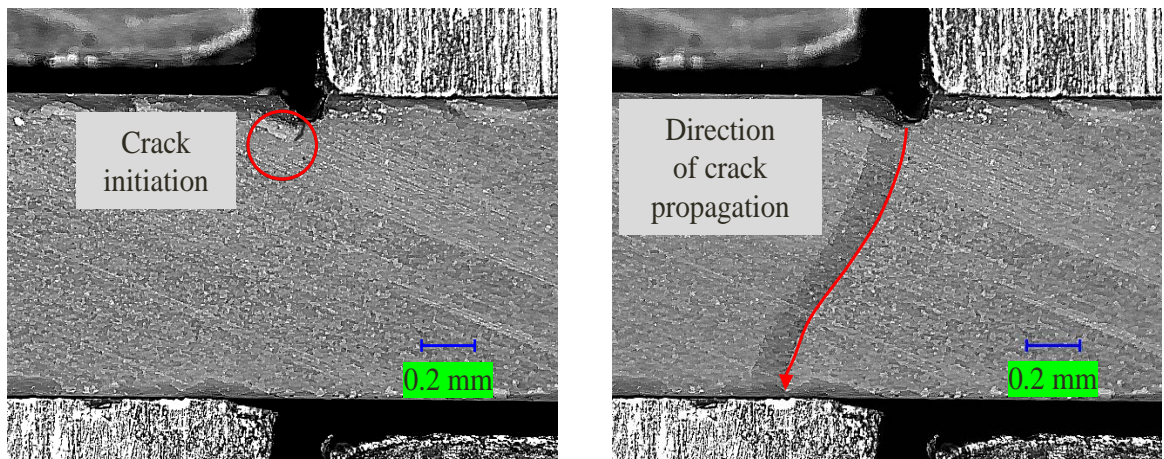
Figure 5-4. Schematic of shearing experiment

These shearing tests were performed on a digital servo-press machine (CYA-3-10, SINTOKOGIO) at the temperature of 296 K and humidity of 50%RH in a controlled room. Here, the downward speed of crosshead(punch) was chosen as 5mm.min⁻¹. During the shearing test, the punching force F N and the displacement of the punch d mm were recorded. To observe the cracking propagation and the side-view of the specimen, a high-speed camera was installed. To evaluate the shear strength of brittle material, typically for ceramics, a significant number of specimens have to be prepared in order to obtain a reliable value. In this experiment, the shearing test was conducted with five specimens for each condition.

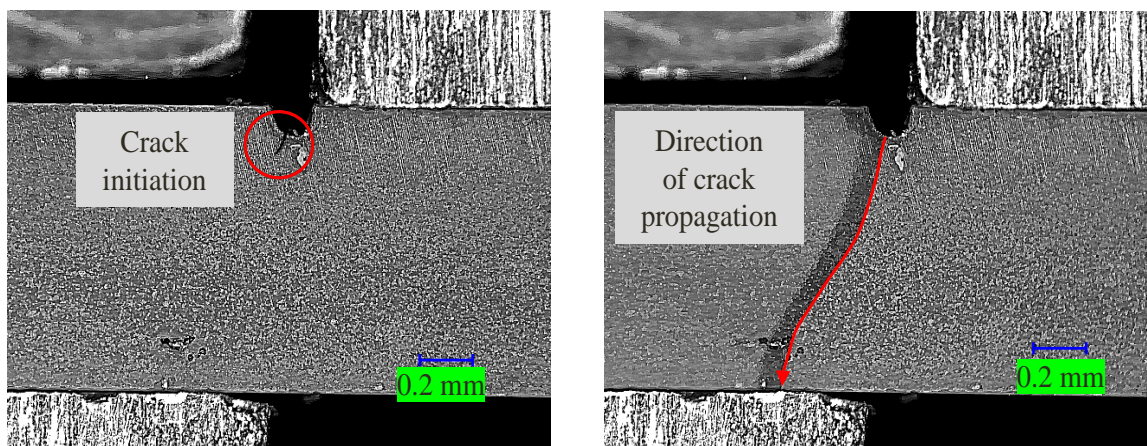
5.2.1.3 Experimental results and discussions

In this experiment, a high-speed camera was used to record the cracking behaviour during the punch indentation. **Figure 5-5(a)** and **(b)** shows the result of cracking behaviour for SNP02 and SNP03 respectively. These cracking propagations

were so fast and catch up by high-speed camera of 1000 frames per second. In two cases, crack initials start at the grooved notch and rapidly to separate into two parts. It was found that the initial crack did not locate at the middle of the notch but occurred at the side face of the notch.



(a). SNP02, at a pre-cracked state $d/t_s=0.021$, and at a crack propagated state $d/t_s=0.023$



(b). SNP03, at a pre-cracked state $d/t_s=0.023$, and at a crack propagated state $d/t_s=0.025$

Figure 5-5. Here, the thickness of plate was $t_s=1$ mm, the feed velocity of punch was $V=5\text{mm}\cdot\text{min}^{-1}$.

The shear strength was defined and calculated by dividing the maximum load by the cross-sectional area of the specimen as shown in Eq (5-4).

$$\tau_{\max} = \frac{F_{\max}}{w \cdot b} \quad (5-4)$$

Here, F_{\max} is the maximum load, $w = 1 - 0.15 = 0.85\text{mm}$ is the distance from notch to lower surface of the workpiece, and $b = 10\text{mm}$ is the width of the workpiece.

Figure 5-6 shows the comparison of load-displacement responses with two types SNP02, SNP03 of Si_3N_4 ceramics. From the load response curves, it was found that SNP02 and SNP03 were brittle elastic behaviour up to the fracture point. The average ultimate failure load and shear strength outcome as **Table 5-2**. The shear strength of SNP02 was approximately 16% higher than that of SNP03, although they had the same chemical structure of Si_3N_4 .

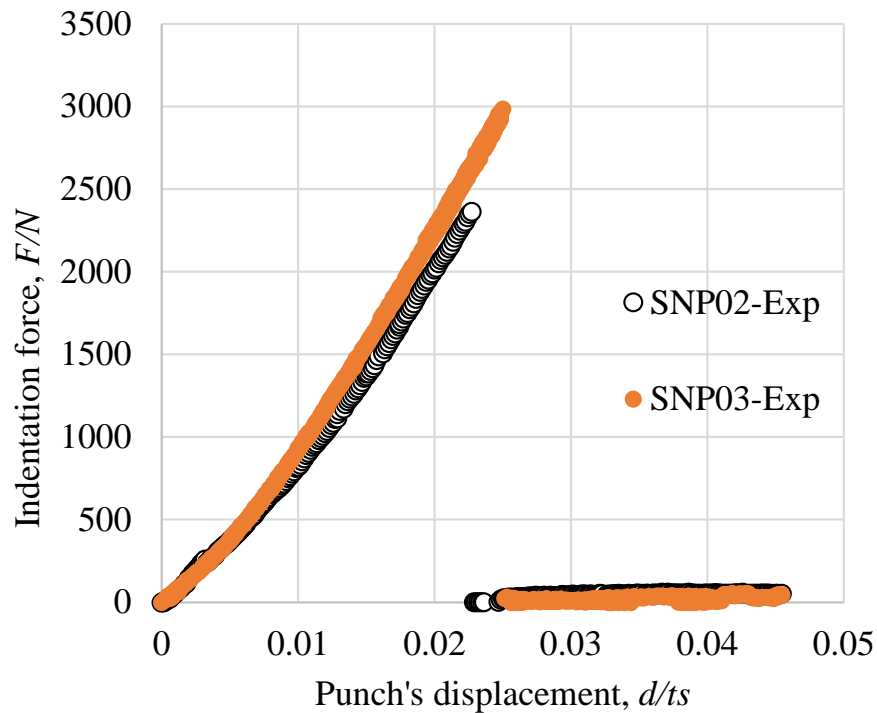


Figure 5-6. Load – displacement response. Here, the thickness was $t_s = 1\text{ mm}$, the feed velocity was $V = 5\text{mm}\cdot\text{min}^{-1}$

Table 5-2. Shear strength of Si₃N₄ workpieces (Average, max-min of 3 samples).

Material code	Ultimate failure load, N	Shear strength, MPa
Si ₃ N ₄ -SNP02	2364 (2250-2760)	278
Si ₃ N ₄ -SNP03	3021 (2750-3270)	355

The surface grinding of two types of Si₃N₄ ceramics was performed using a ML-150P grinding machine in two processes. A coarse polishing was used a grinding wheel with diamond grains of 30 μm. After that, a fine polished surface was performed with diamond particles slurry of 2 μm. After grinding the surface of specimen of SNP02 and SNP03, a scanning electron microscopy SEM (Jeol JSM 6400) was used to observe the surface of these specimens.

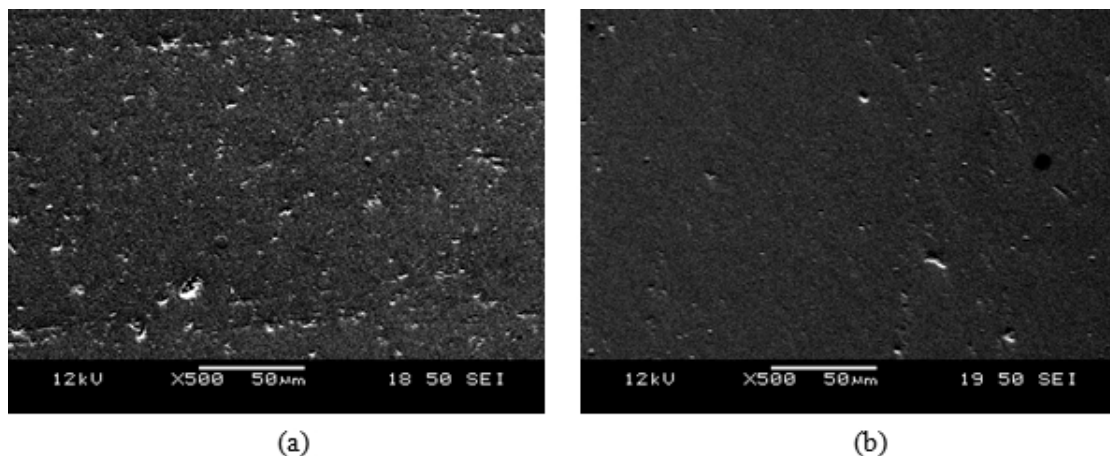


Figure 5-7. Scanning electron microscopy image two type of Si₃N₄ (a). SNP02 and (b). SNP03

In **Figure 5-7**, there were many imperfections including point defects and impurities in the SNP02 in comparison with the SNP03. Synthetically, it was found that a good microstructure (less point defects) contributed to perform the higher shear strength of Si₃N₄ ceramics.

5.2.2 Simulation of cracked behavior

5.2.2.1 Principle of vcct cracking model

Many researchers succeeded to predict an initiated fracture of ductile material in a shearing process [5.1-5.3]. The initiation of fracture was predicted by an integral formulation of Eq. 5-5 [5.2] which reached to a critical threshold value C during the shearing process:

$$\int_0^{\bar{\varepsilon}_p} f(\sigma_m, \bar{\sigma}) d\bar{\varepsilon}_p = C \quad (5-5)$$

Here, $f(\sigma_m, \bar{\sigma})$ is a certain kind of functional form with arguments, and $\bar{\sigma}, \sigma_m, \bar{\varepsilon}_p$ are the Mises equivalent stress, the pressure (average of three normal stresses) and the equivalent plastic strain, respectively. This critical value C was empirically determined from an experimental tensile test. However, the failure behavior of brittle material is apparently different from that of ductile workpiece subjected to a shearing load. In a case of notched brittle material subjected to a shearing load, the critical release energy rate G_C is normally considered to discuss the crack propagation. In this work, the virtual cracking closer technique (VCCT) model based on the Griffith's theory was used to predict the cracking resistance of brittle material [5.19-5.22]. In this theory, there are three modes of cracking propagation: the tensile (mode I), the shearing (mode II) and the tearing (mode III). As for the crack opening and propagation, the total energy release rate of these modes must be equal to the required energy for creating a new surface.

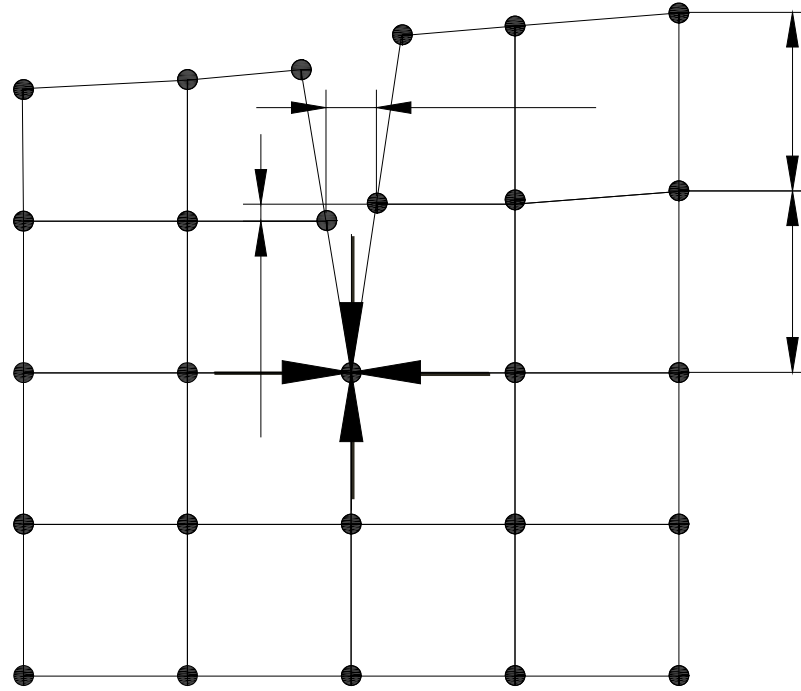


Figure 5-8. Meshed node patterns for explaining the VCCT model

A basic equilibrium of this process was expressed by Eq. (5-6). Here, G_T was the total energy release rate and G_C was the critical release energy rate, which was evaluated from a 3-points bending test of pre-cracked beam.

$$G_T = G_C \quad (5-6)$$

In a case of two-dimensional deformation as the plane strain, the mode III is negligible, and then the total strain energy release rate as a sum of the mode I and the mode II, G_I plus G_{II} , defined as Eq. (5-7) is expressed with a crack length Δa , a shear displacement Δu_k and an opening displacement Δw_k , as shown in Eq. (5-8) [5.4-5.6]. Here, Δa is measured from a node point l to a node point i ; Z_i and X_i are an opening force and a shear force at the crack tip (node point i). Δu_k and Δw_k are calculated from the shear and opening displacement at the node l as shown in **Figure 5-8**.

$$G_T = G_I + G_{II} \quad (5-7)$$

$$G_T = \frac{1}{2\Delta a} \cdot Z_i \cdot \Delta w_k + \frac{1}{2\Delta a} \cdot X_i \cdot \Delta u_k \quad (5-8)$$

In this work, the virtual cracking closer technique (VCCT) was used for investigating the initial cracking and its propagation in a round-notched ceramics specimen using the finite element code MSC. Marc 2015.0.0 (updated Lagrange procedure). **Figure 5-9** shows a two-dimensional shearing FEM model and details of a notched profile. It was constructed as the similar shape with the experimental shearing specimen. The plane strain quadrilateral elements subdivided with 3500 meshes were initially prepared. To focus on the cracking of the workpiece and reduce the calculation time; the punch, dies, counterpunch and strippers were assumed to be rigid bodies, while the workpiece was assumed to be an elastic deformable body.

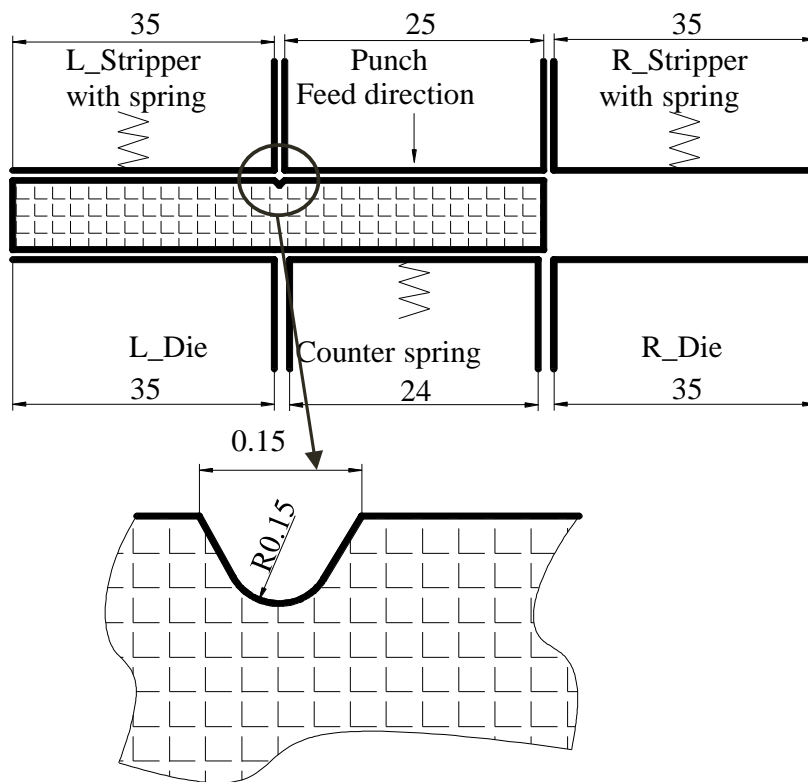


Figure 5-9. A simulation model and notched profile

When discussing the simulation results, the mechanical properties of ceramics were assumed to be same as experimental values described in the section 2.1. The coulomb \tan^{-1} friction model with a relative velocity threshold of 0.01 was considered in this simulation. The friction coefficients of the blank holder and the ceramics: μ_b , the punch and the ceramics: μ_p and the die and the ceramics: μ_d were measured by the friction test based on JIS-K 7125. The results were approximated as $\mu_b = \mu_p = \mu_d = 0.21$.

5.2.2.2 Preliminary simulation for determining the initiation of crack

Preliminary model for detecting the initiation

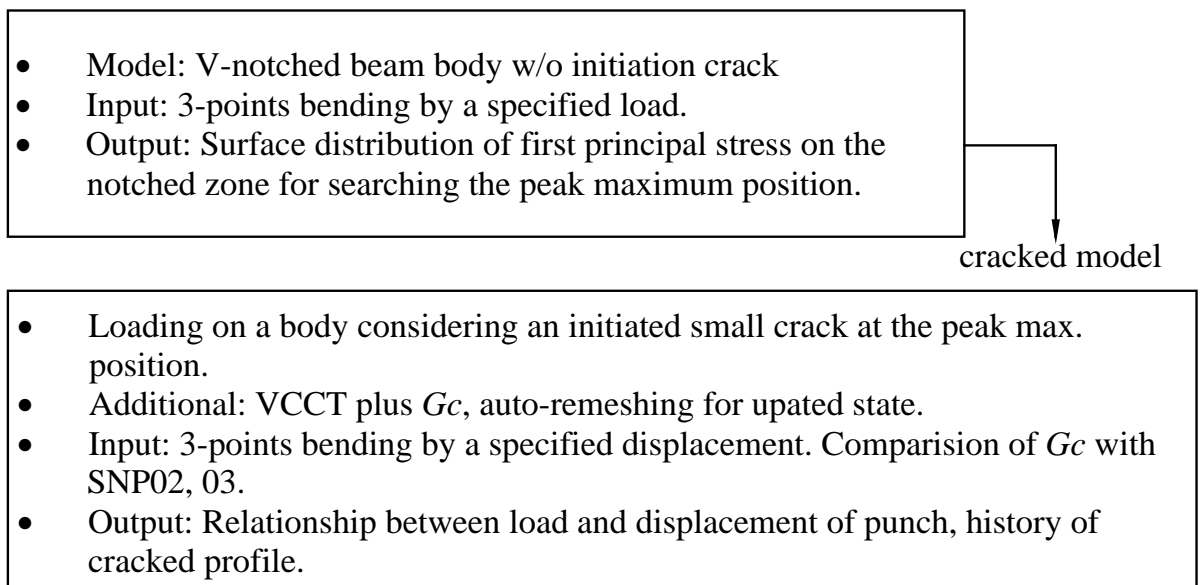


Figure 5-10. Flow schemes of numerical procedure

Figure 5-10 shows the flow schemes of numerical process to simulate the cracking behaviour during a shearing process. Firstly, an FEM model without cracking model was used for determining the stress distribution on the notched surface to detect the crack initiation. The mechanical condition of shearing process and the material properties of ceramics were considered to be same as the experiment described in the section 2.1. There were not any cracks on the surface in the first stage model. In **Figure 5-11**, the circled and triangle sequences show the peak value of maximum principal stress as a tensile state (σ_{p1}) in two cases of SNP02 and SNP03 with respect to the

punch's displacement, respectively. Linear approximations of simulated maximum principal stress σ_{p1} by the least-squares method were derived as Eqs. (5-9, 5-10). The difference of Eqs.(5-9, 5-10) was caused from the difference of Young's modulus of SNP02 and SNP03. The squared sequence shows the tracking position of the peak value of σ_{p1} . Here, the arc-length, L_{srf} , was a distance from the left side of the rounded notch (O) to a peak position of σ_{p1} (P) as shown in **Figure 5-12(a)**. It was found that the peak of σ_{p1} occurred near a 0.1mm off-set position (P) from the groove bottom during the shearing process in two cases of SNP02 and SNP03. This peak position was also corresponded to the position where the initial crack was observed in the shearing experiment. Therefore, a cracked position of the initiation in VCCT model was determined and a 0.012mm depth initiation was defined across to the surface in a meshed model as shown in **Figure 5-12 (b)**.

- for $0.015 < d/t_s < 0.025$ in case of SNP02):

$$\sigma_{p1} = 41124(d/t_s) + 171.44 \text{ at the point P} \quad (5-9)$$

- for $0.015 < d/t_s < 0.025$ in case of SNP03:

$$\sigma_{p1} = 53282(d/t_s) + 106.25 \text{ at the point P} \quad (5-10)$$

From the experiments, it was found that the cracking of groove zone of SNP02 and SNP03 started at the displacement $d/t_s=0.021$ and $d/t_s=0.023$, respectively. Then, the corresponded critical stress of SNP02 and SNP03 was estimated as 1035 and 1331 MPa respectively, using Eqs. (5-9, 5-10). This result was quite similar to the fracture strength which was estimated in [5.12]. Here, a maximum stress value is considered as the fracture strength to predict the cracking behavior in Si_3N_4 subjected to Vickers indentation.

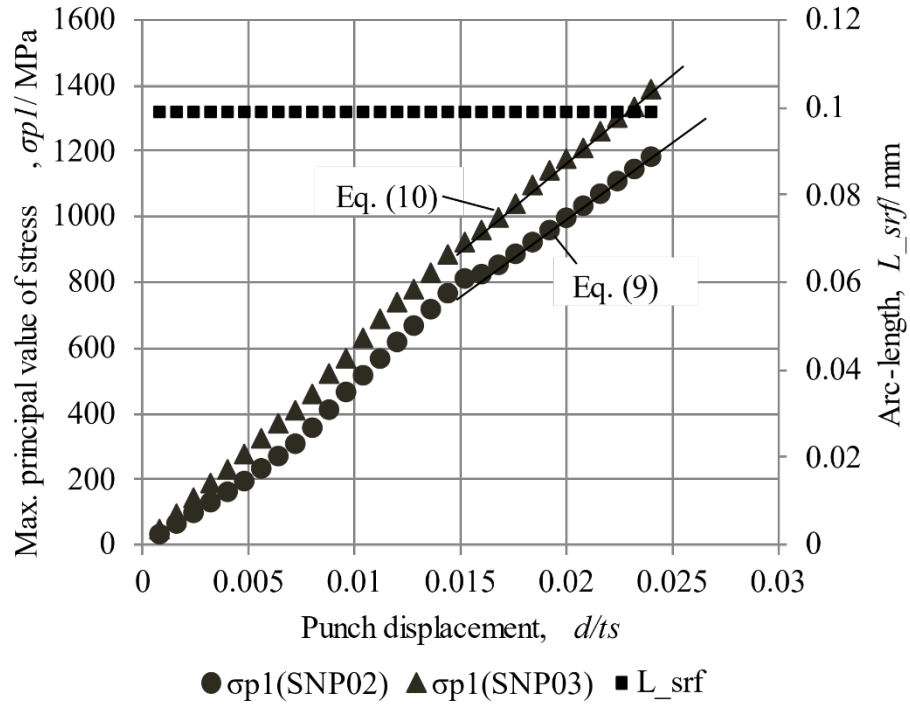


Figure 5-11. Stress distribution on the notch surface

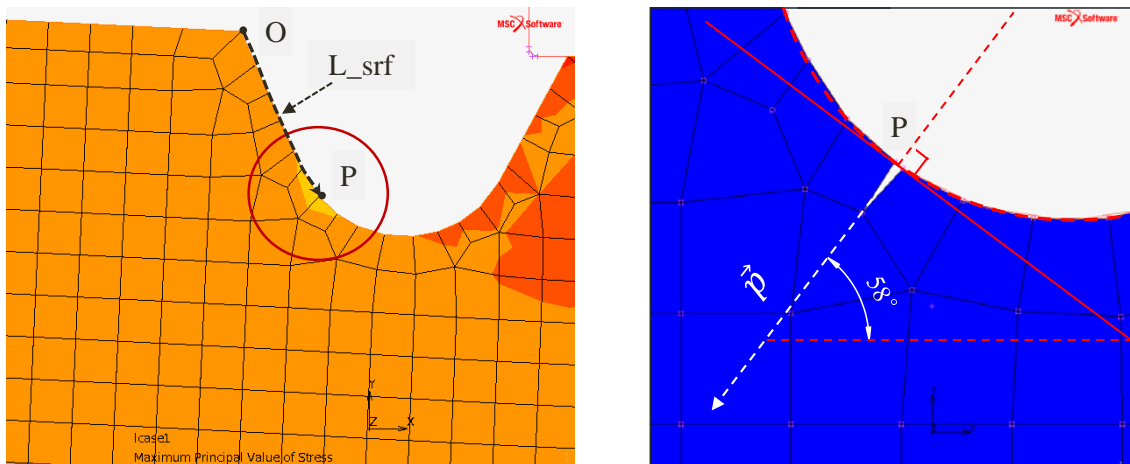


Figure 5-12. Detection of stress severe position and setting of a small crack on a groove surface. (a) Contour band of stress σ_{p1} at $d/t_s = 0.021$ (b) Introduction of a small crack for VCCT

After detecting the initiation position from the preliminary model, a cracking model based on the VCCT method, which was introduced in the section 3.1, was used

to simulate the cracking propagation of ceramics workpiece during the shear process. In this cracking model, the critical release energy rate was assumed to be $0.019 \text{ (N.mm}^{-1}\text{)}$ and $0.021 \text{ (N.mm}^{-1}\text{)}$ for SNP02 and SNP03 respectively from the 3-points bending test of pre-cracked beam that was mentioned in the section 2. The crack grew and propagated whenever the calculated energy release rate was larger than the critical value in the process of punch indentation against the notched workpiece. From the experiment result, it was found that the cracking direction was approximately 58° with the horizontal axis. Therefore, in this simulation, the crack propagation direction was specified by vector \vec{p} as shown in **Figure 5-12** (b). Here, crack propagation direction was approximately perpendicular to the tangent line of notch surface. The crack was propagated by the punch indentation until the workpiece was separated completely.

5.2.2.3 Results of simulation and discussions

To discuss the VCCT based simulation, the initial crack position and the direction of its propagation were numerically measured and compared with the experimental shear results of notched workpiece. **Figure 5-13** shows a simulated process of cracked behavior of SNP02. At the starting position $d/t_s = 0$, a 0.012 mm depth crack was defined on the groove surface as shown in **Figure 5-13** (a).

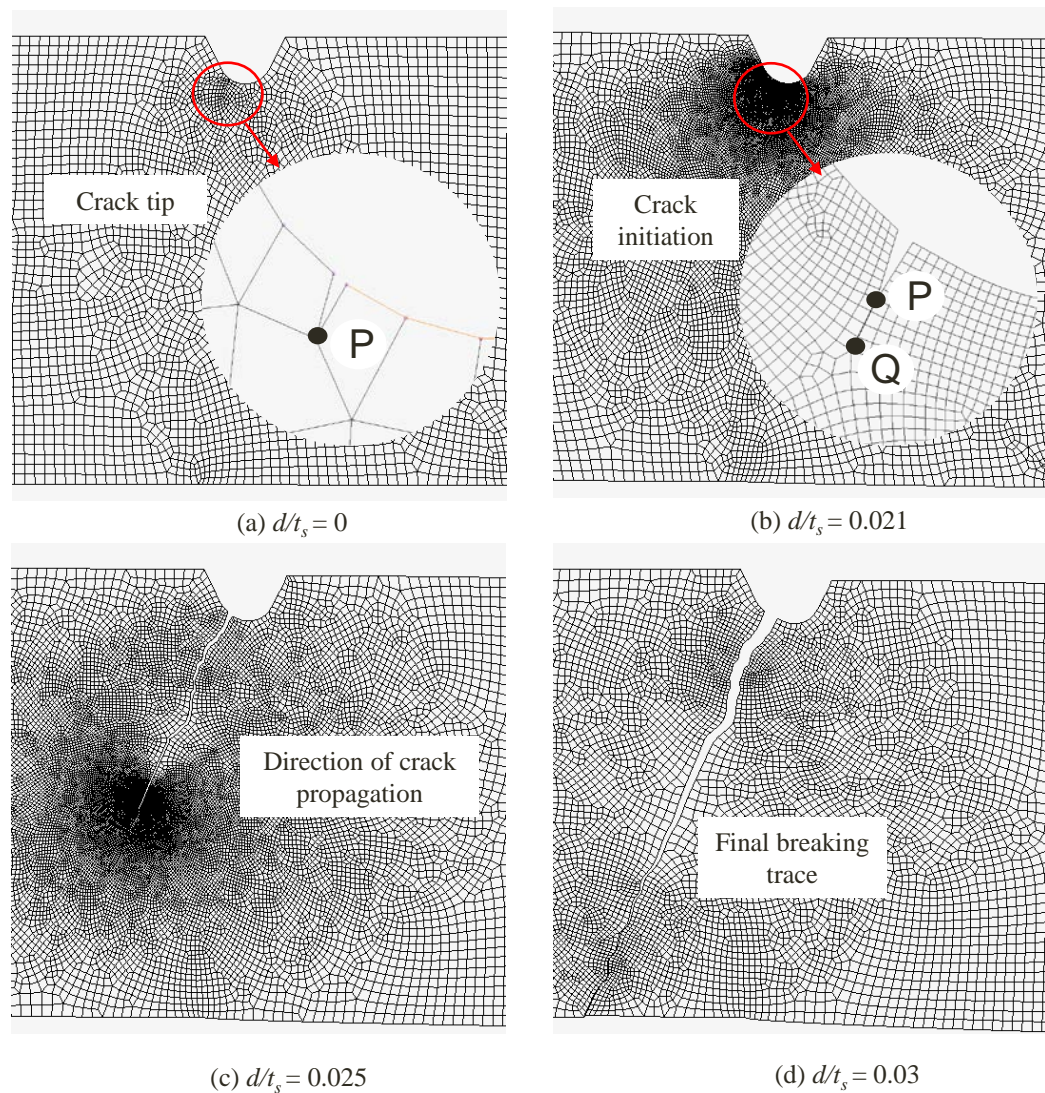


Figure 5-13. Crack propagation in shearing simulation for SNP02

When the punch moved downward, the pushing load increased. Meanwhile, the strain energy increased at the cracked position until the value of G_T (expressed by Eq. (5-8)) exceeded the critical release energy rate G_C , and then the crack started to be enlarged at $d/t_s = 0.021$ (**Figure 5-13** (b)). In this **Figure 5-13** (b), the crack tip was opened from the point P to the point Q in a small incremental step of convergence. Here, when the punch was indented with an incremental step $dx = 8 \times 10^{-4}$ mm, a crack length $da = 0.01$ mm was calculated. The maximum principal stress (σ_{pl}) at the crack tip was estimated as 1047 MPa in this state Fig.12(b). After that, the crack was gradually propagated when the punch

was continuously indented to the workpiece. In order to avoid unexpected stopping of crack growth, a global auto-remeshing function (2D solid: Advancing Front Quad) was used in the FEM simulation. The initial coarse mesh pattern around the focused crack were automatically refined when the crack was propagated in every increment. The automatic-remeshing was performed when the strain change of each element was higher than 0.2 or the inner angle of element was greater than 175° or smaller than 5° . To ensure the mesh resolution which was large enough to generate the new crack tip, the minimum element size was defined as 0.012mm in this simulation. **Figure 5-13(c)** shows a refined remeshing state which was allowed to make a small propagation of crack. Finally, the ceramics workpiece was completely broken at $d/t_s \approx 0.03$ (**Figure 5-13(d)**). The crack was extended and progressed along the initial crack as shown in **Figure 5-14**. In case of simulation, the crack route relatively propagated in a straight line. However, seeing the direction of crack propagation in **Figure 5-14**, especially from the center part to the lower-side of the workpiece, the cracked route of the experiment deviated from the initial line. As the result, the experimental crack path had a slight curve. This mismatching tendency seems to be caused from the high geometry constraints, that was also reported in [5.23-5.24].

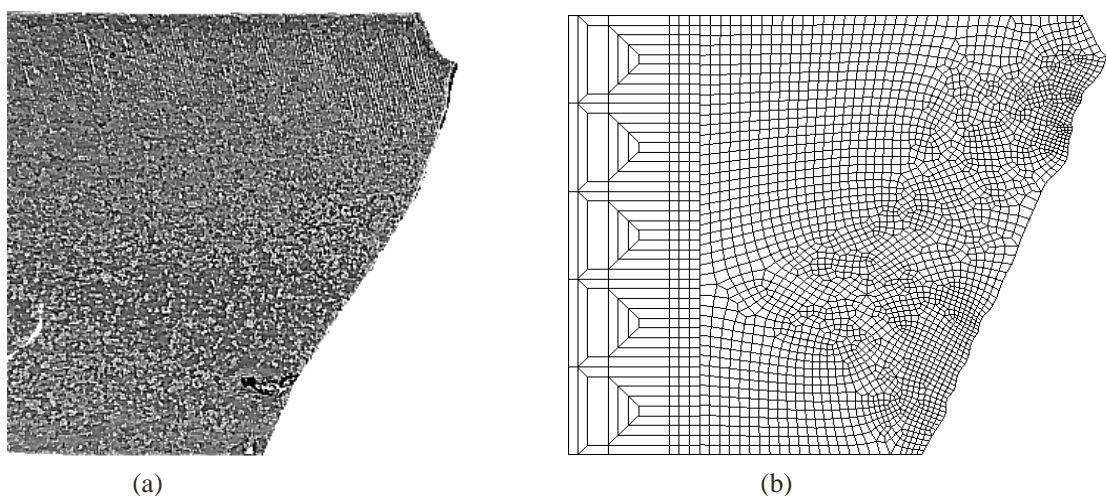


Figure 5-14. Comparing cracking profile between (a). experiment and (b). simulation for SNP02

Comparing the cutting line force as shown in **Figure 5-15**, it was found that the breaking strength was almost similar to that of the experiment. In the simulation, it was easy to detect the initial crack position, although this transition point was not detected clearly in the experiment. Through this development of simulation model, any other loading models or different type of notched workpiece are possible to analyse. After passing the punch stroke $d/t_s > 0.021$ for SNP02 and $d/t_s > 0.023$ for SNP03, the cracking behaviour was different from the experimental results due to some reasons. One reason was a sort of unstable calculation of cracking, and another reason seemed to be caused from the mismatching of dynamic cracking behaviour. The real, experimental behaviour seemed to be affected by a dynamic resistance of cracking, while the G_T based VCCT model was assumed to be a static resistance model.

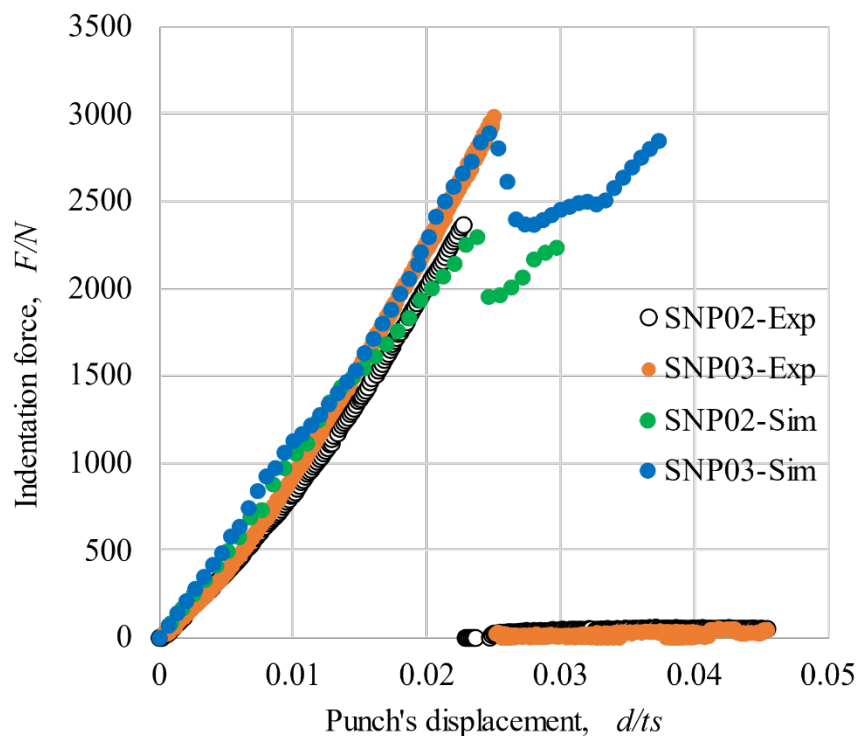


Figure 5-15. Comparing load-displacement response between experiment and simulation

5.3 Apply vcct model in acrylic shearing

5.3.1 Experiment and simulation method

In the previous section, a one-side notch Iosipescu type was used to estimate the shear strength of silicon nitride ceramics. Also, a VCCT method was applicable to predict the cracking behaviour of worksheet during the shearing process. In this section, a similar technique was applied to shearing of the acrylic worksheet. However, a V-notch cutter was used to prepare the two-side notches for acrylic specimen, which has a symmetric pair of round-edges on the top and bottom side. Another experiment condition is similar to the ceramics shearing experiment that was explained in the section 5.2.1. For the FEM simulation, the same VCCT method was applied for predict the cracking behaviour of the acrylic worksheet.

The material properties of AC were obtained from the experiment that was explained in the Chapter 4. In this VCCT model, critical release energy rate was assumed to be $0.59 \text{ (N}\cdot\text{mm}^{-1}\text{)}$, which was calculated from the three-point bending test evaluation as shown in **Table 5-3**.

Table 5-3. Acrylic material properties

Physical parameters		AC
Density, ρ	kg/m ³	1180
Poisson ratio, ν	-	0.39
Young's modulus, E	MPa	2216
Stress intensive factor, K_I	MPa·m ^{1/2}	0.85
Critical energy release rate, G_C	N/mm	0.59

5.3.2 Experiment and simulation results

Figure 5-16 shows the simulated result of cracking behaviour for $0 \leq d/t_S \leq 0.145$. At $d/t_S = 0.12$, the upper crack started to be opened. After that, the lower crack

started to be opened a bit later than the upper crack. Here, the propagation of these cracks could be observed. As illustrated in this figure the cracks were continuously propagated when the depth of the punch was increased. Seeing the direction of crack propagation, it relatively corresponded to the experiment.

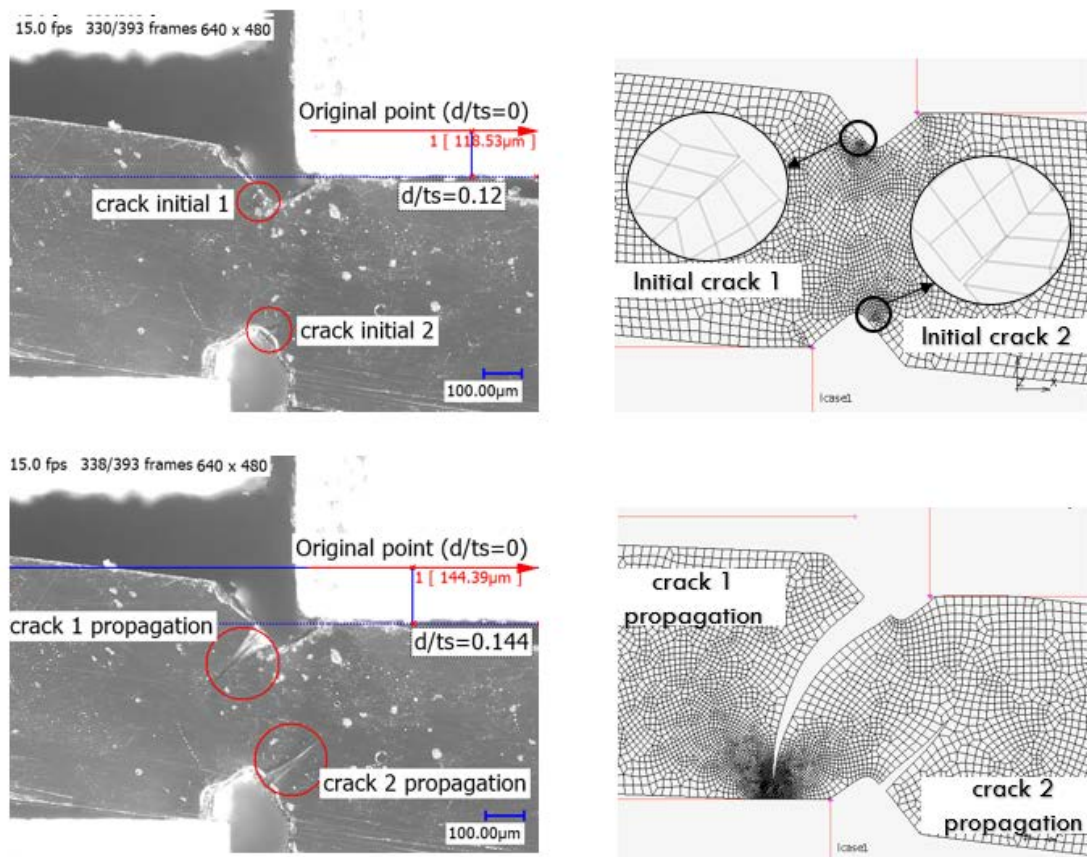


Figure 5-16. Comparing cracking profile between simulated crack propagation and experiment results

Comparing the cutting line force as shown in Fig. 6, it is found that, breaking strength was almost similar to that of the experiment. However, in the simulation, it was easy to detect the initial crack position, while, the experiment could not observe this transition point clearly. After passing the punch stroke $d/t_s > 0.12$, the cracking behaviour is a bit far from with the experiment due to many unstable conditions.

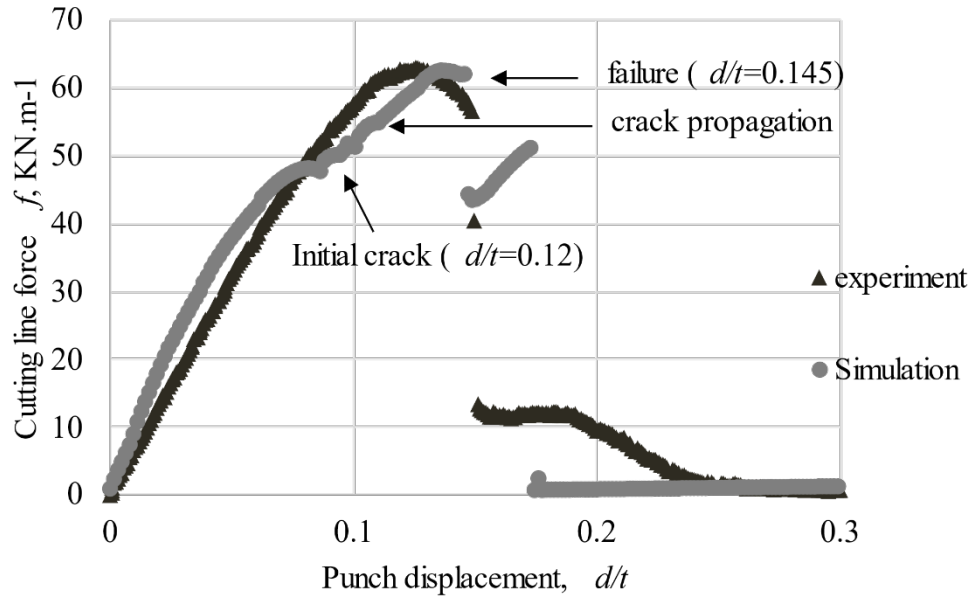


Figure 5-17. Simulated and experimental cutting line force

5.4 Conclusion

In this study, the shear strength of two kinds of ceramics and acrylic material was experimentally and numerically estimated by using a round-notched shear test method. The initial cracking and its propagation direction were analyzed using the VCCT method. The followings were concluded:

The Eq. (5-8) based VCCT model plus the positioning of initiation by the maximum principal stress had a good agreement with the experiment to predict a crack initiation and the direction of crack propagation in a notched Si_3N_4 and AC workpiece.

The developed simulation model using the Eq. (5-8) based VCCT plus the initiation by the maximum principal stress has a possibility to predict the similar crack propagation in notched fragile materials subjected to a shearing tool indentation.

References

- [5.1] Brokken D, Brekelmans WAM, Baaijens FPT (2000) Predicting the shape of blanked products: a finite element approach. *J Mater Process Technol* 103: 51–56.
- [5.2] Goijaerts AM, Govaert LE, Baaijens FPT (2001) Evaluation of ductile fracture models for different metals in blanking. *J Mater Process Technol* 110: 312–323.
- [5.3] Goijaerts AM, Govaert LE, Baaijens FPT (2002) Experimental and Numerical Investigation on the Influence of Process Speed on the Blanking Process. *J Manuf Sci Eng* 124: 416-419.
- [5.4] Zhou Y, Yang W, Hu M, et al. (2016) The typical manners of dynamic crack propagation along the metal/ceramics interfaces: A molecular dynamics study. *Comput. Mater. Sci* 112: 27–33.
- [5.5] Zhou Y, Yang Z, Lu Z (2014) Dynamic crack propagation in copper bicrystals grain boundary by atomistic simulation. *Mater. Sci. Eng. A* 599: 116–124.
- [5.6] Yang Z, Zhou Y, Wang T, et al. (2014) Crack propagation behaviors at Cu/SiC interface by molecular dynamics simulation. *Comput. Mater. Sci* 82: 17–25.
- [5.7] Pusit M, Nagasawa S (2013) Cutting Behavior of Acrylic Thick Sheet Subjected to Squared Punch Shearing. *J Chem Chem En.* 7: 653-665.
- [5.8] Kojima M, Mitsomwang P, Nagasawa S. (2016) Effect of cutter tip angle on cutting characteristics of acrylic worksheet subjected to punch/die shearing. *AIMS Mater Sci* 3: 1728-1747.
- [5.9] Barnes JA, Kumosa M, Hull D (1987) Theoretical and experimental evaluation of the Iosipescu shear test. *Compos Sci Technol* 28: 251–268.
- [5.10] Stojcevski F, Hilditch T, Henderson LC (2018) A modern account of Iosipescu testing. *Compos. Part A Appl. Sci. Manuf* 107: 545–554.
- [5.11] Japan Fine Ceramics Corp, Silicon Nitride, 2020. Available from: <https://www.japan-fc.co.jp/en/products/cate01/cate0101/si3n4.html>.
- [5.12] Kadin Y, Mazaheri M, Zolotarevsky V, et al. (2019) Finite Elements based approaches for the modelling of radial crack formation upon Vickers indentation in silicon nitride ceramics. *J. Eur. Ceram. Soc* 39: 4011-4022.
- [5.13] Zhang L, Zarudi I (2001) Towards a deeper understanding of plastic deformation in mono-crystalline silicon. *Int. J. Mech. Sci* 43: 1985-1996.

- [5.14] ASTM International (2015), ASTM E494-15, Standard Practice for Measuring Ultrasonic Velocity in Materials, West Conshohocken, PA
- [5.15] Birgül R (2009) Hilbert transformation of waveforms to determine shear wave velocity in concrete. *Cem Concr Res* 39: 696–700.
- [5.16] Strobl S, Lube T, Supancic P, et al. (2017) Surface strength of balls made of five structural ceramic materials evaluated with the Notched Ball Test (NBT) *J. Eur. Ceram. Soc* 37: 5065–5070.
- [5.17] Paterson MS, Wong, Teng-fong, (2005) *Fracture Mechanics, Experimental Rock Deformation - The Brittle Field*, 2 Eds., Berlin, Heidelberg: Springer Berlin Heidelberg, 239-246.
- [5.18] Kadin Y, Strobl S, Vieillard C, et al. (2017) In-situ observation of crack propagation in silicon nitride ceramics. *Procedia Structural Integrity* 7: 307-314.
- [5.19] MSC Software Corp (2010) In: *Marc 2010 Volume A: Theory and User Information, Remeshing Techniques*, 154-163.
- [5.20] Krueger R (2004) Virtual crack closure technique: history, approach, and applications. *Appl Mech Rev* 57: 109–143.
- [5.21] Kanda Y, Okada H, Iraha S, et al. (2009) A Virtual Crack Closure-Integral Method for Generalized Finite Element with Drilling and Strain Degrees of Freedoms. *J Comput Sci Technol* 3: 303-314.
- [5.22] Kikuchi H, Kalia RK, Nakano A, et al. (2005) Brittle dynamic fracture of crystalline cubic silicon carbide (3C-SiC) via molecular dynamics simulation. *J. Appl. Phys* 98: 103524.
- [5.23] Ayatollahi MR, Razavi SMJ, Berto F (2018) Crack path stability in brittle fracture under pure mode I loading. *Procedia Structural Integrity* 13: 735–740.
- [5.24] Smith DJ, Ayatollahi MR, Pavier MJ (2001) The role of T-stress in brittle fracture for linear elastic materials under mixed-mode loading. *Fatigue Fract Eng Mater Struct* 24: 137–150.

This page has been intentionally left blank

Chapter 6 :

CONCLUSIONS AND PROSPECTS

6.1 Conclusions

In this research work, the main objective is to reveal the fundamental cutting mechanism and the critical conditions for cutting off a thin worksheet. Deformation behavior and cracking patterns of a thin worksheet during the wedge indentation process were investigated under varying the mechanical conditions such as the punch/die cutting velocity, cutting temperature. As a result, a suitable cutting tool conditions for making a smart sheared edge of the worksheet was proposed. Furthermore, a general-purpose finite element method (FEM) code was applied to develop the cracking model in shearing process of the fragile materials such as ceramics and acrylic. Through experimental and numerical results, the following features were disclosed:

- i. By varying the cutting direction PA6-PE and PE-PA6, the bent-up angle θ of the laminated worksheet and cutting load response were remarkably effect by the laminated structure. A bad cutting profile occurred in this case of normal cutting direction PA6-PE. While a good cutting profile was observed for revered cutting direction PE-PA6. From this result, a good cutting condition can be chosen for a similarity laminated worksheet cutting in the mass industrial. The simulated profile of the nylon film shows good agreement with experimental result. The bent-up angle and the deformation profile of the nylon film mainly depend on the stiffness of upper layer and lower layer of laminated worksheet.
- ii. The bent-up angle and the deformation profile of worksheet remarkably depended on the normalized tip thickness of the cutting blade w/t . When choosing $w/t \leq 0.13$, the bent-up angle was less than 50degrees (72% of saturated maximum angle) and the cutting peak maximum was less than 7 N/mm at normal temperature. This

seemed to be a preferable mechanical condition for smoothly cutting a PA6-PA film off.

- iii. From the study effect of temperature on the cutting characteristics of PA6/PE film, it was found that an appropriate range of the temperature of a blade body, a case of $T = 318\text{K}$ against a room temperature 296K was suitable for cutting the 0.16mm PA6/PE film off during wedge indentation. An FEM model aslo was conducted to reveal the effect of temperature in the deformation of the PA6/PE film. The effect of temperature, velocity was defined by Johnson-Cook parameters that was obtained from series of experiment as various temperature and strain rate. From the simulation results, the simulated cutting load response of the nylon film shows good agreement with experimental result.
- iv. From the study of thermal cutting and equivalency of velocity in cutting characteristics of acrylic worksheet, some features on the cutting resistance and profile deformation mode were revealed as follows. The cutting load response and the deformation profile of the worksheet remarkably depended on the cutting velocity and applied temperature of the cutting blade. An appropriate range of the temperature of a blade body and cutting velocity can be optimized to enhance the quality of the sheared surface of the cutting worksheet.
- v. Moreover, A VCCT model was also applied to simulate a shearing process for investigating the breaking behavior of ceramics and AC workpiece subjected to a shearing-tool indentation. This proposed model can be developed and applied to simulate the AC cutting in wedge indentation process.

6.2 Prospects

In the current study, the FEM simulations of the cracking behavior of Iosipescu specimens subject to shearing process were conducted and discussed subjected to the shearing process. In the near future, the author would like to apply this method to analyse the cracking pattern of the fragile worksheet in wedge indentation process,

which has a completed fracture than the current model. Therefore, the application of this method can be applied to other composite materials.

This page has been intentionally left blank

APPENDIX A

APPARATUSES AND TOOLS

Table A.1 Lists of apparatuses and tools



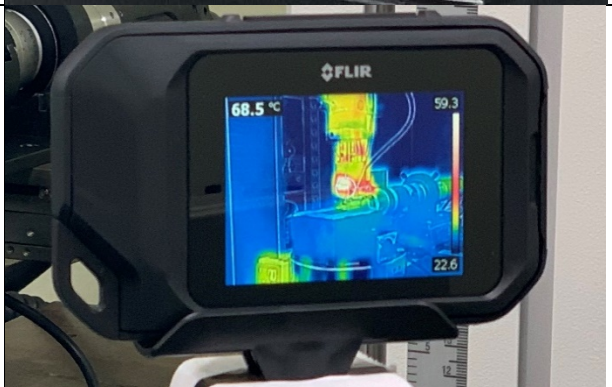



Apparatus/ tool	Photograph of apparatus/tool	Specification/ capacity
Silicone rubber heater		<ul style="list-style-type: none"> - Maximum operating temperature: 473K - Heat generation density: 0.8W/cm² - Voltage: 100 V, - - Power: 10 W
Thermal controller		E5CC-RX3ASM-000
Thermal imaging camera (Flir C3)		<ul style="list-style-type: none"> Thermal sensitive < 0.1 oC Temperature range -263K~ +423K

Table A.1 Lists of apparatuses and tools (Continued)

Apparatus/ tool	Photograph of apparatus/tool	Specification/ capacity
(Instron 3366) Universal testing machine		<ul style="list-style-type: none"> - Load cell = 10 kN - Max. testing speed = 500 mm·min⁻¹ - Vertical test space = 1193 mm
Compression machine (Aiko engineering machine, model 1311DWS)		<ul style="list-style-type: none"> - Power supply: 100 VAC 50/60HZ - Load cell: 50N, 50kgf, 500kgf.
Digital Optical microscope (VHX-2000)		<ul style="list-style-type: none"> - Power supply: 100 ~ 240VAC 50/60HZ, 340VA max. - Shutter speed = 1/15 ~ 1/19000 s. - Image sensor: 2.11 million-pixels.

APPENDIX B
LIST OF PUBLICATIONS

List of journal publications

- [1] **Hanh C. Nguyen**, S. Nagasawa, Cutting characteristics of nylon-polyethylene laminated film subjected to wedge indentation and its thermal dependency, *Advances in Materials and Processing Technologies*, (2020) 1-12.
- [2] **Hanh C. Nguyen**, S. Nagasawa, K. Kaneko, Strength estimation of silicon nitride ceramics using a round-notched specimen subjected to shearing-tool indentation, *AIMS Materials Science*, 7 (2020) 518-533.
- [3] **Hanh C. Nguyen**, S. Nagasawa, Experimental and Numerical Investigation of Cutting Characteristics of PA6/PE Nylon Film Subjected to Wedge Indentation Process, *Materials Science Forum*, 1009 (2020) 129-134.
- [4] **Hanh C. Nguyen**, S. Nagasawa, K. Kaneko, Optimizing boundary surface of ceramics die in deep drawing process, *Transactions on GIGAKU*, Vol.4 No.1 (2017.May,12), Article ID: 04002 [1-7].

List of international conferences

- [1] **Hanh C. Nguyen**, Shigeru Nagasawa, Kensei Kaneko, Strength evaluation of brittle ceramics using iosipecu type specimen subjected to shearing-tool indentation, *5th Asian Symposium on Material and Processing*, Bangkok, Thailand, (2018), No.37, pp.136-137.
- [2] **Hanh C. Nguyen**, Shigeru Nagasawa, Masami Kojima, 5th Asian Symposium on Material and Processing., *Japan Society of Mechanical Engineers Annual Meeting 2018*, Osaka, Japan, (2018).
- [3] Yuto Todoroki, **Hanh C. Nguyen**, and Shigeru Nagasawa., Development of Finite Element Analysis Model of Stress Concentration on Tool Corner for a Tandem Process of Deep Drawing., *The 7th International GIGAKU Conference in Nagaoka*, Nagaoka, Japan (2018), No. RD-003.
- [4] **Hanh C. Nguyen**, and Shigeru Nagasawa, Effects of Cutting Parameters on Cutting Characteristics of Nylon Film Subjected to Wedge Indentation, *The 7th International GIGAKU Conference in Nagaoka*, Nagaoka, Japan, (2018).
- [5] **Hanh C. Nguyen**, Shigeru Nagasawa, Experimental and numerical investigation of cutting parameters on cutting characteristics of nylon film subjected to wedge indentation, *22nd International Conference on Advances in Materials and Processing Technologies*, Taipei, Taiwan, (2019).
- [6] **Hanh C. Nguyen**, Shigeru Nagasawa, Experimental and Numerical Investigation of Cutting Characteristics of PA6/PE Nylon Film Subjected to Wedge Indentation Process, *4th International Conference on Material Engineering and Manufacturing*, Chiba, Japan, (2020).

List of national conferences

- [1] **Hanh C. Nguyen**, Shigeru Nagasawa, Masami Kojima, Predict cracking behavior of Acrylic resin sheet using Iosipescu type specimen subjected to a shearing-tool indentation, *Proceedings of Japan Society of Mechanical Engineers Annual Meeting*, Osaka, Japan, (2018), No. J0450304, pp.1-5.
- [1] **Hanh C. Nguyen**, Shigeru Nagasawa, Cutting characteristics of nylon sheet, *The 14th Seminar on Form Cutting Technology; Japan Composite Material Processing Research Group*, Nagaoka, Japan, (2019).

This page has been intentionally left blank

BIOGRAPHY

Personal details

Full name : NGUYEN CONG HANH
Address : 1603-1 Kamitomioka,
Nagaoka,
Niigata 940-2188, Japan
Place of Birth : Quang Nam, Vietnam.
Date of Birth : August 01, 1988.



Educational background

Sep. 2007 – Aug. 2012. Danang University of Technology, Danang, Vietnam. Bachelor of Engineering in Mechatronics Engineering.
Dec. 2012 – Aug. 2015. Joined Danang University of Technology, Danang, Vietnam, lecturer.
Sep. 2015 – Aug. 2017. Nagaoka University of Technology, Niigata, Japan. Master of Engineering Mechanical Engineering.
Sep. 2017 – Dec. 2020. Nagaoka University of Technology, Niigata, Japan. Doctor of Information Science and Control Engineering.

Working experience

Dec. 2012 – present Joined University of Science and Technology, The University of Danang, Danang, Vietnam, lecturer.

Research field

Material processing technologies: Analysis of advanced sheet material forming processes and finite element analysis (FEM) applied for material processing.

Membership in Academic Societies:

The Japan Society of Mechanical Engineers (JSME)